Pedro Henrique dos Santos Cunha

Scattering Theory for a Wavy Sphere

Volta Redonda, Rio de Janeiro - Brazil
2025

Pedro Henrique dos Santos Cunha

Scattering Theory for a Wavy Sphere

Dissertação de mestrado submetida ao curso de pós-graduação em Física da Universidade Federal Fluminense, como requisito parcial para obtenção do Título de Mestre em Física

Universidade Federal Fluminense - UFF

Instituto de Física

Mestrado Acadêmico em Física

Orientador Dr. Alexandre Grezzi de Miranda Schmidt

Volta Redonda - RJ

20 de setembro de 2025

Ficha catalográfica automática - SDC/BIF
Gerada com informações fornecidas pelo autor

S237s Santos Cunha, Pedro Henrique dos
Scattering Theory for a Wavy Sphere / Pedro Henrique dos Santos Cunha. - 2025.
91 f.: il.

Orientador: Alexandre Grezzi de Miranda Schmidt.
Dissertação (mestrado)-Universidade Federal Fluminense, Instituto de Física, Niterói, 2025.

1. Scattering Theory. 2. Quantum Mechanics. 3. Green's function. 4. Wavy Sphere. 5. Produção intelectual. I. Miranda Schmidt, Alexandre Grezzi de, orientador. II. Universidade Federal Fluminense. Instituto de Física. III. Título.

CDD - XXX

Bibliotecário responsável: Debora do Nascimento - CRB7/6368

Pedro Henrique dos Santos Cunha

Scattering Theory for a Wavy Sphere

Dissertação de mestrado submetida ao curso de pós-graduação em Física da Universidade Federal Fluminense, como requisito parcial para obtenção do Título de Mestre em Física

Aprovado em: 01/09/2025

BANCA AVALIADORA

Membros titulares

Dr. Alexandre Grezzi de Miranda Schmidt
(**UFF**)
Orientador

Dr. Fabiano Manoel de Andrade
(UEPG)

Dr. Reinaldo Faria de Melo e Souza
(IF/UFF)

To my mother, who always encouraged me.

Acknowledgements

I would like to thank, above all, my mother for supporting and encouraging me so that I could make it this far. Without her help, I would never have overcome the obstacles life placed in my path.

My advisor, Alexandre, for his patience and attention throughout this journey.

My girlfriend, Victoria, for her patience on turbulent days, her embrace on cold days, and her comfort on sad days.

My friends, Barbara, Carlos Magno, Miguel, Matheus, Ediward and Victor, for their support, conversations, and laughter along the way.

The entire faculty of Universidade Federal Fluminense, especially Professors Marcos Veríssimo, Ladário da Silva and Rodrigo Garcia Amorim, for the conversations and guidance that extended beyond academic life.

The employees of Universidade Federal Fluminense, both contracted and permanent, who care for and look after the Aterrado Campus, for providing me with a professionally dignified environment in which to study and work.

And last, but by no means least, the whole institution of the Universidade Federal Fluminense for giving me the opportunity to be part of the graduate program in Physics.

"A man that flies from his fear may find that he has only taken a short cut to meet it."

Sador in *Children of Húrin*

Abstract

This thesis investigate how a single rough-like sphere scatters quantum waves. We study two ways to describe the same object. In the first, the shape is smooth but the strength of the barrier changes from point to point, modeling a wavy coupling. In the second, the sphere's shape is deformed by waviness and deformation parameters like a Chebyshev particle.

Starting from the Lippmann–Schwinger equation and its Green-function form of the Helmholtz equation, we find the expressions for the scattering amplitude, the differential and total cross-sections, and also the quantum refractive index. We then compare how each model of roughness alters these quantities.

Keywords: Green's function, Scattering Theory, Wavy Sphere

Resumo

Essa dissertação investiga o fenômeno de espalhamento por uma esfera com rugosidades e heterogeniedades em sua superfície. Estudamos duas maneiras de descrever o mesmo objeto. A primeira abordagem consiste no espalhamento por uma esfera ideal, mas cujo acoplamento varia ponto a ponto, modelando heterogeniedades através de um acoplamento ondular. No segundo caso, a esfera é deformada através de parâmetros de ondulação e deformação que causam irregularidades em sua superfície, como uma partícula de Chebyshev.

Começando pela equação de Lippmann-Schwinger e a função de Green da equação de Helmholtz, nós encontramos as expressões para a amplitude de espalhamento, obtendo a seção de choque diferencial e total, além do indíce de refração quântico. Essas grandezas então são utilizadas para comparar a fenomenologia de cada modelagem.

Palavras-chave: Funções de Green, Teoria de Espalhamento, Esfera ondulada

List of Figures

Contents

1 Introduction

Scattering theory is essential in physics, corroborating our understanding of diverse phenomena such as X-ray imaging, radar systems, and remote sensing applications(BELKIC, 2004). Seminal historical experiments, like Rutherford's α-particle scattering that uncovered the atomic nucleus(E., 1911), and the Franck–Hertz experiment, which significantly contributed to Bohr's atomic model, highlight its pivotal role(BOHR, 1913; FRANCK; HERTZ, 1914).

Non-relativistic quantum scattering phenomena can be described by solving either Schrödinger's differential equation or the Lippmann–Schwinger equation(LIPPMANN; SCHWINGER, 1950). Schrödinger's formulation emphasizes local wavefunction variations, whereas the Lippmann–Schwinger approach uses a global and integral perspective, integrating the wavefunction over specific domains(MAIOLI; SCHMIDT, 2018).

Recent studies have significantly expanded the scope of scattering theory, addressing complex scattering problems from irregularly shaped and rough surfaces. These studies vary in complexity and validity, necessitating comprehensive comparative analyses to ensure their reliability against empirical data, as illustrated by Hermansson et al. (HERMANSSON; FORSSELL; FAGERSTROM, 2003), who thoroughly reviewed scattering models for rough surfaces emphasizing the importance of validating theoretical models against experimental results.

Porous materials add further complexity to scattering analyses due to their intrinsic surface heterogeneity, significantly affecting wave scattering behavior. Chiang et al. (CHIANG et al., 2018) introduced a generalized Porod's scattering law method, capable of quantifying surface heterogeneity in porous media non-invasively. Such advancements underline the importance of accurately characterizing scattering behaviors to understand interactions at microscopic and macroscopic scales.

In the context of electromagnetic and quantum scattering, León-Pérez et al. (LEÓN-PÉREZ et al., 2008) developed modal expansion methods demonstrating that indentations, including arrays of holes and dimples on metal films, significantly scatter surface plasmon polaritons (SPPs). Wolf et al. (WOLF; TERHEIDEN; BRENDEL, 2008) analyzed light scattering in porous silicon, employing Mie's theory and effective refractive indices to describe diffuse propagation, demonstrating the critical interplay between microscopic features and scattering behaviors.

Motivated by these studies, this thesis investigates quantum scattering phenomena specifically by a three-dimensional rough-like sphere, that we call wavy sphere, through a boundary-wall approach(ZANETTI; VICENTINI; LUZ, 2008), that can be model

by two approaches. The first one uses the geometry of the barrier, modeling it as a Chebyshev particle, characterized by waviness and deformation parameters, providing realistic representations of surface irregularities encountered in various physical, chemical, and biological contexts(LAZAREVICH et al., 2004). Because Chebyshev particles reproduce high-frequency, low-amplitude irregularities on an spherical surface, they form a far more realistic model to representing natural imperfections (MISHCHENKO; LACIS, 2003). A notable example is *Neochloris oleoabundans*, microalgal cells whose contours are well captured by Chebyshev descriptors (MISHCHENKO; TRAVIS, 1998). Accurate modeling of these cells corroborate atmospheric optics, photobioreactor design, and diverse biotechnological applications (ZHU et al., 2020; KAHNERT; NOUSIAINEN; LINDQVIST, 2014b; PRUVOST et al., 2011).

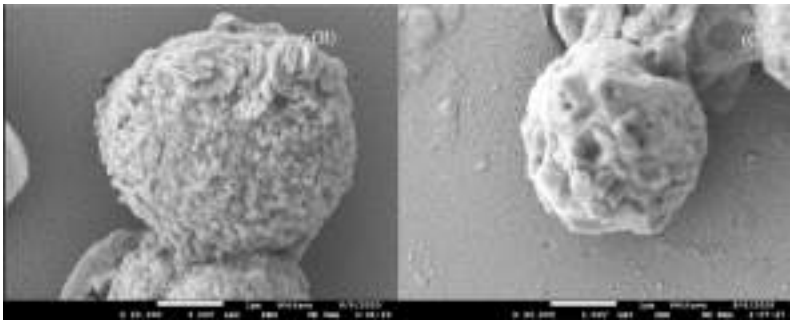

Figure 1 – Example of application related to the modelling of an spherical surface with irregularities: the microalga *Neochloris oleoabundans*, used in the cosmetics industry and in biofuel production (GU; LAN, 2021)

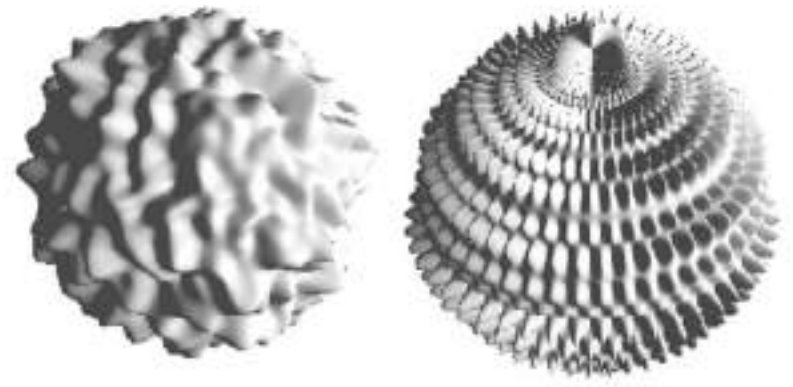

Figure 2 – Example of application related to the modelling of an spherical surface with irregularities: computational modeling of aerosol particles in the atmosphere (KAHNERT; NOUSIAINEN; LINDQVIST, 2014a).

Beyond a purely geometric approach, for the second approach, we present a coupling-function approach: a position-dependent coupling strength of the barrier,

$$\gamma(\phi, \theta)$$

defined on the spherical surface and parameterized by the polar (θ) and azimuthal (ϕ) angles. This function models how each infinitesimal surface element interacts with an incident

plane wave, effectively encoding heterogeneous roughness, compositional inhomogeneities, or electrostatic patches that cannot be captured by shape alone, and can also be used to model porous sphere-like materials.

The objective of this work is an analysis of critical physical quantities, specifically the scattering amplitude, differential and total cross-sections, and the quantum refractive index. Champenois and collaborators (CHAMPENOIS et al., 2008) obtained an expression for the quantum refractive index in gaseous media as:

$$n = 1 + 2\pi N \left(\frac{m_p + m_t}{m_t} \right) \left\langle \frac{f(k_r)}{k_p^2} \right\rangle ,$$

with particle densities N, masses m_p, m_t, and wavenumbers k_r, k_p. In our case we will deal with a plane-wave particle incident on a single scatterer. Thus, under Born's approximation, this refractive index simplifies to:

$$n = 1 + 2\pi\gamma \left\langle \frac{f_0}{k^2} \right\rangle ,$$

where f_0 represents forward scattering amplitudes, γ denotes interaction density, and k is the wave-vector magnitude.

This work is organized as follows. Chapter 2 introduces the mathematical tools of Green's functions, a key element in quantum mechanics scattering theory, and shows their billinear form for the three-dimensional Helmholtz equation in spherical coordinates. Chapter 3 gives a systematic review of scattering theory and its main ideas in quantum mechanics, explaining how the Schrödinger equation connects to the Lippmann–Schwinger equation and defining the physical quantities central to this thesis: the differential scattering cross section, the total scattering cross section, and the quantum refractive index. In Chapter 4, we put these physical and mathematical tools to use in the problem of scattering by a spherical barrier. We start with the simpler case of a smooth spherical barrier, which makes the method clear, and then move on to two more situations: a smooth spherical barrier with wavy coupling and a wavy spherical barrier. For each case, we study the physical quantities mentioned above. Finally, Chapter 5 summarizes the conclusions from the results of Chapter 4 and discusses the related physical insights.

2 Green's Functions

Green functions is one of the most fundamental topics in contemporaneous theoretical physics, being called fundamental solutions of differential operators(PéREZ, 2015).

Specifically, in the quantum physics formulation, the Green Functions play a main role, having a causal relationship with the temporal evolution of the systems and being called propagators (GONIS; BUTLER, 2000).

Green functions G can be defined as solutions of the differential equation

$$\mathbb{L}(\partial)G = \delta \tag{2.1}$$

where $\mathbb{L}(\partial)$ is a differential operator with constant coefficients. In the RHS, δ represents the Dirac delta function, or more rigorously the Dirac delta distribution.

2.1 Distributions

To understand the true nature of the Green functions, first we need to introduce the basic concepts about distributions and the Dirac Delta distribution.

We can define a distribution using a certain class of functions called *test functions*. An *test function* is a function infinitely differentiable with compact support in $\mathbb{R}^n$. We call the set of these test functions as $\boldsymbol{D}(\mathbb{R}^n)$ or simply $\boldsymbol{D}$.

Definition 1. *A compact support of some function f is the closure of all point sets that has $\boldsymbol{x} \in \boldsymbol{X} \subset \mathbb{R}^n$, with $f(\boldsymbol{x}) \neq 0$. Thus*

$$supp(f) = \{\boldsymbol{x} \in \boldsymbol{X} \,|\, f(\boldsymbol{x}) \neq 0\} \tag{2.2}$$

If $supp(f) \subset E$ for some E set, we can say that f is supported in E. Specifically, if $supp(f) \subset U_R \subset \mathbb{R}^n$, where U_R denotes a radius R, we say that f has a compact support in R^n.

By (1), we clearly observe that an test function can not be analytic in the entire $\mathbb{R}^n$. In fact, a good example that demonstrates this characteristic is the test function given by

$$\phi(x) = \begin{cases} C_e e^{-\epsilon^2/(\epsilon^2 - x^2)}, & |x| \leq \epsilon \\ 0, & |x| > \epsilon \end{cases} \tag{2.3}$$

where C_ϵ is a constant such that $\int \phi = 1$.

We define a *distribution*

$$\langle F, \phi \rangle = \int F(\boldsymbol{x})\phi(\boldsymbol{x})d\boldsymbol{x} \tag{2.4}$$

as a continuous linear functional F on the test functions space $\boldsymbol{D}$ where ϕ is the test function. We also denote $\boldsymbol{D'}$ for the distributions space.

The linearity of the functional F is a direct consequence of the integral operator and the continuity is guaranteed by the convergence in $\boldsymbol{D'}$ that can be consulted in (VAZ; OLIVEIRA, 2016).

Therefore, the main value of a distribution is in how it affects other functions (called test functions) when they are integrated along the space in which they are defined. Generally, there are two classes of distributions: the regular distributions and the singular ones (FOLLAND, 1992). The most interesting distributions are the singular distributions, specially the Dirac Delta distribution, which we will discuss later.

2.1.1 Multiplying distributions

One of the operations on distributions that we need to define is the multiplication of distributions. We can consider, in a simple way, two distributions $f \in \boldsymbol{D'}$ and $g \in \boldsymbol{D'}$. For a test function $\phi \in \boldsymbol{D}$, we have:

$$\langle f, \phi \rangle = \int f(\boldsymbol{x})\,\phi(\boldsymbol{x})\,d\boldsymbol{x} \qquad \langle g, \phi \rangle = \int g(\boldsymbol{x})\,\phi(\boldsymbol{x})\,d\boldsymbol{x} \tag{2.5}$$

The product of two distributions is called the direct product, denoted by $f \times g$, and is defined by:

$$\langle f \times g, \phi \rangle = \langle f, \langle g, \phi \rangle \rangle = \langle g, \langle f, \phi \rangle \rangle \tag{2.6}$$

by Fubini's theorem, we know that:

$$\begin{aligned} \langle g, \langle f, \phi \rangle \rangle &= \int f(\boldsymbol{x}) \left(\int g(\boldsymbol{x})\,\phi(\boldsymbol{x})\,d\boldsymbol{x} \right) d\boldsymbol{x} \\ &= \int g(\boldsymbol{x}) \left(\int f(\boldsymbol{x})\,\phi(\boldsymbol{x})\,d\boldsymbol{x} \right) d\boldsymbol{x} = \langle f, \langle g, \phi \rangle \rangle \end{aligned} \tag{2.7}$$

The product $f \times g$ is also a linear functional(OLIVEIRA, 2016), and it can also be shown that it satisfies the commutative and associative properties of the product.

2.1.2 Differentiability in distributions

As mentioned earlier, there are two types of distributions: regular distributions and singular distributions. Regular distributions are those whose $f(\boldsymbol{x})$ satisfies the condition of being locally integrable, and these were discussed in general before. Singular distributions, on the other hand, are more delicate. They do not need to satisfy the local integrability condition because, in general, they are associated with non-differentiable functions. Among these singular distributions, the Dirac Delta distribution stands out, commonly called the Dirac Delta Function, often represented as an infinite pulse in the following way:

$$\delta(x) = \begin{cases} +\infty, & x = 0 \\ 0, & x \neq 0 \end{cases} \tag{2.8}$$

with the condition that the function is normalized, that is,

$$\int \delta(x)\, dx = 1 \tag{2.9}$$

As a distribution, the δ distribution can be represented as a linear functional in the space of test functions, and $\forall \phi \in \boldsymbol{D}$, we have:

$$\delta[\phi] = \int \delta(x)\, \phi(x)\, dx = \phi(0) \tag{2.10}$$

Since $\delta(x) = 0 \quad \forall x \neq 0$ and the integral of δ over the entire space is equal to 1, the result of equation (2.10) is in some cases treated as a property of the delta, where it acts as a sort of filter, selecting the value of $f(x)$ at $x = 0$. This property can also be viewed as a particularly useful notation(OLIVEIRA, 2016) for the right-hand side of equation (2.10). However, we will keep using expression (2.10) as the standard definition of the Dirac Delta distribution.

We can generalize this property[1] to any point $a \in supp(\phi)$ in the following way: Consider the δ function shifted from its origin, that is, $\delta(x - a)$, and perform the variable change $x - a = \zeta$:

$$\int \delta(x - a)\, \phi(x)\, dx = \int \delta(\zeta)\, \phi(\zeta + a)\, d\zeta = \phi(\zeta + a) \tag{2.11}$$

If $\zeta = 0 \rightarrow x = a$, then

$$\int \delta(x - a)\, \phi(x)\, dx = \phi(a) \tag{2.12}$$

Another very important property is the scaling property:

[1] See the reference (BUTKOV, 1968).

$$\delta(ax) = \frac{\delta(x)}{|a|} \qquad a \neq 0 \tag{2.13}$$

this can be easily checked by taking $\zeta = ax$ and integrating over the entire space.

In n dimensions, the normalization condition (2.9) must be respected. Therefore, if $\boldsymbol{x} = \big(x_1, x_2, \ldots, x_n\big)$ are Cartesian coordinates, the delta function is given by

$$\delta^n(\boldsymbol{x}) = \delta(x_1)\,\delta(x_2)\cdots\delta(x_n) \tag{2.14}$$

and by Fubini's Theorem, we guarantee the normalization condition (2.9).

In generalized coordinates, let $\boldsymbol{x} = (x_1, x_2, \ldots, x_n)$ be Cartesian coordinates and $\boldsymbol{\xi} = (\xi_1, \xi_2, \ldots, \xi_n)$ be generalized coordinates related by

$$\begin{aligned} x_1 &= x_1(\xi_1, \xi_2, \ldots, \xi_n) \\ x_2 &= x_2(\xi_1, \xi_2, \ldots, \xi_n) \\ &\vdots \\ x_n &= x_n(\xi_1, \xi_2, \ldots, \xi_n) \end{aligned}$$

let the determinant of the Jacobian matrix be

$$\boldsymbol{J} = \begin{vmatrix} \frac{\partial x_1}{\partial \xi_1} & \cdots & \frac{\partial x_1}{\partial \xi_n} \\ \vdots & \ddots & \vdots \\ \frac{\partial x_n}{\partial \xi_1} & \cdots & \frac{\partial x_n}{\partial \xi_n} \end{vmatrix} \tag{2.15}$$

if $\boldsymbol{x_0}$ is a point in Cartesian coordinates in $\mathbb{R}^n$ and $\boldsymbol{\xi_0}$ is the same point in generalized coordinates, the δ function defined in terms of the generalized coordinates is given by:

$$\delta(\boldsymbol{x} - \boldsymbol{x_0}) = \frac{1}{|\boldsymbol{J}|}\,\delta(\boldsymbol{\xi} - \boldsymbol{\xi_0}) \tag{2.16}$$

according to (2.14), we can rewrite (2.16) as:

$$\prod_{i=1}^{n} \delta\big(x_i - x_{0_i}\big) = \frac{1}{|\boldsymbol{J}|} \prod_{i=1}^{n} \delta\big(\xi_i - \xi_{0_i}\big) \tag{2.17}$$

The absolute value of the determinant of the Jacobian matrix in the denominator is necessary because we must respect the normalization condition (2.9). When we change the coordinate system, the differentials in the multiple integral are adjusted through the scale factors of the chosen metric.

2.1.3 Convolution

The study of Convolution is quite extensive and goes beyond the scope of this work. Here, our focus will be to define the convolution between a distribution and a function ψ.

Let f, g be differentiable functions in $\mathbb{R}^n$. The convolution operation $(g * f)$ is given by:

$$(g * f)(\boldsymbol{x}) = \int f(\boldsymbol{y})\, g(\boldsymbol{x} - \boldsymbol{y})\, d\boldsymbol{y} \tag{2.18}$$

since they are differentiable, it also holds that

$$(g * f)' = g' * f = f * g' \tag{2.19}$$

Definition 2. *Let $F \in \boldsymbol{D}'$ and $\psi \in \boldsymbol{D}(\mathbb{R}^n)$. Following (PéREZ, 2015), we define a convolution between a distribution F and a function ψ as:*

$$\langle F * \psi, \phi \rangle = \langle F, \tilde{\psi} * \phi \rangle \qquad \forall \phi \in \boldsymbol{D}(\mathbb{R}^n) \tag{2.20}$$

where $\tilde{\psi}$ is the transpose[2] of ψ:

$$\tilde{\psi}(-\boldsymbol{y}) = \psi(\boldsymbol{y}) \tag{2.21}$$

Example 2.1.1. *The most important example of the convolution of a distribution is the convolution involving the distribution δ. Thus, with $\psi, \phi \in \mathbb{S}(\mathbb{R}^n)$, we have:*

$$\langle \delta * \psi, \phi \rangle = \langle \delta, \tilde{\psi} * \phi \rangle = (\tilde{\psi} * \phi)(0) = \int \tilde{\psi}(-\boldsymbol{y})\, \phi(\boldsymbol{y})\, d\boldsymbol{y} = \int \psi(\boldsymbol{y})\, \phi(\boldsymbol{y})\, d\boldsymbol{y} = \langle \psi, \phi \rangle \tag{2.22}$$

in other words, the distribution δ is the identity element of the convolution operation.

$$\delta * \psi = \psi, \qquad \forall \psi \in \mathbb{S}(\mathbb{R}^n) \tag{2.23}$$

.

2.2 The Green's function as a Fundamental Solution of Differential Operators

Let $\mathbb{L}$ be a linear operator of order m in the form

[2] The reason for the name "transpose" is that this flipping is the adjoint/transpose operation when you move the convolution kernel from one slot of the pairing to the other (it plays the role of the transpose of an integral kernel). It is not the matrix transpose. For more details, see (HÖRMANDER, 2015), chapter 4.

$$\mathbb{L}(\boldsymbol{x}, \partial) = \sum_{|\alpha|=0}^{m} a_\alpha(\boldsymbol{x})\, \partial^\alpha \tag{2.24}$$

applied to a distribution $u(\boldsymbol{x})$. We define the non-homogeneous differential equation

$$\mathbb{L}(\boldsymbol{x}, \partial)\, u(\boldsymbol{x}) = f \tag{2.25}$$

where $f, u \in \boldsymbol{D}'$ and the coefficients $a_\alpha(\boldsymbol{x})$ belong to $\boldsymbol{D}(\mathbb{R}^n)$.

In the particular case where these coefficients are constants, we can simplify the notation and write

$$\mathbb{L}(\partial)\, u(\boldsymbol{x}) = f. \tag{2.26}$$

Definition 3. *Let $\mathbb{L}(\partial)$ be a differential operator with constant coefficients. We say that a distribution G is a fundamental solution if*

$$\mathbb{L}(\partial)\, G = \delta, \tag{2.27}$$

where $G \in \boldsymbol{D}'$.

The link between studying distributions and studying fundamental solutions will be based on convolution, using the concepts mentioned earlier.

Theorem 2.2.1. *Let $\mathbb{L}(\partial)$ be a differential operator with constant coefficients, and let G be a fundamental solution of that operator. Let $f \in \boldsymbol{D}(\mathbb{R}^n)$ be a test function. The solution of the equation*

$$\mathbb{L}(\partial)\, u = f \tag{2.28}$$

is given by

$$u = G * f. \tag{2.29}$$

Demonstração. Suppose u is a solution of the differential operator. Then

$$\mathbb{L}(\partial)\, \Big(G * f\Big) = f. \tag{2.30}$$

by the rule for differentiating convolutions, we have

$$\mathbb{L}(\partial)\, \Big(G * f\Big) = \Big(\mathbb{L}(\partial)\, G\Big) * f. \tag{2.31}$$

since $\mathbb{L}(\partial)\, G = \delta$ by definition and δ is the identity element of convolution, it follows that

$$\Big(\mathbb{L}(\partial)\, G\Big) * f = \delta * f = f. \tag{2.32}$$

and because $\mathbb{L}(\partial)\, G = \delta$ is a solution, $G * f$ is also a solution, thus yielding the desired result. ■

As a consequence, we can say u is indeed a solution related to the fundamental solution G. Since u is, in the sense of distributions, a convolution, we can also write (BARATA, 2020):

$$u(\boldsymbol{x}) = \int G(\boldsymbol{x} - \boldsymbol{y})\, f(\boldsymbol{y})\, d\boldsymbol{y} \tag{2.33}$$

as the solution of the differential equation. It is important to note that the operator $\mathbb{L}$ does not need to have constant coefficients and can be generalized (BARATA, 2020). The notation

$$u(\boldsymbol{x}) = \int G(\boldsymbol{x} \mid \boldsymbol{y})\, f(\boldsymbol{y})\, d\boldsymbol{y} \tag{2.34}$$

is often used for clearer interpretation.

In many problems, one needs the solution of $\mathbb{L}(\partial)(u) = f$ to satisfy certain boundary conditions (Dirichlet, Neumann, or mixed) on the boundary of an open domain $\Omega \subset \mathbb{R}^n$. Fundamental solutions that lead to such solutions are called Green's Functions. We chose the letter G for the fundamental solution precisely to introduce the concept of Green's Functions.

Green's Functions are important because they depend on the differential operator and the chosen boundary conditions, but not on the function f. Physically, the Green's function holds all the essential information of a physical system described by a function u under the boundary conditions, when a stimulus f is applied. An illustrative example for understanding this result is the case of a stretched string with a point force f applied (BUTKOV, 1968).

Example 2.2.1. *Consider a stretched string of length L, initially at rest, with a point force per unit length $f(x)$ acting on it. The displacement $u(x)$ of the string satisfies the differential equation*[3]*:*

$$T\frac{d^2u(x)}{dx^2} = F(x) \qquad \frac{d^2u(x)}{dx^2} = \frac{F(x)}{T} = f(x) \tag{2.35}$$

Subject to the boundary conditions $u(0) = u(L) = 0$.

If the applied force F_0 is concentrated at a point $x = \xi$, it is reasonable from a physical perspective that $f(x)$ is given by:

$$f(x) = \frac{F_0}{T}\,\delta(x - \xi) \tag{2.36}$$

By definition (3), we can rewrite the differential equation, except for a constant, as

[3] This differential equation can be seen as the one-dimensional Laplace equation.

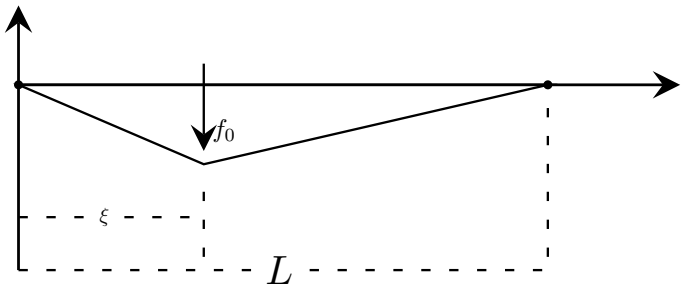

Figure 3 – Stretched string with force applied at $x = \xi$.

$$\frac{d^2G(x,\xi)}{dx^2} = \delta(x-\xi), \tag{2.37}$$

where, according to the development of Green Functions, $G(x|\xi)$ is the *Green's function* of our physical problem, since we have Dirichlet boundary conditions. Furthermore, the boundary conditions applied to $G(x|\xi)$ are:

$$G(0,\xi) = G(L,\xi) = 0. \tag{2.38}$$

Notice that, initially, at $x = \xi$ we have an indeterminacy, due to the nature of the Dirac delta distribution. Therefore, the solution of our differential equation for G must be written in a way that lets us handle this indeterminacy, so we define:

$$\begin{aligned} G(x,\xi) &= Ax + B \qquad 0 \leq x < \xi, \\ G(x,\xi) &= A'x + B' \qquad \xi < x \leq L. \end{aligned} \tag{2.39}$$

by applying the boundary conditions, we find $B = 0$ and $B' = -A'L$. Thus, the solution becomes:

$$\begin{aligned} G(x,\xi) &= Ax, \qquad 0 \leq x < \xi, \\ G(x,\xi) &= A'(x-L), \qquad \xi < x \leq L. \end{aligned} \tag{2.40}$$

To determine the constants A and A', we impose the condition that, despite the nature of the delta distribution δ, the solution must be continuous at $x = \xi$. More formally, we require continuity of the solution for $\xi - \epsilon$ and $\xi + \epsilon$, where ϵ can be chosen arbitrarily small. Since this is a physical problem of a stretched string, the point $x = \xi$ must exist. Therefore, at $x = \xi$:

$$A\xi = A'(\xi - L). \tag{2.41}$$

from this, we can write A' in terms of A:

$$A' = \frac{A\,\xi}{(\xi - L)}. \tag{2.42}$$

hence, our solution becomes:

$$\begin{aligned} G(x,\xi) &= Ax, \qquad 0 \le x < \xi, \\ G(x,\xi) &= \frac{A\,\xi}{(\xi - L)}\Big(x - L\Big), \qquad \xi < x \le L. \end{aligned} \tag{2.43}$$

consequently, the partial derivatives with respect to x must exist:

$$\begin{aligned} \frac{\partial G(x,\xi)}{\partial x} &= A, \qquad 0 \le x < \xi, \\ \frac{\partial G(x,\xi)}{\partial x} &= \frac{A\,\xi}{(\xi - L)}, \qquad \xi < x \le L. \end{aligned} \tag{2.44}$$

we can use this information to determine the constant A. We just integrate equation (2.37) with respect to x over the interval $\xi - \epsilon$ to $\xi + \epsilon$ and let $\epsilon \to 0$. Therefore:

$$\frac{\partial G(\xi + \epsilon, \xi)}{\partial x} - \frac{\partial G(\xi - \epsilon, \xi)}{\partial x} = 1. \tag{2.45}$$

substituting the expressions found for the partial derivatives, we get:

$$\frac{A\,\xi}{(\xi - L)} - A = 1, \tag{2.46}$$

$$A = \frac{\xi - L}{L}. \tag{2.47}$$

finally, we write our Green's function $G(x|\xi)$ as follows:

$$\begin{cases} G(x|\xi) = -\dfrac{x\,(L - \xi)}{L}, & 0 \le x < \xi, \\ G(x|\xi) = -\dfrac{\xi\,(L - x)}{L}, & \xi < x \le L. \end{cases} \tag{2.48}$$

according to Theorem (2.2.1), the solution $u(x)$ is given by:

$$u(x) = \int_0^L G(x|\xi)\, f(\xi)\, d\xi. \tag{2.49}$$

Naturally, as the differential operator changes, finding the Green functions becomes harder. An illustrative example for a more general and physically important differential operator is the Sturm-Liouville operator.

Example 2.2.2. *The Sturm-Liouville operator is relevant in many physical problems. It provides an intuitive introduction to the search for eigenvalues and eigenfunctions and has several applications.*

Consider the non-homogeneous differential equation:

$$\frac{d}{dx}\Big[p(x)\,\frac{dy}{dx}\Big] + s(x)\,y = -f(x), \qquad a \le x \le b \tag{2.50}$$

subject to the boundary conditions:

$$\alpha_1\,y(a) + \alpha_2\,y'(a) = 0, \qquad \beta_1\,y(b) + \beta_2\,y'(b) = 0, \tag{2.51}$$

where $p(x)$ and $s(x)$ must be analytic for $a \le x \le b$. If $s(x)$ is of the form $s(x) = q(x) + \lambda\,r(x)$, the differential equation becomes a Sturm-Liouville equation:

$$\frac{d}{dx}\Big[p(x)\,\frac{dy}{dx}\Big] + \Big(q(x) + \lambda\,r(x)\Big)\,y = -f(x), \qquad a \le x \le b, \tag{2.52}$$

where λ is called the eigenvalue of the differential operator. In this sense, finding values of λ for which (2.52) has a nontrivial solution under the given boundary conditions is equivalent to solving both $\mathbb{L}(y) = f$ and $\Big(\mathbb{L} + \lambda r\Big)y = f$.

To find the Green's function for the Sturm-Liouville operator, following the approach of Definition (3), we have:

$$\frac{d}{dx}\Big[p(x)\,\frac{dG(x|\xi)}{dx}\Big] + \Big(q(x) + \lambda\,r(x)\Big)\,G(x|\xi) = \delta(x-\xi). \tag{2.53}$$

Similar to the example in the previous section, we require the Green's function $G(x|\xi)$ to satisfy certain conditions for its existence:

- G must satisfy the homogeneous equation except at $x = \xi$.
- G must satisfy the imposed boundary conditions.
- G must be continuous at $x = \xi$.
- $\dfrac{dG}{dx}$ must have a jump discontinuity at $x = \xi$.

The last condition assumes that integrating over the limits $\xi - \epsilon$ to $\xi + \epsilon$ yields a finite value as $\epsilon \to 0$. Indeed, integrating in x over these limits, we have:

$$p(x)\,\frac{dG(x|\xi)}{dx}\bigg|_{\xi-\epsilon}^{\xi+\epsilon} + \int_{\xi-\epsilon}^{\xi+\epsilon} s(x)\,G(x|\xi)\,dx = 1. \tag{2.54}$$

since $s(x)$ and $G(x|\xi)$ are both continuous at $x = \xi$, that integral is zero. Therefore,

$$\lim_{x\to\xi} p(x)\left[\frac{dG(\xi+\epsilon|\xi)}{dx} - \frac{dG(\xi-\epsilon|\xi)}{dx}\right] = 1. \tag{2.55}$$

assume that the differential equation (2.52) has two nontrivial solutions $y_1(x)$ and $y_2(x)$. In the region $a \leq x < \xi$, the solution is $y_1(x)$. Since $G(x|\xi)$ and $y_1(x)$ satisfy the same differential equation (the homogeneous one)(DUFFY, 2015), the same boundary conditions hold:

$$\alpha_1 y_1(a) + \alpha_2 y_1'(a) = 0,$$
$$\alpha_1 G(a|\xi) + \alpha_2 G'(a|\xi) = 0.$$

Note that α_1 and α_2 must not make the solution trivial. Therefore, the Wronskian[4] of (y_1, G) must be zero at $x = a$. Because $y_1(x)$ and $G(x|\xi)$ satisfy the same homogeneous differential equation, the same relationship holds in the region considered. That is,

$$G(x|\xi) = C_1 y_1(x), \qquad a \leq x < \xi. \tag{2.57}$$

similarly, using the boundary conditions at $x = b$ and taking $y_2(x)$ in the interval $\xi < x \leq b$, we have:

$$G(x|\xi) = C_2 y_2(x), \qquad \xi < x \leq b. \tag{2.58}$$

enforcing continuity of G, y_1, and y_2 at $x = \xi$, and the fact that G' has a jump discontinuity at $x = \xi$, we obtain (DUFFY, 2015):

$$C_1\, y_1(\xi) - C_2\, y_2(\xi) = 0, \qquad C_1\, y_1'(\xi) - C_2\, y_2'(\xi) = \frac{1}{p(\xi)}. \tag{2.59}$$

This system of equations has a unique solution (BUTKOV, 1968):

$$C_1 = \frac{y_2(\xi)}{p(\xi)\, W(\xi)}, \qquad C_2 = \frac{y_1(\xi)}{p(\xi)\, W(\xi)}, \tag{2.60}$$

where $W(\xi)$ is the Wronskian of $\Big(y_1(\xi), y_2(\xi)\Big)$. Hence, the Green's function is given by:

[4] The Wronskian of (y_1, y_2) is defined as:

$$W(y_1, y_2) = \begin{vmatrix} y_1(x) & y_2(x) \\ y_1'(x) & y_2'(x) \end{vmatrix} = y_1 y_2' - y_2 y_1'. \tag{2.56}$$

$$\begin{cases} G(x|\xi) = \dfrac{y_1(x)\, y_2(\xi)}{p(\xi)\, W(\xi)}, & a \leq x < \xi, \\ G(x|\xi) = \dfrac{y_2(x)\, y_1(\xi)}{p(\xi)\, W(\xi)}, & \xi < x \leq b. \end{cases} \tag{2.61}$$

Clearly, $W(\xi) \neq 0$. Since this holds for the entire interval $a \leq x \leq b$, we say $W(y_1, y_2) \neq 0$. Thus, $y_1(x)$ and $y_2(x)$ must be linearly independent. On the other hand, if the associated homogeneous differential equation has only one nontrivial solution, it follows that y_1 and y_2 are linearly dependent (DUFFY, 2015). If the differential equation is of the form

$$\Big(\mathbb{L} + \lambda r\Big)\, y = f, \tag{2.62}$$

where λ is the eigenvalue of the associated homogeneous equation, then if there are nontrivial solutions of

$$\Big(\mathbb{L} + \lambda r\Big)\, y = 0, \tag{2.63}$$

and such a solution is called y_0, y_1 and y_2 will be multiples of y_0 and thus linearly dependent. In that case, the Green's function does not exist.[5]

Therefore, according to Theorem (2.2.1), the solution of our differential equation is

$$y(x) = \int_a^b G(x|\xi)\, f(\xi)\, d\xi. \tag{2.64}$$

2.3 Eigenfunction Series Expansion of Green's function

In the case where the associated homogeneous differential equation is separable in the chosen coordinate system, the most common and widely used method for constructing the Green's function is the eigenfunction series expansion method. To illustrate this method, consider the one-dimensional differential equation

$$\mathbb{L}y(x) = f(x), \qquad a \leq x \leq b \tag{2.65}$$

where $\mathbb{L}$ is the Sturm-Liouville differential operator, and $f(x)$ is analytic for $x \in [a, b]$. For boundary conditions, consider homogeneous Dirichlet conditions such that

$$\mathcal{B}y(a) = \mathcal{B}y(b) = 0 \tag{2.66}$$

[5] This idea is analogous to the case of linear systems of equations. For the non-homogeneous equation $\boldsymbol{A}y = f$, where y and f are both column vectors, a nontrivial solution exists only if $\boldsymbol{A}^{-1}$ exists. If $\boldsymbol{A}^{-1}$ does not exist, then the homogeneous equation $\boldsymbol{A}y = 0$ has a nontrivial solution.

where $\mathcal{B}$ is an operator that generalizes the boundary condition (2.66).

According to the development, our Green's function $G(x|\xi)$ must satisfy:

$$\mathbb{L}G = \delta(x-\xi), \qquad \mathcal{B}G = 0 \tag{2.67}$$

The functions used in the series expansion must be eigenfunctions of the operator $\mathbb{L}$ with respect to its eigenvalues. Due to (2.63), the eigenfunctions $\varphi_n(x)$ must satisfy:

$$\mathbb{L}\varphi_n(x) = (\lambda - \lambda_n)r(x)\varphi_n(x), \qquad \mathcal{B}\varphi_n = 0 \tag{2.68}$$

If the set φ_n is complete, we ensure that the expansion in terms of φ_n remains within the space of our function $y(x)$, and therefore, the series expansion will satisfy the boundary conditions. Hence, if $G(x|\xi)$ exists, it can be represented as

$$G(x|\xi) = \sum_{n=1}^{\infty} \gamma_n(\xi)\varphi_n(x) \tag{2.69}$$

and applying the operator $\mathbb{L}$, we obtain:

$$G(x|\xi) = \sum_{n=1}^{\infty} \gamma_n(\xi)\mathbb{L}\varphi_n(x) = \sum_{n=1}^{\infty} \gamma_n(\xi)(\lambda - \lambda_n)r(x)\varphi_n(x) \tag{2.70}$$

but according to (2.67), we have:

$$\sum_{n=1}^{\infty} \gamma_n(\xi)(\lambda - \lambda_n)r(x)\varphi_n(x) = \delta(x-\xi) \tag{2.71}$$

since in this case the set $\varphi_n(x)$ is complete and we ensure the expansion in terms of $\varphi_n(x)$ is contained in our space, it is finite within this space[6]. Multiplying both sides by φ_m and integrating with respect to the variable x over the entire space of our solution, we can interchange the sum and the integral, obtaining:

$$\sum_{n=1}^{\infty} \gamma_n(\xi)(\lambda - \lambda_n) \int_a^b r(x)\varphi_m(x)\varphi_n(x)dx = \varphi_m(\xi) \tag{2.72}$$

If φ_m and φ_n are orthonormal functions of the space associated with the differential operator, the term inside the integral satisfies the orthonormality condition

$$\int_a^b r(x)\varphi_m(x)\varphi_n(x) = \delta_{n,m} \tag{2.73}$$

where $\delta_{n,m}$ is a Kronecker delta. Such a condition is necessary to find a solution in terms of eigenfunctions φ (DUFFY, 2015). Thus, the eigenfunction series expansion assumes the form

[6] It is therefore implicitly understood that $\varphi_n(x) \geq 0$ for all n.

$$G(x|\xi) = \sum_{n=1}^{\infty} \frac{\varphi_n(\xi)\varphi_n(x)}{\lambda - \lambda_n} \tag{2.74}$$

where $\gamma_n(\xi) = \dfrac{\varphi_n(\xi)}{\lambda - \lambda_n}$. Equation (2.74) is called the bilinear (or spectral) expansion of the Green's function and can naturally be extended to more than one variable, provided the separability conditions of the differential operator and the orthonormality of the eigenfunctions associated with the given space are satisfied.

2.4 Green's function for the Helmholtz Equation in 3-dimensions

The Helmholtz differential equation plays a crucial role in quantum mechanics due to its connection with the time-independent Schrödinger equation for the free particle, governing the behavior of non-relativistic quantum systems. Specifically, the Helmholtz equation arises when proposing the use of the separation of variables technique to solve the wave equation, splitting its solution into spatial and temporal parts. This nature will be better explored in the next chapter, however, formalizing its solution is necessary. The Helmholtz differential operator applied to the Green's function is given by the equation

$$(\nabla^2 + k^2)G(\boldsymbol{r}|\boldsymbol{r'}) = \delta(\boldsymbol{r} - \boldsymbol{r'}) \tag{2.75}$$

Taking the Fourier transform on both sides, we expand the equation to

$$\begin{aligned} (k^2 - s^2)\frac{1}{(2\pi)^3}\int_{-\infty}^{\infty} G(\boldsymbol{r}|\boldsymbol{r'})e^{-i\boldsymbol{s}\cdot\boldsymbol{r}}d\boldsymbol{r} &= \frac{1}{(2\pi)^3}\int_{-\infty}^{\infty}\delta(\boldsymbol{r} - \boldsymbol{r'})e^{-i\boldsymbol{s}\cdot\boldsymbol{r}}d\boldsymbol{r} \\ \tilde{G}(\boldsymbol{s}|\boldsymbol{r'}) &= \frac{e^{-i\boldsymbol{s}\cdot\boldsymbol{r'}}}{k^2 - s^2} \end{aligned} \tag{2.76}$$

where $\tilde{G}$ represents the transformed Green's function. Taking the inverse transform, we find the integral

$$G(\boldsymbol{r}|\boldsymbol{r'}) = \frac{1}{(2\pi)^3}\int_{-\infty}^{\infty}\frac{e^{i\boldsymbol{s}\cdot(\boldsymbol{r}-\boldsymbol{r'})}}{k^2 - s^2}d\boldsymbol{s} \tag{2.77}$$

to be solved. Using Cauchy's integral formula and residue calculus (BUTKOV, 1968), the result of this integral leads to the Helmholtz Green's function (GRIFFITHS; SCHROETER, 2018), given by

$$G(\boldsymbol{r}|\boldsymbol{r'}) = -\frac{1}{4\pi}\frac{e^{ik|\boldsymbol{r}-\boldsymbol{r'}|}}{|\boldsymbol{r} - \boldsymbol{r'}|} \tag{2.78}$$

2.4.1 Separability Conditions

Another representation of the Green's function can be obtained by invoking the concept of an eigenfunction series expansion of the space. This, however, presupposes that the differential operator admits a separable solution in the chosen coordinate system and, moreover, that well-defined eigenfunctions of the operator exist within the space of our problem.

The work of Moon and Spencer(MOON; SPENCER, 1952) shows that, for an arbitrary orthogonal coordinate system (ξ_1, ξ_2, ξ_3) in three-dimensional space, the Helmholtz equation for

$$\psi(\xi_1, \xi_2, \xi_3) = \zeta_1(\xi_1)\zeta_2(\xi_2)\zeta_3(\xi_3) \tag{2.79}$$

assumes the form

$$\sum_{i=1}^{3} \frac{1}{\zeta_i} \frac{\partial}{\partial \xi_i} \left[\frac{\sqrt{\det \boldsymbol{g}}}{g_{ii}} \frac{\partial \zeta}{\partial \xi_i} \right] + k^2 \sqrt{\det \boldsymbol{g}} = 0, \tag{2.80}$$

where $\boldsymbol{g}$ is the metric tensor, which, under an orthogonal coordinate system, satisfies $g_{ij} = 0$ for $i \neq j$. Moon and Spencer further demonstrate that the separability conditions are fulfilled if the term $\frac{\sqrt{\det \boldsymbol{g}}}{g_{ii}}$ can be expressed as a product of the form

$$\frac{\sqrt{\det g}}{g_{ii}} = f_i(\xi_i)\, F_i(\xi_j, \xi_k), \qquad j, k \neq i. \tag{2.81}$$

To guarantee this separation, the auxiliary function Φ_{ij} is defined by

$$\Phi_{ij}(\xi_i) = -\frac{1}{f_i} \frac{\partial}{\partial \alpha_j} \left(\frac{1}{\zeta_i} \frac{d}{d\xi_i} \left(f_i \frac{d\zeta_i}{d\xi_i} \right) \right), \tag{2.82}$$

which leads to the linear system

$$\begin{aligned} f_1 F_1 \Phi_{11}(\xi_1) + f_2 F_2 \Phi_{21}(\xi_2) + f_3 F_3 \Phi_{31}(\xi_3) &= \sqrt{\det g}, \\ f_1 F_1 \Phi_{12}(\xi_1) + f_2 F_2 \Phi_{22}(\xi_2) + f_3 F_3 \Phi_{32}(\xi_3) &= 0, \\ f_1 F_1 \Phi_{13}(\xi_1) + f_2 F_2 \Phi_{23}(\xi_2) + f_3 F_3 \Phi_{33}(\xi_3) &= 0. \end{aligned} \tag{2.83}$$

A necessary condition for a non-trivial solution of this system is that the Stäckel determinant(MORSE; FESHBACH, 1946)

$$S = \begin{vmatrix} \Phi_{11} & \Phi_{12} & \Phi_{13} \\ \Phi_{21} & \Phi_{22} & \Phi_{23} \\ \Phi_{31} & \Phi_{32} & \Phi_{33} \end{vmatrix}, \tag{2.84}$$

be non-zero ($S \neq 0$). The solutions are then expressed through the cofactors M_{i1} of Φ_{i1} in the Stäckel determinant, giving rise to two other important separability conditions. First, we need that the metric tensor can be directly related to the cofactors M_{i1} via

$$g_{ii} = \frac{S}{M_{i1}}. \tag{2.85}$$

The second one is the multiplicative relation for the determinant of the metric tensor

$$\frac{\sqrt{\det g}}{S} = \prod_{i=1}^{3} f_i(\xi_i). \tag{2.86}$$

With these conditions, the separated Helmholtz equation is cast into three independent ordinary differential equations, one for each variable ξ_i:

$$\frac{1}{g_{ii} f_i \zeta_i} \frac{d}{d\xi_i}\left(f_i \frac{d\zeta_i}{d\xi_i}\right) + \sum_{j=1}^{3} \alpha_j \frac{\Phi_{ij}}{g_{ii}} = 0, \tag{2.87}$$

where the constants α_j are obtained from the boundary conditions of the physical problem. Combining these equations returns the original Helmholtz equation in separated form:

$$\sum_{n=1}^{3} \frac{M_n}{S f_n} \frac{\partial}{\partial \xi_n}\left(f_n \frac{\partial \psi}{\partial \xi_n}\right) + k^2 \psi = 0. \tag{2.88}$$

Once the separability condition for the differential operator is satisfied, the second requirement for constructing a bilinear expansion of the Green's function is the existence of a complete set of eigenfunctions of the space. Assume that the coordinates employed to seek the system's eigenfunctions are ξ_2 and ξ_3, associated with k_2 and k_3. In this case, we have the eigenfunctions $\zeta_{2,m}$ and $\zeta_{3,n}$. To simplify the notation we denote every product $\zeta_{2,m}\zeta_{3,n}$ using indices p, q to map the tuple (n, m). In this system, the separability condition(AZADO; MAIOLI; SCHMIDT, 2021) reads

$$\int\int U_q(\xi_2, \xi_3)\, U_p(\xi_2, \xi_3)\, \rho(\xi_2, \xi_3)\, d\xi_2\, d\xi_3 = \delta_{p,q}, \tag{2.89}$$

where $\rho(\xi_2, \xi_3)$ is a weight function obtained from the Jacobian of the coordinate system. Assuming this is the case, the Green's function can be expanded as

$$G_k(\mathbf{r}|\mathbf{r}') = \sum_q X_{1q}(\xi_1|\xi_1')\, B_q(\xi_2', \xi_3')\, U_q(\xi_2, \xi_3). \tag{2.90}$$

Here X_{1q} and B_q are functions to be determined. Substituting this expansion into the differential equation that defines the Green's function,

$$\sum_{n=1}^{3} \frac{M_n}{S f_n} \frac{\partial}{\partial \xi_n}\left(f_n \frac{\partial G}{\partial \xi_n}\right) + k^2 G = -\frac{4\pi\, \delta(\xi_1 - \xi_1')\, \delta(\xi_2 - \xi_2')\, \delta(\xi_3 - \xi_3')}{h_1 h_2 h_3}, \tag{2.91}$$

and using the properties of the eigenfunctions U_q, the three-dimensional problem reduces to a one-dimensional differential equation for X_{1q}:

$$\frac{1}{f_1} \frac{d}{d\xi_1}\left(f_1 \frac{dX_{1q}}{d\xi_1}\right) + X_{1q} \sum_{m=1}^{3} \alpha_{mq} \Phi_{1m} = -\frac{4\pi\, \delta(\xi_1 - \xi_1')}{f_1}. \tag{2.92}$$

This equation corresponds to a Sturm–Liouville-type differential operator, discussed earlier. The general solution to the inhomogeneous equation is obtained via the independent functions y_{1q} and y_{2q}, solutions to the associated homogeneous equation

$$\frac{1}{f_1} \frac{d}{d\xi_1}\left(f_1 \frac{dy}{d\xi_1}\right) + y \sum_{m=1}^{3} \alpha_{mq} \Phi_{1m} = 0, \tag{2.93}$$

using the standard Wronskian method $W(y_{1q}, y_{2q})$:

$$X_{1q}(\xi_1|\xi_1') = -\frac{4\pi}{W(y_{1q}, y_{2q}) f_1(\xi_1')} \begin{cases} y_{1q}(\xi_1)\, y_{2q}(\xi_1'), & \xi_1 \leq \xi_1' \\ y_{1q}(\xi_1')\, y_{2q}(\xi_1), & \xi_1 \geq \xi_1' \end{cases}. \tag{2.94}$$

The function $B_q(\xi_2', \xi_3')$ is, in turn, found to be

$$B_q(\xi_2', \xi_3') = \frac{h_1}{h_2 h_3}\, \rho(\xi_2', \xi_3')\, U_q(\xi_2', \xi_3'). \tag{2.95}$$

Finally, inserting these results into the initial expansion yields the complete expression of the Green's function expanded in eigenfunctions:

$$\begin{aligned} G_k(\mathbf{r}|\mathbf{r}') = -4\pi \frac{h_1}{h_2 h_3}\, \rho(\xi_2', \xi_3') \sum_q U_q(\xi_2', \xi_3') U_q(\xi_2, \xi_3) \\ \times \frac{1}{W(y_{1q}, y_{2q})} \begin{cases} y_{1q}(\xi_1)\, y_{2q}(\xi_1'), & \xi_1 \leq \xi_1' \\ y_{1q}(\xi_1')\, y_{2q}(\xi_1), & \xi_1 \geq \xi_1' \end{cases} \end{aligned} \tag{2.96}$$

This general representation makes it straightforward to construct the Green's function to different coordinate systems, requiring only the specification of the orthogonal eigenfunction set U_q, the scale factors h_i, and the weight function $\rho(\xi_2, \xi_3)$.

2.4.2 Bilinear Expansion in Spherical Coordinates

In the case of spherical coordinates, the choice of the two coordinates ξ_2 and ξ_3 becomes evident, since we have two angles mapped onto a finite interval that also exhibit periodicity. In spherical coordinates we therefore map

$$\xi_1 = r, \quad \xi_2 = \theta, \quad \xi_3 = \phi, \tag{2.97}$$

with the well-known scale factors:

$$h_1 = 1, \quad h_2 = r, \quad h_3 = r \sin\theta. \tag{2.98}$$

The weight function associated with the Jacobian of the coordinate system, required for the orthonormality of the eigenfunctions, is given by

$$\rho(\theta, \phi) = \sin\theta. \tag{2.99}$$

In this context, the orthonormal eigenfunctions are the spherical harmonics $Y_{\ell,m}(\theta, \phi)$, which satisfy the familiar orthonormality relation(ARFKEN; WEBER, 1999):

$$\int_0^{2\pi} \int_0^{\pi} Y_{\ell,m}^*(\theta, \phi)\, Y_{\ell',m'}(\theta, \phi)\, \sin\theta\, d\theta\, d\phi = \delta_{\ell,\ell'} \delta_{m,m'}. \tag{2.100}$$

The homogeneous radial equation resulting from separation of the Helmholtz equation in this system takes the form of the Bessel differential equation:

$$\frac{1}{r^2}\frac{d}{dr}\left(r^2\frac{dy}{dr}\right)+\left(k^2-\frac{\ell(\ell+1)}{r^2}\right)y=0, \tag{2.101}$$

whose independent solutions are the spherical Bessel functions $j_\ell(kr)$ and the spherical Hankel functions of the first kind $h_\ell^{(1)}(kr)$.

The Wronskian associated with these solutions is

$$W\left[j_\ell(kr),h_\ell^{(1)}(kr)\right]=\frac{i}{kr^2}. \tag{2.102}$$

Consequently, the general expression for the Green's function obtained previously in an arbitrary coordinate system particularises to the well-known representation in spherical coordinates:

$$G_k(\mathbf{r}|\mathbf{r}')=-ik\sum_{\ell=0}^{\infty}\sum_{m=-\ell}^{\ell}j_\ell(kr_<)\,h_\ell^{(1)}(kr_>)\,Y_{\ell,m}^*(\theta',\phi')\,Y_{\ell,m}(\theta,\phi), \tag{2.103}$$

where the standard notation $r_< = \min(r,r')$ and $r_> = \max(r,r')$ is used. Expression (2.103) is the required form that will be employed in this work.

3 Scattering Theory

3.1 Fundamental Concepts

Scattering problems can, in principle, be formulated for macroscopic objects—for example, the separation of two billiard balls (rigid spheres) after their collision—or even for astronomical bodies. In such cases, however, there are more direct ways of obtaining information about the system. Therefore, scattering theory finds its richest application at atomic and sub-atomic scales, where the dynamics obey the laws of quantum mechanics. Many concepts introduced in this domain, such as the differential cross section, already appear in classical mechanics, which makes it an ideal starting point for introductory studies of this theory.(TAYLOR, 2004) Below, we present a brief review of scattering in classical mechanics.

Every scattering experiment begins with a projectile that, from a great distance (incident asymptotic regime), approaches the target practically free of external forces and thus possesses essentially kinetic energy.(TAYLOR, 2004) Upon entering the interaction region—which rarely exceeds a few atomic diameters—the projectile is deflected, and its trajectory obeys Newton's equations of motion. Comparing the states of the projectile before and after this brief interaction already provides relevant information about the system.

To characterize the trajectory, consider the projectile advancing in a straight line toward the target. A line parallel to this trajectory is drawn through the center of the target, and the impact parameter s is defined as the distance between the two lines. This parameter quantifies how close the projectile passes to the target and, consequently, the intensity of the deflection.[1] After the collision, the projectile emerges asymptotically with a new direction that forms the scattering angle with respect to the incident trajectory, as shown in Figure 4.

From a general perspective, instead of dealing with a single projectile, we can imagine a large number of projectiles—a beam—being launched toward a scattering center, which will produce the scattering of this beam. Since the beam will consist of projectiles whose impact parameters, although sufficiently close, are different, it is natural to consider the scattering direction as a solid angle and to monitor the number of projectiles in the beam scattered within this solid angle. Following this reasoning and considering the number of scattered projectiles per unit time (or flux), we define the differential cross

[1] In quantum mechanics, Heisenberg's uncertainty principle prevents the direct determination of the impact parameter.

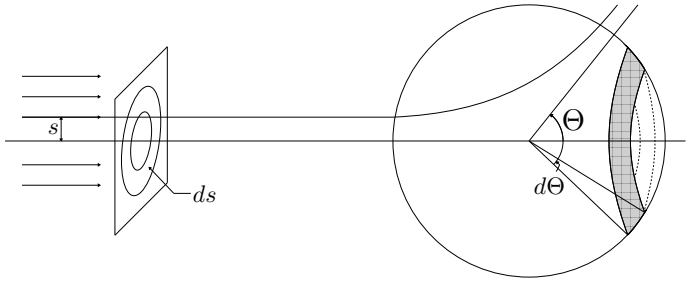

Figure 4 – Illustration of the scattering process in classical mechanics, of the impact parameter and the scattering angle. In this figure, the projectile moves from left to right with impact parameter s as a free particle and is scattered by an angle Θ by a force center.

section:

$$\sigma(\Omega)d\Omega = \frac{d\sigma}{d\Omega} = \frac{\text{Number of particles scattered per unit time}}{\text{Incident particle flux}} \tag{3.1}$$

In general, the differential cross section also depends on the angle around the axial axis relative to the particle trajectory, i.e., $\sigma(\Omega) = \sigma(\Theta, \phi)$. However, if the target possesses spherical symmetry or exerts a force field with spherical symmetry, the scattering will have axial symmetry, as in the case of Rutherford scattering.(E., 1911)

We also define the total scattering cross section(JOSE; SALETAN, 1998) by integrating $\sigma(\Omega)$ over all solid angles $d\Omega$:

$$\sigma_{tot} = \int \sigma(\Omega)d\Omega \tag{3.2}$$

although less frequently used, the total scattering cross section also reveals important characteristics about the dynamical system in question.

3.2 Quantum Scattering and the Lippmann-Schwinger Equation

The quantum description of scattering processes, is based on the characterization of the state $|\Psi\rangle$, which obeys the time-dependent Schrödinger equation:

$$i\hbar\frac{\partial}{\partial t}|\Psi\rangle = H|\Psi\rangle \tag{3.3}$$

In general, the full Hamiltonian H is expressed as

$$H = H_0 + V\,. \tag{3.4}$$

Throughout this work we consider a time-independent potential, so we later set $V = V(\boldsymbol{r})$. The operator H_0 represents the kinetic-energy operator whose eigenvalues are

$$E_{\boldsymbol{k}} = \frac{\hbar^2\boldsymbol{k}^2}{2m}\,, \tag{3.5}$$

where the values $E_{\boldsymbol{k}}$ are known; therefore an initial state of H_0, denoted $|i\rangle$—which intuitively represents the incident wave-function in the scattering problem—is completely known. Once $V \neq 0$ in (3.4), transitions to other states $|n\rangle$ occur as (3.4) evolves in time. In our problem we imagine the particle experiencing the potential V only in its immediate vicinity, i.e., the incident particle interacts with the potential and is then scattered as $r \to \infty$.

From the postulates of quantum mechanics(COHEN-TANNOUDJI; DIU; LALOE, 1986), we know that an eigenstate $|\alpha\rangle$ evolves in time through a time-evolution operator:

$$\begin{aligned} |\alpha\rangle_t &= e^{iH_0(t-t_0)/\hbar}|\alpha\rangle \\ &= U(t,t_0)|\alpha\rangle\,. \end{aligned} \tag{3.6}$$

Our strategy is to examine the time-evolution operator $U(t,t_0)$ in its interaction representation, $U_I(t,t_0)$, since the particle interacts with the potential only during a short interval and subsequently propagates freely. This viewpoint simplifies the development of the tools we employ, given that our potential is time independent.

The time-evolution operator in the interaction picture is defined as(SAKURAI; NAPOLITANO, 2017)

$$U_I(t,t_0) = e^{iH_0t/\hbar}\,U(t,t_0)\,e^{-iH_0t/\hbar}\,. \tag{3.7}$$

taking the time derivative of both sides of (3.6) yields

$$\begin{aligned} i\hbar\frac{\partial}{\partial t}|\alpha\rangle_t &= i\hbar\frac{\partial}{\partial t}\left(e^{iH_0(t-t_0)/\hbar}|\alpha\rangle\right) \\ &= -H_0e^{iH_0(t-t_0)/\hbar}|\alpha\rangle + e^{iH_0(t-t_0)/\hbar}(H_0+V)|\alpha\rangle \\ &= e^{iH_0(t-t_0)/\hbar}V|\alpha\rangle\,. \end{aligned} \tag{3.8}$$

writing the state $|\alpha\rangle$ through the operator $U_I(t,t_0)$ we obtain

$$i\hbar\frac{\partial}{\partial t}U_I(t,t_0) = V_I\,U_I(t,t_0)\,, \tag{3.9}$$

where $V_I = e^{iH_0(t-t_0)/\hbar}V\,e^{-iH_0(t-t_0)/\hbar}$, and the initial condition $U_I(t,t_0) = 1$ at $t = t_0$ is satisfied.

The differential equation (3.9) with its initial condition is equivalent to the integral equation

$$U_I(t,t_0) = 1 - \frac{i}{\hbar}\int_{t_0}^{t} V_I(t')\,U_I(t',t_0)\,dt'\,. \tag{3.10}$$

Given two eigenstates of H_0, $|i\rangle$ and $|n\rangle$, the transition amplitude(SAKURAI; NAPOLITANO, 2017) from state $|i\rangle$ to state $|n\rangle$ is obtained by acting with $\langle n|$ and $|i\rangle$ on (3.10). For a time-independent potential, as in our case, we write

$$\langle n|U_I(t,t_0)|i\rangle = \delta_{n,i} - \frac{i}{\hbar}\sum_m\langle n|V|m\rangle\int_{t_0}^{t} e^{i\omega_{nm}t'}\,\langle m|U_I(t',t_0)|i\rangle\,dt'\,, \tag{3.11}$$

where $\omega_{nm} = E_n - E_m$. Because we are dealing with scattering problems, the initial state $|i\rangle$ and the final state $|n\rangle$ exist only asymptotically; thus we take $t \to \infty$ and $t_0 \to -\infty$.

Making a first-order approximation in (3.11) gives $\langle m|U_I|i\rangle = \delta_{m,i}$, yielding

$$\langle n|U_I(t,t_0)|i\rangle = \delta_{n,i} - \frac{i}{\hbar}\langle n|V|i\rangle \int_{t_0}^{t} e^{i\omega_{ni}t'}\, dt' \,. \tag{3.12}$$

We must accommodate both states as $t \to \infty$ and $t_0 \to -\infty$. We therefore define a T-matrix such that

$$\langle n|U_I|i\rangle = \delta_{n,i} - \frac{i}{\hbar}T_{n,i} \int_{t_0}^{t} e^{i\omega_{ni}t' + \epsilon t'} dt' \,, \tag{3.13}$$

where $e^{+\epsilon t}$ acts as a convergence factor with $\epsilon > 0$ and $t \leq 1/\epsilon$. The limit $\epsilon \to 0$ must be taken before $t \to \infty$.

The integral can be evaluated for $|i\rangle \neq |n\rangle$; taking $t_0 \to -\infty$ yields

$$\langle n|U_I(t,-\infty)|i\rangle = -\frac{i}{\hbar}T_{n,i}\frac{e^{i\omega_{ni}t+\epsilon t}}{i\omega_{ni}+\epsilon} = \frac{1}{\hbar}T_{n,i}\frac{e^{i\omega_{ni}t+\epsilon t}}{-\omega_{ni}+i\epsilon} \,. \tag{3.14}$$

Inserting (3.14) into the integrand of (3.11) we find

$$\begin{aligned}\langle n|U_I(t,-\infty)|i\rangle = \frac{1}{\hbar}\langle n|V|i\rangle\frac{e^{i\omega_{ni}t+\epsilon t}}{-\omega_{ni}+i\epsilon} - \frac{i}{\hbar^2}\sum_m \langle n|V|m\rangle\frac{T_{m,i}}{-\omega_{mi}+i\epsilon} \\ \times \int_{-\infty}^{t} e^{i\omega_{nm}t' + i\omega_{mi}t' + \epsilon t'} dt' \,.\end{aligned} \tag{3.15}$$

The integral is straightforward, and by definition $\omega_{nm} + \omega_{mi} = \omega_{ni}$, which can be taken out of the sum, giving

$$\langle n|U_I(t,-\infty)|i\rangle = \frac{1}{\hbar}\frac{e^{i\omega_{ni}t+\epsilon t}}{-\omega_{ni}+i\epsilon}\left[\langle n|V|i\rangle + \frac{1}{\hbar}\sum_m \langle n|V|m\rangle\frac{T_{m,i}}{-\omega_{mi}+i\epsilon}\right] . \tag{3.16}$$

Comparing (3.16) with (3.14) we obtain

$$T_{n,i} = \langle n|V|i\rangle + \frac{1}{\hbar}\sum_m \langle n|V|m\rangle\frac{T_{m,i}}{-\omega_{mi}+i\epsilon} \,. \tag{3.17}$$

Expanding $T_{n,i}$ over a set of states $|\psi^+\rangle$ in a basis $|j\rangle$ we write

$$T_{n,i} = \sum_j \langle n|V|j\rangle\langle j|\psi^+\rangle = \langle n|V|\psi^+\rangle \,. \tag{3.18}$$

Approximating, without loss of generality, $i\hbar\epsilon = i\epsilon$ and $\hbar\omega_{mi} = E_m - E_i$, equation (3.17) becomes

$$\langle n|V|\psi^+\rangle = \langle n|V|i\rangle + \sum_m \langle n|V|m\rangle\frac{\langle m|V|\psi^+\rangle}{E_i - E_m + i\epsilon} \,. \tag{3.19}$$

Because $|n\rangle$ is an eigenstate of H_0, (3.19) must hold for every $|n\rangle$, leading to

$$\begin{aligned} |\psi^+\rangle &= |i\rangle + \sum_m |m\rangle \frac{\langle m|V|\psi^+\rangle}{E_i - E_m + i\epsilon} \\ &= |i\rangle + \sum_m \frac{1}{E_i - E_m + i\epsilon} |m\rangle\langle m|V|\psi^+\rangle \,. \end{aligned} \tag{3.20}$$

If E_m is the energy eigenvalue of H_0, we arrive at

$$|\psi^+\rangle = |i\rangle + \frac{1}{E - H_0 + i\epsilon} V|\psi^+\rangle \,. \tag{3.21}$$

Equation (3.21) is the Lippmann–Schwinger equation for the state $|\psi^+\rangle$. The superscript + appears because we used the positive convergence factor $e^{+\epsilon t}$ in (3.13); an analogous result is obtained with the negative sign. The choice of sign is linked to the principle of causality, which we discuss later. In general we write the Lippmann–Schwinger equation for a state $|\psi^\pm\rangle$ as

$$|\psi^\pm\rangle = |i\rangle + \frac{1}{E - H_0 \pm i\epsilon} V|\psi^\pm\rangle \,. \tag{3.22}$$

Projecting (3.22) onto the position basis $\langle \boldsymbol{r}|$ gives

$$\langle \boldsymbol{r}|\psi^\pm\rangle = \langle \boldsymbol{r}|i\rangle + \langle \boldsymbol{r}| \frac{1}{E - H_0 \pm i\epsilon} |\boldsymbol{r'}\rangle\langle \boldsymbol{r'}|V|\psi^\pm\rangle \,. \tag{3.23}$$

We identify the Green's function

$$G(\boldsymbol{r}, \boldsymbol{r'}) \equiv \frac{\hbar^2}{2m} \langle \boldsymbol{r}| \frac{1}{E - H_0 \pm i\epsilon} |\boldsymbol{r'}\rangle \,, \tag{3.24}$$

and finally write the Lippmann–Schwinger equation in position representation:

$$\psi(\boldsymbol{r}) = \varphi(\boldsymbol{r}) + \frac{2m}{\hbar^2} \int G(\boldsymbol{r}, \boldsymbol{r'})\, V(\boldsymbol{r'})\, \psi(\boldsymbol{r'})\, d\boldsymbol{r'} \,. \tag{3.25}$$

This is the form of the Lippmann–Schwinger equation we shall use in this work.

3.3 Green's Function in Scattering Theory

According to Definition 3 in Chapter 2, the Green's function is a fundamental solution of the differential operator. For this reason, it plays a central role in scattering theory, and its analysis reveals important aspects of the scattering phenomenon. In this section we shall develop an explicit expression for the Green's function introduced earlier in (3.24). One way to proceed is to exploit the fact that the eigenstates of H_0 are more easily calculated in the momentum basis and, by inserting a complete set of states $|\boldsymbol{k}\rangle$ in (3.24), obtain a discretized expression for the Green's function that can then be extended to the continuous spectrum.

We start from the time-dependent Schrödinger equation (3.3) in its position representation:

$$\left(i\hbar\frac{\partial}{\partial t} - H\right)\Psi(\boldsymbol{r},t) = 0\,. \tag{3.26}$$

Since the full Hamiltonian is given by (3.4), we can write

$$\left(\frac{\partial}{\partial t} - H_0\right)\Psi(\boldsymbol{r},t) = V(\boldsymbol{r},t)\Psi(\boldsymbol{r},t)\,. \tag{3.27}$$

In agreement with Theorem (2.2.1), the Green's function is obtained by solving

$$\left[\frac{\partial}{\partial t} - H_0\right] G_0(\boldsymbol{r},t\,|\,\boldsymbol{r'},t') = \delta(\boldsymbol{r}-\boldsymbol{r'})\,\delta(t-t')\ . \tag{3.28}$$

As a fundamental solution, the Green's function describes how the wave function at the point $(\boldsymbol{r},t)$ connects to the inhomogeneous (source) term at $(\boldsymbol{r'},t')$. Observe that G_0 behaves like a wavefront: any point in space where the wave function is non-zero at $t = t'$ acts as a source that determines the wave function at a later time t. This is an interesting connection with Huygens' principle.[2] However, the Green's function for the time-dependent Schrödinger equation differs from the one describing light propagation in Huygens' principle, mainly because the wave velocity in Schrödinger's equation depends critically on energy, whereas, in vacuum, light waves propagate at an energy-independent speed.(GONIS; BUTLER, 2000)

The partial differential equation (3.27) can be cast in integral form:

$$\Psi(\boldsymbol{r},t) = \chi(\boldsymbol{r},t) + \int G_0(\boldsymbol{r},t\,|\,\boldsymbol{r'},t')\,V(\boldsymbol{r'},t')\,\Psi(\boldsymbol{r'},t')\,d\boldsymbol{r'}\,dt'. \tag{3.29}$$

The wave functions are related to the time-independent functions through

$$\begin{aligned}\Psi(\boldsymbol{r},t) &= \psi(\boldsymbol{r})e^{-iEt}\,,\\ \chi(\boldsymbol{r},t) &= \varphi(\boldsymbol{r})e^{-iEt}\,.\end{aligned} \tag{3.30}$$

The calculation of $G_0(\boldsymbol{r},t\,|\,\boldsymbol{r'},t')$ is well-known(LANDIM; RODRIGUES, 2022) and yields

$$\begin{aligned}G_0^+ &= -i\left[\frac{1}{4\pi i(t-t')}\right]^{3/2}\Theta(t-t')\,\exp\!\left[i\,\frac{|\boldsymbol{r}-\boldsymbol{r'}|^2}{4(t-t')}\right],\\ G_0^- &= i\left[\frac{1}{4\pi i(t-t')}\right]^{3/2}\Theta(t'-t)\,\exp\!\left[i\,\frac{|\boldsymbol{r}-\boldsymbol{r'}|^2}{4(t-t')}\right],\end{aligned} \tag{3.31}$$

[2] Christiaan Huygens proposed that each point on a wavefront acts as a new point source: at every instant the front itself generates infinitesimal new waves from each of its points, producing the next wavefront one instant later. He also assumed that only the waves propagating in the forward direction carry enough energy to generate secondary waves, which prevents, for example, light from propagating backward into regions hidden behind objects.

where $\Theta(t-t')$ is the Heavside step function.

To respect causality in the scattering problem we choose G_0^+ as our Green's function. It is also called the retarded function, or propagator(LANDIM; RODRIGUES, 2022), in reference to Huygens' principle. Its counterpart, G_0^-, is known as the advanced function.(GONIS; BUTLER, 2000)

Assuming a time-independent potential, we naturally recover the Lippmann–Schwinger equation (3.25). It is therefore sensible to look for a form of the Green's function that is likewise time independent.

In Chapter 2 we saw that any Green's function arises from convolution with the Dirac delta distribution δ. Being a singular distribution, δ belongs to the Schwartz space (PéREZ, 2015), on which the Fourier transform is an automorphism. Hence applying the transform to our Green's function preserves its fundamental properties, ensuring that the result remains the appropriate Green's function for the problem.

Because time t and frequency ν are Fourier conjugates, and frequency relates to energy through Planck's constant, the passage to the frequency domain eliminates t-dependence and converts it into a direct energy dependence. This energy-space form fits naturally into the Lippmann–Schwinger equation.

Substituting (3.30) into (3.29) we obtain

$$\psi(\boldsymbol{r})e^{-iEt} = \varphi(\boldsymbol{r})e^{-iEt} + \int G_0(\boldsymbol{r}, t \,|\, \boldsymbol{r'}, t')\, V(\boldsymbol{r'})\, \psi(\boldsymbol{r'})e^{-iEt'}\, d\boldsymbol{r'}\, dt'. \tag{3.32}$$

Inserting the expression for G_0^+ found in (**??**) into (3.32) and using the causality condition $t > t'$ gives

$$\psi(\boldsymbol{r})e^{-iEt} = \varphi(\boldsymbol{r})e^{-iEt} - \lim_{\epsilon\to 0^+} i(2\pi)^{-3} \int e^{-\epsilon(t-t')} e^{-iEt'} e^{i\boldsymbol{k}\cdot\boldsymbol{R}} e^{-ik^2(t-t')}\, d\boldsymbol{k} \int V(\boldsymbol{r'})\psi(\boldsymbol{r'})\, d\boldsymbol{r'}\, dt'. \tag{3.33}$$

The t' terms can be grouped into a single integral I:

$$\int_{-\infty}^{t} e^{i(k^2-E-i\epsilon)t'}\, dt' = -i\, \frac{e^{i(k^2-E-i\epsilon)t}}{k^2 - E - i\epsilon}\,. \tag{3.34}$$

Substituting into (3.33) and cancelling the common factor e^{-iEt} yields

$$\psi(\boldsymbol{r}) = \varphi(\boldsymbol{r}) + \lim_{\epsilon\to 0^+} (2\pi)^{-3} \int \frac{e^{i\boldsymbol{k}\cdot\boldsymbol{R}}}{k^2 - E - i\epsilon}\, V(\boldsymbol{r'})\psi(\boldsymbol{r'})\, d\boldsymbol{r'}\, d\boldsymbol{k}. \tag{3.35}$$

Re-arranging (3.35) we find

$$\psi(\boldsymbol{r}) = \varphi(\boldsymbol{r}) + \int \Big[\lim_{\epsilon\to 0^+} (2\pi)^{-3} \frac{e^{i\boldsymbol{k}\cdot\boldsymbol{R}}}{k^2 - E - i\epsilon}\, d\boldsymbol{k} \Big] V(\boldsymbol{r'})\psi(\boldsymbol{r'})\, d\boldsymbol{r'}. \tag{3.36}$$

That is,

$$\psi(\boldsymbol{r}) = \varphi(\boldsymbol{r}) + \int G_0^+(\boldsymbol{r} \,|\, \boldsymbol{r'}; E)\, V(\boldsymbol{r'})\psi(\boldsymbol{r'})\, d\boldsymbol{r'}\,, \tag{3.37}$$

where the time-independent (energy-dependent) Green's function is

$$G_0^+(\boldsymbol{r} \,|\, \boldsymbol{r'}; E) = (2\pi)^{-3} \lim_{\epsilon \to 0^+} \int \frac{e^{i\boldsymbol{k}\cdot\boldsymbol{R}}}{k^2 - E - i\epsilon}\, d\boldsymbol{k}. \tag{3.38}$$

Setting $E = k'^2$, we can rewrite (3.38) as

$$G_0^+(\boldsymbol{r} \,|\, \boldsymbol{r'}; E) = G_0^+(\boldsymbol{r} \,|\, \boldsymbol{r'}) = \lim_{\epsilon \to 0^+} (2\pi)^{-3} \int \frac{e^{i\boldsymbol{k}\cdot\boldsymbol{R}}}{k^2 - k'^2 - i\epsilon}\, d\boldsymbol{k}. \tag{3.39}$$

In three dimensions we may choose spherical coordinates to perform the integral:

$$G_0^+(\boldsymbol{r} \,|\, \boldsymbol{r'}) = \lim_{\epsilon \to 0^+} (2\pi)^{-3} \int_0^\infty dk\, k \int_0^{2\pi} d\phi \int_0^\pi d\theta\, \sin\theta\, \frac{e^{ikR\cos\theta}}{k^2 - k'^2 - i\epsilon}. \tag{3.40}$$

After integrating over the angles the integral becomes

$$G_0^+(\boldsymbol{r} \,|\, \boldsymbol{r'}) = \lim_{\epsilon \to 0^+} \frac{1}{4\pi^2 R} \int_{-\infty}^\infty \frac{k \sin(kR)}{k^2 - k'^2 - i\epsilon}\, dk. \tag{3.41}$$

We evaluate this integral in the complex plane using a semicircular contour along the real axis, as shown in Figure 5. Applying Cauchy's residue theorem(ABLOWITZ; FOKAS, 2003) we obtain

$$\begin{aligned} G_0^+(\boldsymbol{r} \,|\, \boldsymbol{r'}) &= -\frac{1}{4\pi} \frac{e^{ik'R}}{R} \\ &= -\frac{1}{4\pi} \frac{e^{i\sqrt{E}\,|\boldsymbol{r}-\boldsymbol{r'}|}}{|\boldsymbol{r}-\boldsymbol{r'}|}\,. \end{aligned} \tag{3.42}$$

In the time domain, G_0^+ can be recognized as the solution of the eigenvalue equation $H_0 G = EG$(SAKURAI; NAPOLITANO, 2017), i.e., the Green's function of the Helmholtz equation given in (2.75).

This interpretation is important: the time-independent Green's function in scattering theory is simply the free-particle Green's function of the Schrödinger equation. We therefore refer to it as the free Green's function, or the Green's function of a free particle.

3.4 Scattering Amplitude and Cross Sections

In scattering processes we are normally interested in the effect of the scatterer on the outgoing wave at a distance far beyond the range of the potential[3]. This is crucial

[3] Obviously, the incident plane wave is infinite. From a practical and realistic standpoint, however, we consider a wave-packet that approaches the scattering center. Before it encounters the target, the packet behaves like a plane wave front, and after the interaction we have both the original packet and an emerging spherical wave front.(GOLDBERGER; WATSON, 1967)

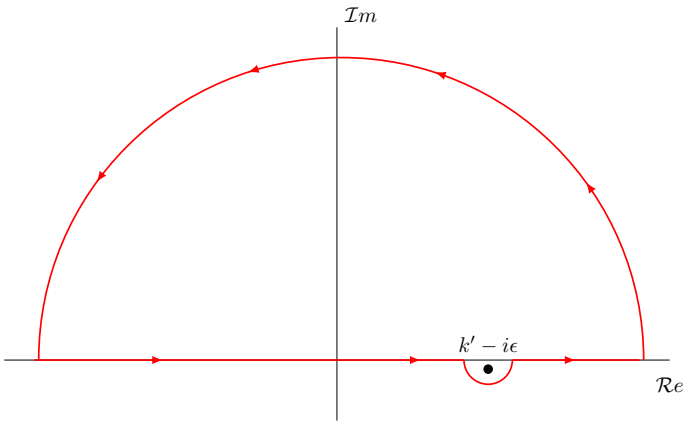

Figure 5 – Integration contour used in the calculation of the time-independent Green's function.

experimentally, because we cannot place a detector very close to the target.(SAKURAI; NAPOLITANO, 2017)

Under these conditions it is reasonable to seek solutions which, in three dimensions for $|\boldsymbol{r} - \boldsymbol{r'}| \to \infty$, take the generic form

$$\psi(\boldsymbol{r})_{r\to\infty} = A\left[e^{i\boldsymbol{kr}} + f(\Omega)\frac{e^{ikr}}{r}\right], \tag{3.43}$$

where the first term represents the incident plane wave and the second term the scattered spherical wave; here $r = |\boldsymbol{r} - \boldsymbol{r'}|$. The factor $1/r$ in the spherical term is required so that $|\psi|^2$ falls off as $1/r^2$, ensuring probability conservation.(GRIFFITHS; SCHROETER, 2018)

The cross section defined in (3.1) as the number of particles scattered per unit time divided by the incident flux equals the scattered flux through a spherical surface element $r^2 d\Omega$ divided by the incident flux. To evaluate these quantities we may[4] consider the probability that the incident wave ψ_{in} crosses an infinitesimal area $d\sigma$ in time dt while travelling with speed v:

$$dP = |\psi_{in}|^2 dV = |A|^2 (v\,dt)\,d\sigma, \tag{3.44}$$

and the probability that the scattered wave ψ_{out} crosses a spherical element $r^2 d\Omega$ in time dt with speed v:

$$dP = |\psi_{out}|^2 dV = \frac{|A|^2 |f(\Omega)|^2}{r^2}(v\,dt)\,r^2 d\Omega. \tag{3.45}$$

These probabilities must be equal(GRIFFITHS; SCHROETER, 2018), giving

$$d\sigma = |f(\Omega)|\,d\Omega, \tag{3.46}$$

and hence the differential cross section (3.1) becomes

$$\frac{d\sigma}{d\Omega} = |f(\Omega)|^2. \tag{3.47}$$

[4] A more rigorous treatment uses the probability-current density associated with the time-independent Schrödinger equation; see (JOACHAIN, 1979), Chapter 3.

and the total cross section

$$\sigma_{tot} = \int \frac{d\sigma}{d\Omega} d\Omega = \int |f(\Omega)|^2 d\Omega. \tag{3.48}$$

Equation (3.47) links the differential cross section, of primary experimental interest, to the scattering amplitude extracted from the wave function, making it a remarkably powerful bridge between theory and experiment.

The main difficulty now lies in determining the amplitude $f(\Omega)$. Among the techniques for computing it, the partial-wave analysis and the Born approximation are prominent whenever the scattering problem allows such methods. The partial wave method expands both incident and scattered waves in angular-momentum eigenfunctions, applying suitable boundary conditions; the Born approximation, generally used at high energies, relies on convergence criteria because it is an approximative approach.

In our case we aim to develop a methodology that yields either exact solutions of the Lippmann–Schwinger equation or, at least, a system of equations that can be solved numerically to obtain the scattering solution. Consequently, we seek solutions of the form (3.43) for $|\boldsymbol{r} - \boldsymbol{r'}| \to \infty$.

As we shall see, when taking $|\boldsymbol{r} - \boldsymbol{r'}| \to \infty$ we must also adopt *asymptotic* expressions for the free Green's function, employing asymptotic expansions of the eigenfunctions involved.(ARFKEN; WEBER, 1999)

3.5 Quantum Refractive Index

In optics, the propagation of light waves in a material medium is described by what we call the refractive index. The term *refractive index* was coined by Thomas Young(YOUNG, 1845), but its first appearances and measurements date back to the 18th century, notably in the works of Newton(NEWTON, 1730) and Hauksbee(HAUKSBEE, 1710).

Like the propagation of the light, the propagation of matter waves in a material medium can be described through a quantity analogous to the refractive index of optical theory. This idea was first introduced in the mid-20th century by Foldy(FOLDY, 1945) and Lax(LAX, 1951) and has been refined over the years.

In this context, the refractive index describes how the propagation of the incident wave is modified upon entering the scatterer and its medium. Because the waves are infinite in extent, the scattered wave interferes with the incident wave, altering its phase and amplitude. The phase change induces a change in the propagation speed of the wave within the medium.

An intuitive way to obtain the quantum refractive index is to consider a wave travelling through a medium under the Born approximation, where the medium is characterized by a well-localized finite potential. According to (SMITH et al., 1997), in a scattering phenomenon under these conditions, at a distance $r = R$ the wave function is given by

$$\psi \approx e^{inkR}\varphi, \tag{3.49}$$

where the number n is called the quantum refractive index. This is generally a complex quantity: its real part produces a phase shift in the emerging wave, while its imaginary part accounts for attenuation. Indeed, one can show that for $r = R$ the wave function is expected to take the form

$$\psi \approx e^{ikR}\, e^{i\phi\gamma R}\, e^{-\gamma R\sigma_{tot}/2}\varphi, \tag{3.50}$$

and comparison of (3.49) with (3.50) yields

$$n = 1 + \frac{\gamma}{k}\left(\phi + i\frac{\sigma_{tot}}{2}\right) = 1 + 2\pi\gamma\,\frac{f(k)}{k}, \tag{3.51}$$

since, by the optical theorem,

$$\begin{cases} \operatorname{Im} f(k,0) \;\longrightarrow\; \dfrac{k\sigma_{tot}}{4\pi}, \\[2ex] \operatorname{Re} f(k,0) \;\longrightarrow\; \dfrac{k\phi}{2\pi}. \end{cases} \tag{3.52}$$

Many researchers have examined and discussed the formulation of a quantum refractive index for atomic particles, comparing their equations with experimental results(VIGUÉ, 1995; AUDOUARD; DUPLAA; VIGUÉ, 1995; AL, 1997; FORREY et al., 1996). Based on these studies, C. Champenois(CHAMPENOIS et al., 2008) derived an expression that agrees with the available experimental data on particle collisions and with the theoretical results of statistical physics and the quantum Boltzmann equation(VACCHINI; HORNBERGER, 2009). For the particles of a gas, Champenois proposed

$$n = 1 + 2\pi N\left(\frac{m_p + m_t}{m_t}\right)\left\langle\frac{f(k_r)}{k_p^2}\right\rangle, \tag{3.53}$$

where N is the number of scatterers per unit volume, m_p is the particle mass, m_t the target mass, k_r the incident particle's wave number in the centre-of-mass frame, and k_p its wave number in its own frame. The function f denotes the forward scattering amplitude.

In our problem we deal with a plane-wave particle incident on a single scatterer, so N represents the potential-barrier coupling that we denote $\gamma(\boldsymbol{r})$. Moreover, the wave number reduces to the standard k used in the preceding sections, and under the Born approximation(SAKURAI; NAPOLITANO, 2017) we may assume $m_t \gg m_p$.

Thus the quantum refractive index for our system is defined by

$$n = 1 + 2\pi\gamma(\boldsymbol{r})\left\langle \frac{f_0}{k^2} \right\rangle, \tag{3.54}$$

where f_0 is the forward scattering amplitude (scattering angle zero). The advantage of Champenois's expression is that the average accommodates both plane-wave scattering—where the average is taken over incidence angles—and beam scattering, where the average is taken over momenta k, while in both cases including all possible initial velocities.

4 Applications

4.1 Smooth Spherical Surface

To illustrate the methodology used, we first consider scattering by a target shaped as a spherical shell built from the sum of Dirac delta functions, called a δ wall. This potential barrier was originally proposed by *da Luz et al.*(LUZ; LUPU-SAX; HELLER, 1997) and can be defined through the integral representation

$$V(\boldsymbol{r}') = \int_S \gamma\, \delta(\boldsymbol{r}' - \boldsymbol{r}'')\, d\boldsymbol{a}', \tag{4.1}$$

where, in our case, S is a spherical surface of radius R parametrized by $\boldsymbol{r}'(\phi', \theta')$ with $0 \leq \phi' < 2\pi,\ 0 \leq \theta' \leq \pi$—that is, a surface integral. The factor γ describes the coupling strength of the potential barrier, i.e. the intensity of the potential that produces the scattering.

This potential will be used in the Lippmann–Schwinger equation (3.25) developed in the previous chapter,

$$\psi(\boldsymbol{r}) = \varphi(\boldsymbol{r}) + \mu \int G(\boldsymbol{r} \,|\, \boldsymbol{r}') V(\boldsymbol{r}')\, \psi(\boldsymbol{r}')\, d\boldsymbol{r}', \tag{4.2}$$

where we integrate over all space, $G(\boldsymbol{r} \,|\, \boldsymbol{r}')$ is the three-dimensional Green's function, and $\mu = 2m/\hbar^2$.

Rewriting the Lippmann–Schwinger equation in spherical coordinates and substituting the potential gives

$$\begin{aligned} \psi(\boldsymbol{r}) = \varphi(\boldsymbol{r}) + \mu \int_0^{\infty} \int_0^{2\pi} \int_0^{\pi} G(\boldsymbol{r} \,|\, \boldsymbol{r}') \times \\ \left(\int_0^{2\pi} \int_0^{\pi} \gamma(\phi', \theta') \frac{\delta(r' - R)\delta(\theta' - \theta'')\delta(\phi' - \phi'')}{|J|}\, R^2 \sin\theta''\, d\theta''\, d\phi'' \right) \times \\ \psi(\boldsymbol{r}')|J|\, dr'\, d\theta'\, d\phi' \end{aligned} \tag{4.3}$$

where the δ integrals can be carried out.

Thus we arrive at the integral equation in which the source terms represent the spherical shell:

$$\psi(\boldsymbol{r}) = \varphi(\boldsymbol{r}) + \mu\gamma R^2 \int_0^{2\pi} \int_0^{\pi} G(r, \phi, \theta \,|\, R, \phi', \theta')\, \gamma(\phi', \theta')\, \psi(R, \phi', \theta')\, \sin\theta'\, d\theta'\, d\phi', \tag{4.4}$$

where $G(r, \phi, \theta \,|\, R, \phi', \theta')$ is the free-particle Green's function, denoted $G_0^+(\boldsymbol{r} \,|\, \boldsymbol{r}')$. In spherical coordinates the Green's function is expressed through its bilinear expansion (2.103),

$$G_0^+(\boldsymbol{r} \,|\, \boldsymbol{r}') = -ik \sum_{\ell=0}^{\infty} \sum_{m=-\ell}^{\ell} j_\ell(kr_<)\, h_\ell^{(1)}(kr_>)\, Y_\ell^m(\theta, \phi)\, Y_\ell^{*m}(\theta', \phi'), \tag{4.5}$$

where j_ℓ and $h_\ell^{(1)}$ are spherical Bessel and Hankel functions, respectively, and

$$r_> = \max(r, r'), \qquad r_< = \min(r, r').$$

This notation sets our position relative to the barrier: choosing $r_< = r,\ r_> = R$ corresponds to points *inside* the barrier, while $r_< = R,\ r_> = r$ refers to the *exterior* region.

Inserting the bilinear expansion of the Green's function into (4.4) gives the integral equation we must solve:

$$\begin{aligned}\psi(\boldsymbol{r}) = \varphi(\boldsymbol{r}) - ik\mu R^2 \sum_{\ell=0}^{\infty}\sum_{m=-\ell}^{\ell} Y_\ell^m(\theta,\phi)\int_0^{2\pi}\int_0^{\pi} d\phi' d\theta' \sin(\theta')\gamma(\phi',\theta')\times \\ j_\ell(kr_<)h_\ell^{(1)}(kr_>)Y_\ell^{*m}(\theta',\phi')\psi(r',\phi',\theta')\end{aligned} \tag{4.6}$$

4.1.1 Constant coupling

In general the coupling γ may be a function, but in this first case we assume a homogeneous barrier with $\gamma = \text{const}$.

Starting from (4.6) we rewrite

$$\begin{aligned}\psi(\boldsymbol{r}) = \varphi(\boldsymbol{r}) - ik\mu\gamma R^2 \sum_{\ell=0}^{\infty}\sum_{m=-\ell}^{\ell} Y_\ell^m(\theta,\phi) j_\ell(kr_<)h_\ell^{(1)}(kr_>) \\ \int_0^{2\pi}\int_0^{\pi} d\phi' d\theta' \sin(\theta') Y_\ell^{*m}(\theta',\phi')\psi(R,\phi',\theta'),\end{aligned} \tag{4.7}$$

which can be solved analytically by choosing an appropriate expansion for $\psi(R,\phi',\theta')$. A natural choice is an expansion in the eigenfunctions of the problem, i.e. spherical harmonics:

$$\psi(R,\phi',\theta') = \sum_{\ell'=0}^{\infty}\sum_{m'=-\ell'}^{\ell'} A_{\ell',m'}(R)\, Y_{\ell'}^{m'}(\theta',\phi'),$$

with coefficients $A_{\ell',m'}(R)$ to be determined. Substituting into (4.7) we obtain

$$\begin{aligned}\psi(\boldsymbol{r}) = \varphi(\boldsymbol{r}) - ik\mu\gamma R^2 \sum_{\ell=0}^{\infty}\sum_{m=-\ell}^{\ell} Y_\ell^m(\theta,\phi) j_\ell(kr_<)h_\ell^{(1)}(kr_>) \sum_{\ell'=-\infty}^{\infty}\sum_{m'=-\ell'}^{\ell'} A_{\ell',m'}(R) \\ \int_0^{2\pi}\int_0^{\pi} d\phi' d\theta' \sin(\theta') Y_\ell^{*m}(\theta',\phi') Y_{\ell'}^{m'}(\theta',\phi')\end{aligned} \tag{4.8}$$

The integral is familiar—it is the orthogonality condition for spherical harmonics(ARFKEN; WEBER, 1999):

$$\int_0^{2\pi}\int_0^{\pi} Y_\ell^{*m}(\theta',\phi')\, Y_{\ell'}^{m'}(\theta',\phi')\, \sin\theta'\, d\theta'\, d\phi' = \delta_{\ell,\ell'}\delta_{m,m'}.$$

Hence the Lippmann–Schwinger equation becomes

$$\psi(\boldsymbol{r}) = \varphi(\boldsymbol{r}) - ik\mu\gamma R^2 \sum_{\ell=0}^{\infty}\sum_{m=-\ell}^{\ell} Y_\ell^m(\theta,\phi)\, j_\ell(kr_<)\, h_\ell^{(1)}(kr_>)\, A_{\ell,m}(R). \tag{4.9}$$

To find the coefficients $A_{\ell',m'}$ we also expand the left-hand wave function:

$$\psi(r,\phi,\theta) = \sum_{\ell',m'} A_{\ell',m'}(r)\, Y_{\ell'}^{m'}(\theta,\phi). \tag{4.10}$$

The incident plane wave $\varphi(\boldsymbol{r})$ is expanded in the usual way(GOTTFRIED, 2018):

$$\varphi(r,\phi,\theta,\boldsymbol{k}) = 4\pi \sum_{\ell'',m''} i^{\ell''} j_{\ell''}(kr)\, Y_{\ell''}^{m''}(\theta,\phi)\, Y_{\ell''}^{*m''}(\boldsymbol{k}), \tag{4.11}$$

where $\boldsymbol{k}$ denotes the incident direction.

Substituting these expansions into (4.9), multiplying by $Y_\ell^{*m}(\theta,\phi)\sin\theta$, and integrating over θ,ϕ yields

$$A_{\ell,m}(r) = 4\pi\, i^\ell\, j_\ell(kr)\, Y_\ell^{*m}(\boldsymbol{k}) - ik\mu\gamma R^2\, j_\ell(kr_<)\, h_\ell^{(1)}(kr_>)\, A_{\ell,m}(R). \tag{4.12}$$

Evaluating at $r = R$ gives the coefficients explicitly:

$$A_{\ell,m}(R,\boldsymbol{k}) = \frac{4\pi\, i^\ell\, j_\ell(kR)\, Y_\ell^{*m}(\boldsymbol{k})}{1 + ik\mu\gamma R^2\, j_\ell(kR)\, h_\ell^{(1)}(kR)}. \tag{4.13}$$

and finally, inserting these coefficients into (4.9) we obtain the full wave function:

$$\begin{aligned}\psi(r,\phi,\theta) = \sum_{\ell=0}^{\infty}\sum_{m=-\ell}^{\ell}\Bigg[& 4\pi i^\ell j_\ell(kR) - ik\mu\gamma R^2 j_\ell(kr_<) h_\ell^{(1)}(kr_>) \\ & \left(\frac{4\pi i^\ell j_\ell(kR)}{1 + ik\mu\gamma R^2 j_\ell(kR) h_\ell^{(1)}(kR)}\right)\Bigg] Y_\ell^m(\theta,\phi) Y_\ell^{*m}(\boldsymbol{k})\end{aligned} \tag{4.14}$$

which is the wave equation for a particle scattered by a spherical-shell barrier with constant coupling. With this result, by choosing $r_>$ and $r_<$ we can study the wave function inside and outside the barrier. Inside the barrier ($r_> = R,\ r_< = r$) the spherical Bessel function j_ℓ causes the wave to exhibit resonant behaviour when k coincides with one of its zeros. Outside, the spherical Hankel function $h_\ell^{(1)}$ governs the propagation of the scattered wave, and from the exterior solution we can compute the scattering amplitude and the physical quantities of interest in this work.

Figure 6 provides a detailed view of the probability-density both outside and inside the spherical barrier, using level surfaces to highlight the regions of highest values. With $k = 2$, because of the shorter wavelength, the incident wave is largely reflected and couples only weakly to the interior region. The probability thus remains strongly localized outside the barrier, but we can still see a tunneling effect happening.

By contrast, Figure 7 illustrates the case of $k = \pi$. Here the de Broglie wavelength provides enough kinetic energy for the wave to penetrate deeply into the potential, producing multiple internal scatterings and interference patterns. The exterior probability

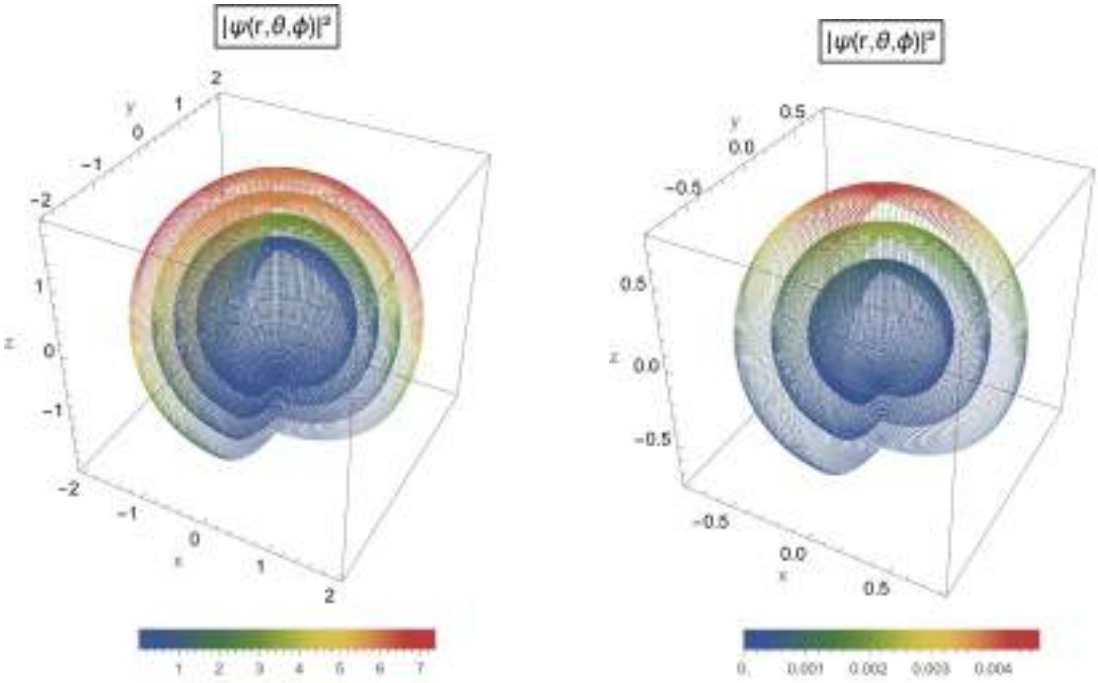

Figure 6 – Visualization of the probability density of the wave function in the region outside the barrier (left image) and inside the barrier (right image) using spherical level surfaces. The potential barrier is located at $R = 1.0$, and the level surfaces are positioned at $r = 1.1$, $r = 1.4$, $r = 1.7$, and $r = 2.0$ for the exterior region, and at $r = 0.4$, $r = 0.6$, and $r = 0.8$ for the interior region. The incident plane wave has angle $\theta_k = \pi$ and $\phi_k = 0$. In both figures, the parameters used were $k = 2$, $\gamma = 50$, and $\mu = 1$, and the series was truncated at $l = l_{\max} = 7$.

density also changes dramatically because of the diffraction of the wave, redistributing probability angularly.

Finally, note that in both scenarios the incident wave is a plane wave and therefore non-normalizable. In addition, since 4.14 represents a infinite summation, we truncate the sum at $l_{\max} = 7$ which is a good value for convergence of the solution(MAIOLI; SCHMIDT, 2018). This justification for the truncation of the infinite sum will be the same for the other visualizations of the results presented in this work.

4.1.2 Wavy Coupling

As mentioned earlier, the coupling γ can take the form of a function that depends on the surface-parameter coordinates. In this situation, an analytical solution is possible provided that the coupling function γ can be expanded in terms of spherical harmonics (AZADO; MAIOLI; SCHMIDT, 2021).

With this in mind, we can model the coupling γ so as to reproduce a possible wavy nature of the barrier that, in our case, is the scattering target. Such modelling is particularly useful for studying scattering from surfaces with imperfections or even cavities

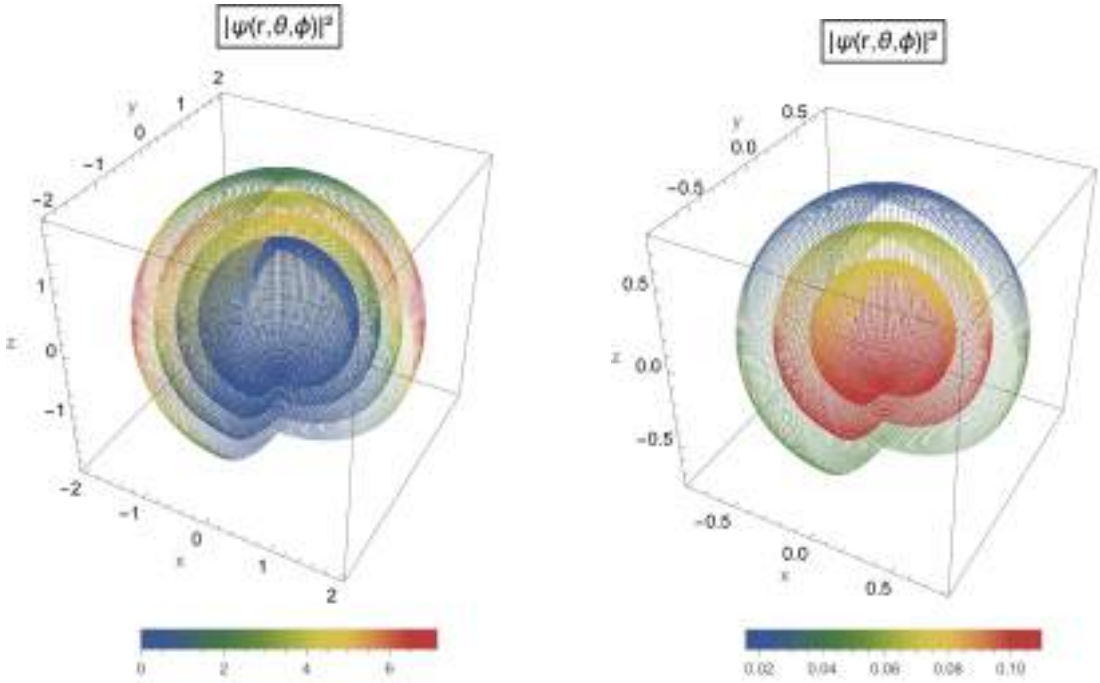

Figure 7 – Visualization of the probability density of the wave function in the region outside the barrier (left image) and inside the barrier (right image) using spherical level surfaces. The potential barrier is located at $R = 1.0$, and the level surfaces are positioned at $r = 1.1$, $r = 1.4$, $r = 1.7$, and $r = 2.0$ for the exterior region, and at $r = 0.4$, $r = 0.6$, and $r = 0.8$ for the interior region. The incident plane wave has angle $\theta_k = \pi$ and $\phi_k = 0$. In both figures, the parameters used were $k = \pi$, $\gamma = 50$, and $\mu = 1$, and the series was truncated at $l = l_{\max} = 7$.

(porosity)[1], enabling a deeper understanding of these processes in quantum scattering.

For that reason, suppose that the coupling $\gamma(\phi, \theta)$ we wish to describe is a wavy coupling given by

$$\gamma(\phi, \theta) = \gamma_0 + \eta \cos(\beta\phi) \cos(\alpha\theta) \tag{4.15}$$

where η is a constant that can be tuned to model the deformation of the coupling over the surface. We can expand $\gamma(\phi, \theta)$ in spherical harmonics[2] as follows:

$$\gamma(\phi, \theta) = \gamma_0 + \eta \cos(\beta\phi) \cos(\alpha\theta) = \gamma_0 + \frac{\eta}{2}\left[\sum_{a=\beta}^{\infty} c_a \left(Y_a^{\beta}(\theta, \phi) + Y_a^{-\beta}(\theta, \phi)\right)\right] \tag{4.16}$$

where

$$c_a = \frac{2a+1}{2} \frac{(a-\beta)!}{(a+\beta)!} \int_0^{\pi} \cos(\alpha\theta)\, P_a^{\beta}(\cos\theta)\, \sin\theta\, d\theta \tag{4.17}$$

provides the coefficients c_a required for the expansion. A solution to this integral is obtained by setting $x = \cos\theta$, leading to an integral involving Chebyshev polynomials (GRIER,

[1] You can think in pick N random points which $\gamma = 0$, and in this case the solution will simply be the incident wave, i.e, $\psi = \varphi$ on that point, which you could introduce in your fully solution with specific boundary conditions. There's a lot of methods capable to generate this points in a randomness way, for more details see (MULLER, 1959).

[2] See Appendix A.

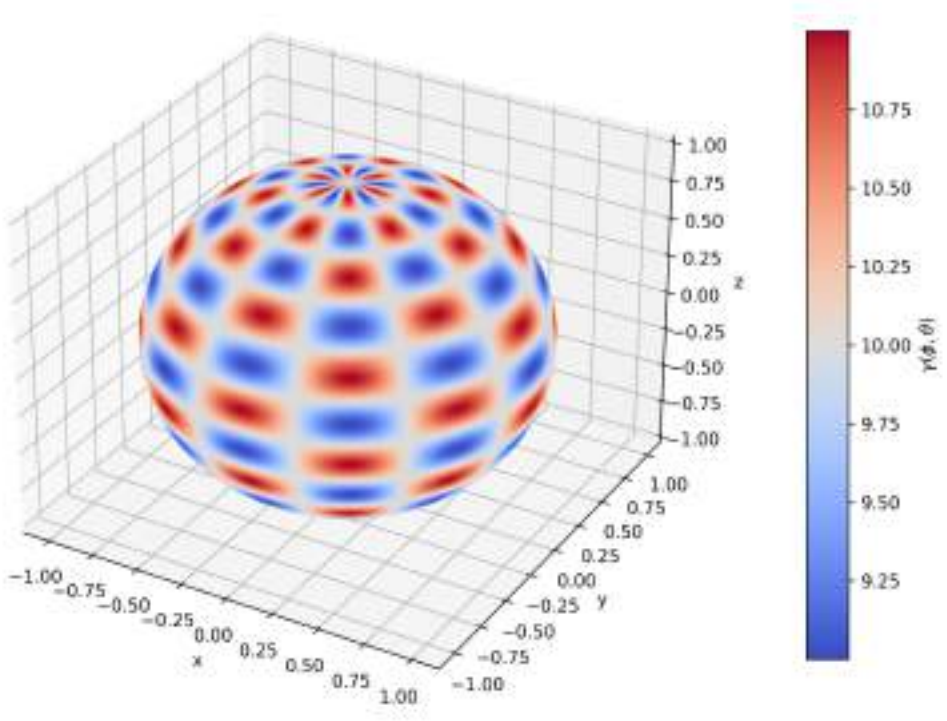

Figure 8 – Modelling of the potential coupling over a spherical-shell barrier. The values used were $\gamma_0 = 10$, $\eta = 1$, and $R = 1$.

2006):

$$c_a = \frac{2a+1}{2}\frac{(a-\beta)!}{(a+\beta)!}\int_1^{-1} T_\alpha(x)\, P_a^\beta(x)\, dx, \tag{4.18}$$

and the Chebyshev polynomials admit the series expansion (ABRAMOWITZ; STEGUN, 1948)

$$T_\alpha(x) = \frac{\alpha}{2}\sum_{k=0}^{\alpha/2}(-1)^k \frac{2^{\alpha-2k}\,(\alpha-k-1)!}{k!\,(\alpha-2k)!}\, x^{\alpha-2k}, \qquad \alpha > 0.$$

Because α is a positive integer, substituting this series into (4.18) yields

$$c_a = \frac{\alpha(2a+1)}{4}\frac{(a-\beta)!}{(a+\beta)!}\sum_{k=0}^{\alpha/2}(-1)^{k+1} \frac{2^{\alpha-2k}\,(\alpha-k-1)!}{k!\,(\alpha-2k)!}\int_{-1}^{1} x^{\alpha-2k}\, P_a^\beta(x)\, dx,$$

and after the change of variable $x = 2u - 1$ the integral can be evaluated[3] provided

[3] Gradshteyn & Ryzhik (GRADSHTEYN; RYZHIK, 2014), 7th ed., p. 771, Eq. 7.126-2.

$\mathrm{Re}(\alpha - 2k) > -1$:

$$c_a = \frac{\alpha(2a+1)}{4}\frac{(a-\beta)!}{(a+\beta)!}\sum_{k=0}^{\alpha/2}(-1)^{k+1}\frac{2^{\alpha-2k+1}\,(\alpha-k-1)!}{k!(\alpha-2k)!} \times \left[\frac{(-1)^\beta\sqrt{\pi}\;2^{-2\beta-1}\Gamma(\frac{1+\alpha-2k}{2})\Gamma(1+\beta+a)}{\Gamma(\frac{1}{2}+\frac{\beta}{2})\Gamma(\frac{3}{2}+\frac{\alpha}{2}-k-\frac{\beta}{2})\Gamma(1-\beta+a)}\right] \times {}_3F_2\left(\frac{\beta+a+1}{2},\frac{\beta-a}{2},\frac{\beta}{2}+1;\beta+1;\frac{3+\alpha-2k+\beta}{2};1\right) \quad \text{where } Re(\alpha-2k)>-1; \quad \beta\in\mathbb{Z} \tag{4.19}$$

Since α and k are integers, the condition $\mathrm{Re}(\alpha - 2k) > -1$ becomes $\alpha > 2k - 1$, which is satisfied because k ranges from 0 to $\alpha/2$. Hence the problem admits an analytic solution.

Analogous to the case of constant coupling, suppose the wave function $\psi(r', \phi', \theta')$ can be expanded as

$$\psi(r',\phi',\theta') = \sum_{p=0}^{\infty}\sum_{q=-p}^{p} A_{p,q}(R)\, Y_p^q(\theta',\phi'). \tag{4.20}$$

Then

$$\psi(\boldsymbol{r}) = \varphi(\boldsymbol{r}) - ikR^2\mu\sum_{\ell=0}^{\infty}\sum_{m=-\ell}^{\ell}\sum_{p=0}^{\infty}\sum_{q=-p}^{p} A_{p,q}(R)Y_\ell^m(\theta,\phi)j_\ell(kr_<)h_\ell^{(1)}(kr_>)\times \int_0^{2\pi}\int_0^{\pi} d\phi' d\theta' \sin(\theta')Y_\ell^{*m}(\theta',\phi')Y_p^q(\theta',\phi')\times \left[\gamma_0 + \frac{\eta}{2}\left(\sum_{a=\beta}^{\infty} c_a\left(Y_a^\beta(\theta,\phi) + Y_a^{-\beta}(\theta,\phi)\right)\right)\right] \tag{4.21}$$

which becomes

$$\psi(\boldsymbol{r}) = \varphi(\boldsymbol{r}) - ikR^2\mu\gamma_0\sum_{\ell=0}^{\infty}\sum_{m=-\ell}^{\ell}\sum_{p=0}^{\infty}\sum_{q=-p}^{p} A_{p,q}(R)Y_\ell^m(\theta,\phi)g_\ell(r|R) \int_0^{2\pi}\int_0^{\pi} d\phi' d\theta' \sin(\theta')Y_\ell^{*m}(\theta',\phi')Y_p^q(\theta',\phi') - \frac{ikR^2\mu\eta}{2}\sum_{\ell=0}^{\infty}\sum_{m=-\ell}^{\ell}\sum_{p=0}^{\infty}\sum_{q=-p}^{p}\sum_{a=\beta}^{\infty} c_a A_{p,q}(R)Y_\ell^m(\theta,\phi)g_\ell(r|R) \left[\int_0^{2\pi}\int_0^{\pi} d\phi' d\theta' \sin(\theta')Y_\ell^{*m}(\theta',\phi')Y_p^q(\theta',\phi')Y_a^\beta(\theta',\phi') + \int_0^{2\pi}\int_0^{\pi} d\phi' d\theta' \sin(\theta')Y_\ell^{*m}(\theta',\phi')Y_p^q(\theta',\phi')Y_a^{-\beta}(\theta',\phi')\right] \tag{4.22}$$

where $g_\ell(r|R) = j_\ell(kr_<)h_\ell^{(1)}(kr_>)$. These integrals are known once we use the property $Y_a^{*b}(\theta,\phi) = (-1)^b Y_a^{-b}(\theta,\phi)$; their results can be found in (ARFKEN; WEBER, 1999; TRIFONOV, 2011):

$$\int_0^{2\pi}\int_0^{\pi} Y_a^{*b}Y_p^q \sin\theta\, d\theta\, d\phi = \delta_{a,p}\delta_{b,q},$$

$$
\begin{aligned}
(-1)^b \int_0^{2\pi} \int_0^{\pi} Y_a^{-b}(\theta,\phi) Y_p^q(\theta,\phi) Y_s^t(\theta,\phi) \sin(\theta)\, d\theta\, d\phi \\
= (-1)^b \sqrt{\frac{(2a+1)(2p+1)(2s+1)}{4\pi}} \begin{pmatrix} a & p & s \\ 0 & 0 & 0 \end{pmatrix} \begin{pmatrix} a & p & s \\ -b & q & t \end{pmatrix},
\end{aligned} \tag{4.23}
$$

where the last two factors are 3-j symbols, an alternative to Clebsch–Gordan coefficients in angular-momentum addition.

To streamline subsequent calculations, we define a function of the parameters

$$
J_3(\ell, -m, p, q, a, \pm\beta) = (-1)^m \sqrt{\frac{(2\ell+1)(2p+1)(2a+1)}{4\pi}} \begin{pmatrix} \ell & p & a \\ 0 & 0 & 0 \end{pmatrix} \begin{pmatrix} \ell & p & a \\ -m & q & \pm\beta \end{pmatrix},
$$

equivalent to the integral now evaluated. Combining these results with (4.22) gives

$$
\begin{aligned}
\psi(\boldsymbol{r}) = \varphi(\boldsymbol{r}) - ikR^2\mu\gamma_0 \sum_{\ell=0}^{\infty} \sum_{m=-\ell}^{\ell} A_{\ell,m}(R) Y_\ell^m(\theta,\phi) g_\ell(r|R) \\
- \frac{ikR^2\mu\eta}{2} \sum_{\ell=0}^{\infty} \sum_{m=-\ell}^{\ell} \sum_{p=0}^{\infty} \sum_{q=-p}^{p} \sum_{a=\beta}^{\infty} c_a A_{p,q}(R) Y_\ell^m(\theta,\phi) g_\ell(r|R) \times \\
[J_3(\ell, -m, p, q, a, +\beta) + J_3(\ell, -m, p, q, a, -\beta)]
\end{aligned} \tag{4.24}
$$

Note that (4.24) represents a wave function comprising two potential contributions: one with $\gamma = \text{const}$ and the other with the proposed wavy γ. The first term after the incident wave is exactly the contribution found for constant coupling, whereas the second term stems from the wavy part. The incident plane wave $\varphi(\boldsymbol{r})$ can also be expanded in spherical harmonics:

$$
\varphi = 4\pi \sum_b \sum_{c=-b}^{b} i^b j_b(kr)\, Y_b^c(\theta,\phi)\, Y_b^{*c}(\hat{k}), \tag{4.25}
$$

with $\hat{k}$ the incident direction. Using (4.20) for the left-hand side and (4.25) for the incident wave, we get

$$
\begin{aligned}
\sum_{\ell'}^{\infty} \sum_{m'=-\ell'}^{\ell'} A_{\ell',m'}(r) Y_{\ell'}^{m'}(\theta,\phi) = 4\pi \sum_b^{\infty} \sum_{c=-b}^{b} i^b j_b(kr) Y_b^c(\theta,\phi) Y_b^{*c}(\hat{k}) \\
- ikR^2\mu\gamma_0 \sum_{\ell=0}^{\infty} \sum_{m=-\ell}^{\ell} A_{\ell,m}(R) Y_\ell^m(\theta,\phi) g_\ell(r|R) \\
- \frac{ikR^2\mu\eta}{2} \sum_{\ell=0}^{\infty} \sum_{m=-\ell}^{\ell} \sum_{p=0}^{\infty} \sum_{q=-p}^{p} \sum_{a=\beta}^{\infty} c_a A_{p,q}(R) Y_\ell^m(\theta,\phi) g_\ell(r|R) \\
[J_3(\ell, -m, p, q, a, +\beta) + J_3(\ell, -m, p, q, a, -\beta)]
\end{aligned} \tag{4.26}
$$

Multiplying by $Y_s^t(\theta,\phi)\sin\theta$, integrating, and using orthogonality yields

$$
\begin{aligned}
A_{s,t}(r) = 4\pi i^s j_s(kr) Y_s^{*t}(\hat{k}) - ikR^2\mu\gamma_0 A_{s,t}(R) g_s(r|R) \\
- \frac{ikR^2\mu\eta}{2} \sum_{p=0}^{\infty} \sum_{q=-p}^{p} \sum_{a=\beta}^{\infty} c_a A_{p,q}(R) g_s(r|R) \\
[J_3(s, -t, p, q, a, +\beta) + J_3(s, -t, p, q, a, -\beta)]
\end{aligned} \tag{4.27}
$$

Writing the right-hand side as

$$A_{s,t}(r) = \sum_{p,q} A_{p,q}(r)\,\delta_{p,s}\delta_{q,t},$$

and evaluating at $r = R$ we group terms into

$$\sum_{p,q} A_{p,q}(R)\Big\{\delta_{p,s}\delta_{q,t}\Big[1 + ikR^2\mu\gamma_0 g_s(R)\Big] + W^{t,q}_{s,p}\Big\} = 4\pi\, i^s j_s(kR)\, Y^{*t}_s(\hat{k}), \tag{4.28}$$

where

$$W^{t,q}_{s,p} = \frac{ikR^2\mu\eta}{2} g_s(R) \sum_{a=\beta}^{\infty} c_a(R)\,[J_3(s,-t,p,q,a,+\beta) + J_3(s,-t,p,q,a,-\beta)] \tag{4.29}$$

collects the terms involving the 3-j symbols. Equation (4.28) shows how to compute the coefficients $A_{s,t}$; it can be viewed as the inner product of a matrix with a vector, of the form $(1 + \mathbb{F}) \cdot \boldsymbol{A} = 4\pi\boldsymbol{B}$ (AZADO; MAIOLI; SCHMIDT, 2021).

4.1.3 Scattering Amplitude and Physical Quantities

The most important physical quantity in a scattering process is the scattering amplitude, obtained by analysing the wave function in a region far from the scattering potential. This region is called the *asymptotic region* and is reached in the limit $r \to \infty$.

We can obtain the scattering amplitude from the exterior wave function, i.e. by taking $r_< = R$ and $r_> = r$, so that in the asymptotic limit the wave function has the form of equation (3.43). In this limit the spherical Hankel function is replaced by its asymptotic representation (ARFKEN; WEBER, 1999):

$$h^{(1)}_\ell(kr)_{r\to\infty} \longrightarrow (-i)^{\ell+1}\frac{e^{ikr}}{kr} \tag{4.30}$$

It is easy to see that, for constant coupling, substituting (4.30) into the exterior wave function (4.14), with $r_< = R$ and $r_> = r$, and comparing with (3.43), the scattering amplitude is

$$f(\phi,\theta,\boldsymbol{k}) = \mu\gamma R^2 \sum_{\ell=0}^{\infty}\sum_{m=-\ell}^{\ell} (-i)^{\ell+2} j_\ell(kR) A_{\ell,m}(R,\boldsymbol{k}) Y^m_\ell(\theta,\phi) \tag{4.31}$$

where the coefficients $A_{\ell,m}(R,\boldsymbol{k})$ are given by equation (4.13). With $f(\phi,\theta,\boldsymbol{k})$ we can compute the quantum refractive index and also the differential cross section through (3.54) and (3.47) respectively. Thus,

$$\begin{aligned}\frac{d\sigma}{d\Omega} = |f(\phi,\theta,\boldsymbol{k})|^2 = \mu^2\gamma^2R^4 \sum_{\ell,m}\sum_{\ell',m'} (-i)^{\ell+2}(+i)^{\ell'+2}(-1)^{m'} j_\ell(kR) j_{\ell'}(kR) \\ Y^m_\ell(\theta,\phi) Y^{-m'}_{\ell'}(\theta,\phi) A_{\ell,m}(R,\boldsymbol{k}) A^*_{\ell',m'}(R,\boldsymbol{k})\end{aligned} \tag{4.32}$$

and for the total cross section,

$$\sigma_{tot} = \int \frac{d\sigma}{d\Omega} d\Omega = \int |f(\phi, \theta, \boldsymbol{k})|^2 d\Omega = \sigma^2 \gamma^2 R^4 \sum_{\ell=0}^{\infty} \sum_{m=-\ell}^{\ell} j_\ell^2(kR) |A_{\ell,m}(R, \boldsymbol{k})|^2 \tag{4.33}$$

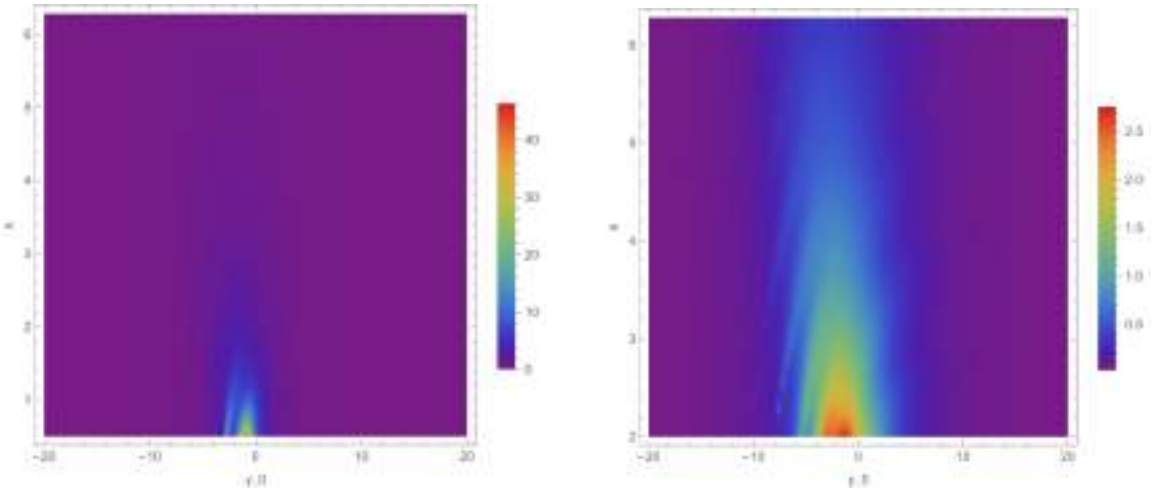

Figure 9 – Visualization of the total cross section (4.33) for the scattering of a plane wave by a spherical barrier with constant coupling strength. Here we used the parameters $R = 1$, $\mu = 1$ and $\theta_k = \phi_0 = 0$ for the incident angles. We truncate the series at $l_{max} = 9$.

In figure 9 we can visualize the total cross section, as function of both the incident wavenumber k and the coupling strength γ_0, (4.33) considering that we truncate the sum at $l_{max} = 9$. The total cross section is well-behaved for positive coupling strength (repulsive potential). For negative coupling strength, it has some peaks with local maxima and minima and some narrow marks. In the figure on the right we emphasizes this narrow-marks behavior when we increase the value of the wavenumber k. These peaks are due to interference phenomena between the incident wave and the wave that can enter the barrier and suffers multiple reflections inside of it.

In figure 10 we have the real and imaginary part of the quantum refractive index as a function of the incident wavenumber. We observe that when $\gamma_0 > 0$ and $\gamma_0 < 0$ there is two opposite behavior and its due to multiple scattering inside the barrier (PINSKER, 2016). The imaginary part is usually a positive value related to the absorption of the incident wave by the medium and is called extinction coefficient (SCHMIDT; PEREIRA, 2023), and negative values often occur in the study of CdS quantum dots in dieletric layers (CHEN et al., 2013).

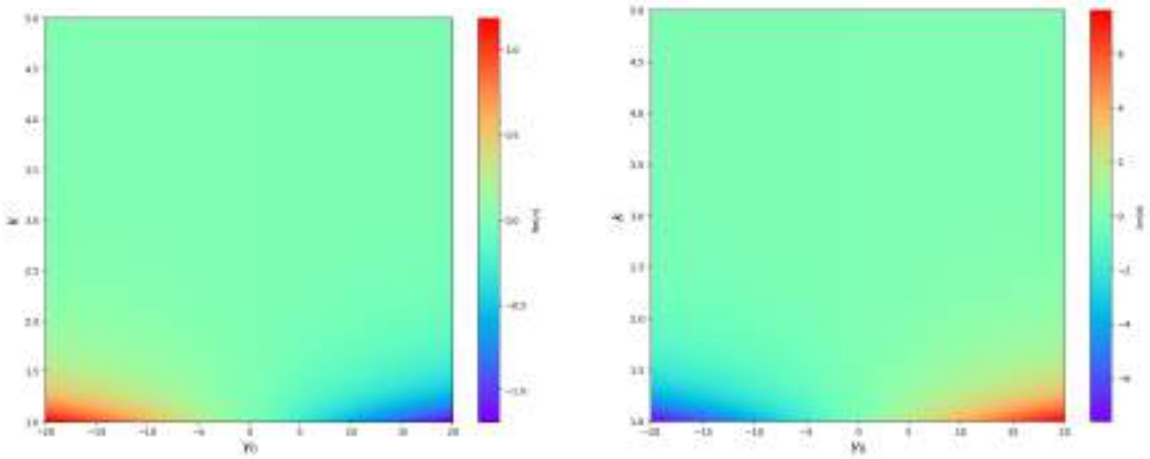

Figure 10 – Real and imaginary part of quantum refractive index for the scattering of a plane wave by a spherical barrier with wave-number k and coupling strength γ_0. Here we used the parameters $R = 1$, $\mu = 1$ and we truncate the series at $l_{max} = 7$.

In the other scenario, for wavy coupling, we must first rewrite equation (4.24) as

$$\psi(\boldsymbol{r}) = \varphi(\boldsymbol{r}) - ikR^2\mu \sum_{\ell=0}^{\infty}\sum_{m=-\ell}^{\ell} j_\ell(kr)h_\ell^{(1)}(kR)Y_\ell^m(\theta,\phi)\times \\ \left\{\gamma_0 A_{\ell,m}(R) + \frac{\eta}{2}\sum_{p=0}^{\infty}\sum_{q=-p}^{p}\sum_{a=\beta}^{\infty} c_a A_{p,q}(R)\times \right. \\ \left. [J_3(\ell,-m,p,q,a,+\beta) + J_3(\ell,-m,p,q,a,-\beta)]\right\} \tag{4.34}$$

Analogously, using the asymptotic expansion (4.30) and comparing with (3.43), the scattering amplitude is

$$f(\phi,\theta,\boldsymbol{k}) = \mu R^2 \sum_{\ell=0}^{\infty}\sum_{m=-\ell}^{\ell} (-i)^{\ell+2} j_\ell(kR)Y_\ell^m(\theta,\phi) \\ \left\{\gamma_0 A_{\ell,m}(R,\boldsymbol{k}) + \frac{\eta}{2}\sum_{p=0}^{\infty}\sum_{q=-p}^{p}\sum_{a=\beta}^{\infty} c_a A_{p,q}(R,\boldsymbol{k})\times \right. \\ \left. [J_3(\ell,-m,p,q,a,+\beta) + J_3(\ell,-m,p,q,a,-\beta)]\right\} \tag{4.35}$$

where the coefficients $A_{\ell,m}$ and $A_{p,q}$ are determined from equation (4.28). Defining,

$$B_{\ell,m}(R,\boldsymbol{k}) = \left\{\gamma_0 A_{\ell,m}(R,\boldsymbol{k}) + \frac{\eta}{2}\sum_{p=0}^{\infty}\sum_{q=-p}^{p}\sum_{a=\beta}^{\infty} c_a A_{p,q}(R,\boldsymbol{k})\times \right. \\ \left. [J_3(\ell,-m,p,q,a,+\beta) + J_3(\ell,-m,p,q,a,-\beta)]\right\} \tag{4.36}$$

the differential cross section is given by

$$\frac{d\sigma}{d\Omega} = |f(\phi,\theta,k)|^2 = \mu^2 R^4 \sum_{\ell,m}\sum_{\ell',m'} (-i)^{\ell+2}(+i)^{\ell'+2}(-1)^{m'} j_\ell(kR)\, j_{\ell'}(kR) \\ Y_\ell^m(\theta,\phi)\, Y_{\ell'}^{-m'}(\theta,\phi) B_{\ell,m}(R,\boldsymbol{k})\, B^*_{\ell' m'}(R,\boldsymbol{k}). \tag{4.37}$$

and the total cross section

$$\sigma_{tot} = \int \frac{d\sigma}{d\Omega} d\Omega = \int |f(\phi,\theta,k)|^2 d\Omega = \mu^2 R^4 \sum_{\ell=0}^{\infty}\sum_{m=-\ell}^{\ell} j_\ell^2(kR)|B_{\ell,m}(R,\boldsymbol{k})|^2 \tag{4.38}$$

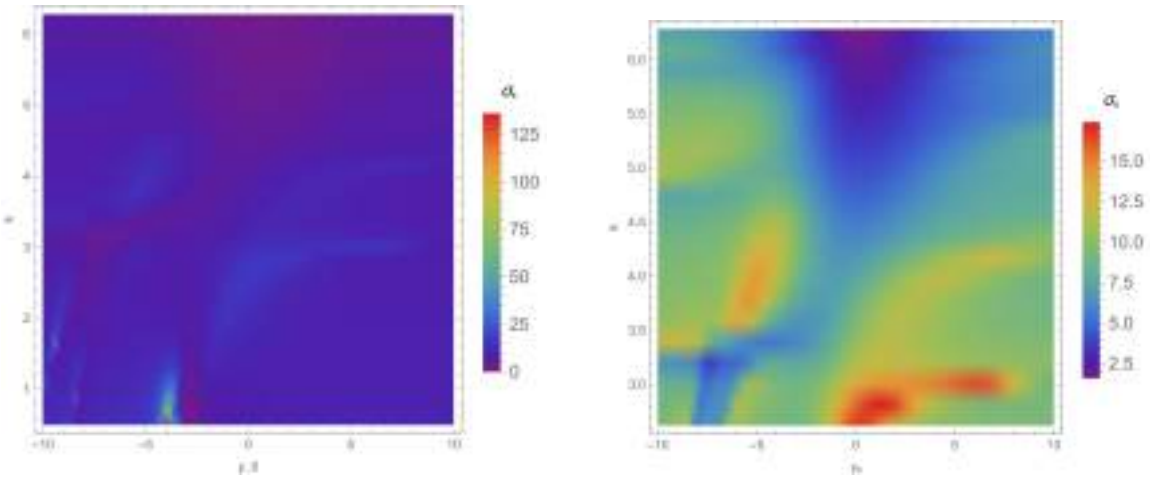

Figure 11 – Visualization of the total cross section (4.38) for the scattering of a plane wave by a spherical barrier with wavy coupling strength. Here we use the parameters $R = 1$, $\mu = 1$, $\eta = 5$, $\beta = 4$, $\alpha = 6$ and $\theta_k = \phi_0 = 0$ for the incident angles. We truncate the series at $l_{max} = 5$.

As same as before, in figure 11 we can visualize the total cross section, as function of both the incident wavenumber k and the constant part of the wavy coupling strength γ_0. In this case we truncate the sum at $l_{max} = 5$. In this case we still have some peaks with local maxima and minima but the total cross section is no longer well-behaved. This occur due to the wavy behavior of the coupling strength, allowing waves to penetrate the barrier in different locations and producing many interference phenomena between the incident wave and the scattered wave.

In figure 12 and 13 we have the real and imaginary part of the quantum refractive index for the wavy coupling barrier. We can observe that, again, we have a opposite behavior for the imaginary part when $\gamma < 0$ and $\gamma > 0$, which makes sense if we compare with the constant coupling strength scenario. Also, we notice that this time we needed a higher value for k to increase the absolute value of n_{im}. Furthermore, for the real part, we notice that there is a curious behavior around $k = \pi$, even with the opposite values of γ_0, which suggests a relationship with the de Broglie wavelength. On the other hand, for the imaginary part, the behavior at $k = \pi$ is softer, being just an inflection point.

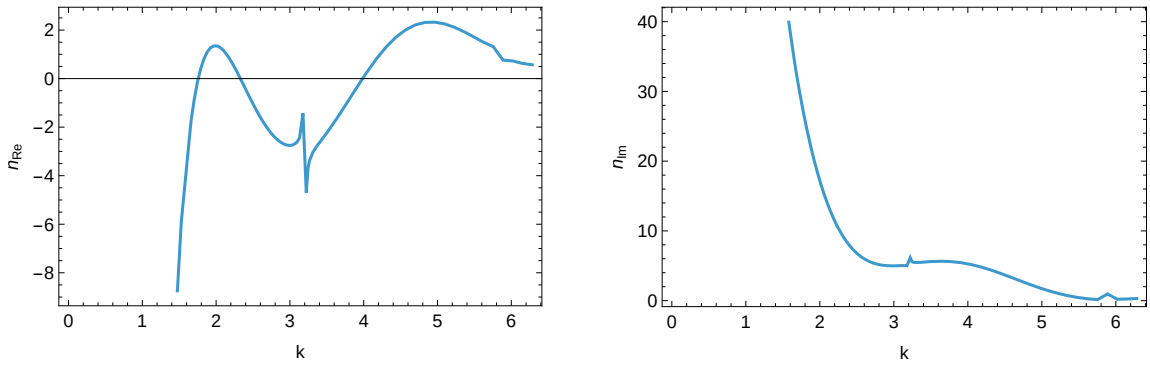

Figure 12 – Real and imaginary part of quantum refractive index for the scattering of a plane wave by a spherical barrier with wavy coupling strength. Here we use the parameters $R = 1$, $\mu = 1$ and $\gamma_0 = -50$, $\eta = 10$, $\alpha = 3$ and $\beta = 3$. We truncate the series at $l_{max} = 4$.

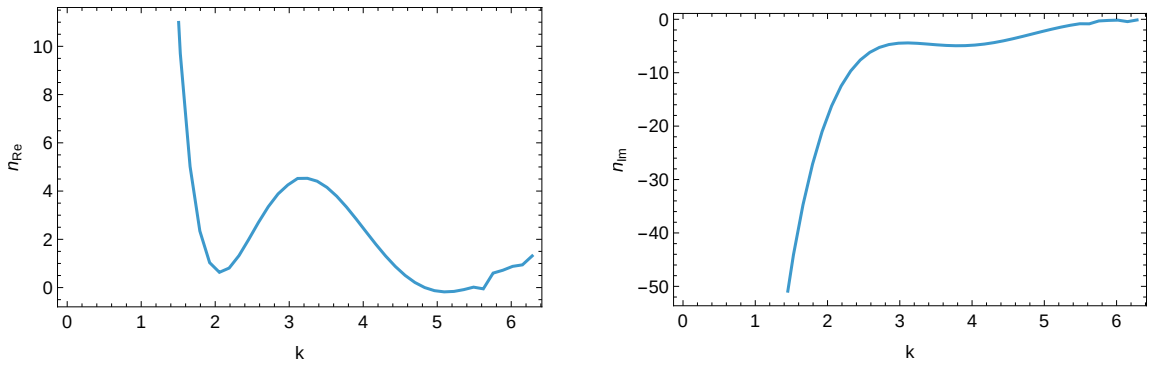

Figure 13 – Real and imaginary part of quantum refractive index for the scattering of a plane wave by a spherical barrier with wavy coupling strength. Here we use the parameters $R = 1$, $\mu = 1$ and $\gamma_0 = 50$, $\eta = 10$, $\alpha = 3$ and $\beta = 3$. We truncate the series at $l_{max} = 4$.

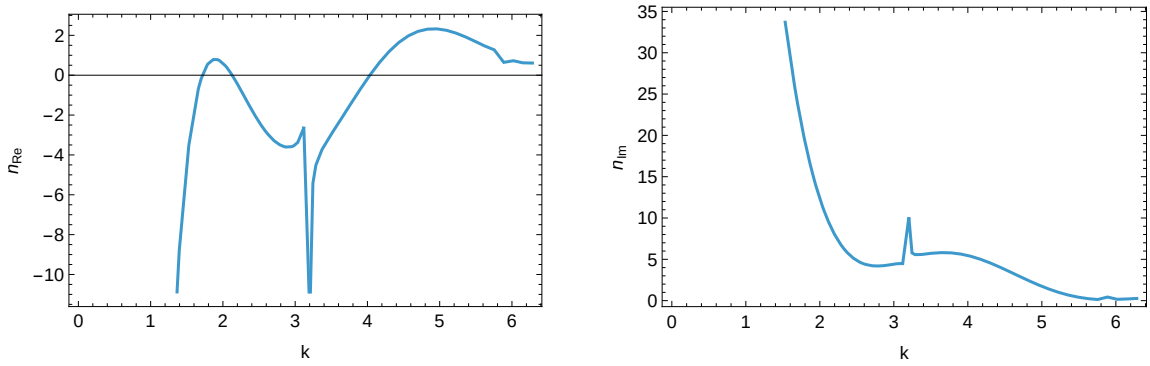

Figure 14 – Real and imaginary part of quantum refractive index for the scattering of a plane wave by a spherical barrier with wavy coupling strength. Here we use the parameters $R = 1$, $\mu = 1$ and $\gamma_0 = -50$, $\eta = 25$, $\alpha = 3$ and $\beta = 3$. We truncate the series at $l_{max} = 4$.

In figure 14 we have another scenario when $\gamma_0 < 0$, but in this case $\eta = 25$, half of the absolute value of γ_0. We notice that, in this case, both real and imaginary parts have local peaks of maxima and minima at $k = \pi$. For the real part, since it is negative,

this local minima at $k = \pi$ suggests a greater occurrence of multiple scattering within the potential barrier for this wavenumber. For the imaginary part, this local maxima suggests greater absorption of the incident wave by the barrier.

The dimensional analysis can give us more insights about these behaviors. Note that we are in Rydberg Atomic units, so $[k] = a_0^{-1}$, $[\gamma] = Ry$ and also $[E] = Ry\ a_0^2$. Therefore, the adimensional

$$\Pi = \frac{\gamma}{k^2} \tag{4.39}$$

plays an important role for the physical observations here. Note that if $\Pi > 1$, the kinetic energy will play a more relevant role in characterizing the results obtained than the potential interaction, so the plane wave will pass throught the barrier without great interactions. This can be clearly observed in the results for the quantum refractive index, for example the figure 14, which suggests that $n \to 0$ as k increase. We will observe that this will also be the case in the next application.

4.2 Wavy Spherical Surface

Another way to model an irregular surface in a scattering phenomenon is to build a parametrization that can be used together with the boundary-wall method to describe the scattering potential. In this alternative—unlike the previous case, where we modelled the coupling γ—the irregularities are applied directly to the geometry of the scatterer's surface.

For this model we consider a surface parametrized by

$$r(\phi,\theta) = R + \varepsilon\cos(\beta\phi)\cos(\alpha\theta), \qquad \phi\in[0,2\pi], \quad \theta\in[0,\pi] \tag{4.40}$$

which represents a *wavy sphere* whose radius varies point-by-point. Here R is the radius of the undeformed sphere, β is a non-negative integer, and ε is the deformation parameter. The surface-area element, with $\boldsymbol{r}$ the usual spherical coordinates, is

$$d\boldsymbol{a} = \left|\frac{\partial\boldsymbol{r}}{\partial\phi}\times\frac{\partial\boldsymbol{r}}{\partial\theta}\right| = \sqrt{\left(\frac{\partial\boldsymbol{r}}{\partial\theta}\right)^2\left(\frac{\partial\boldsymbol{r}}{\partial\phi}\right)^2 - \left(\frac{\partial\boldsymbol{r}}{\partial\phi}\cdot\frac{\partial\boldsymbol{r}}{\partial\theta}\right)}\,d\phi\,d\theta$$

$$\begin{aligned} d\boldsymbol{a} =& \Big\{\Big[\Big(\tfrac{\partial r}{\partial\phi}\Big)^2 + r^2(\phi,\theta)\sin^2\theta\Big]\Big[\Big(\tfrac{\partial r}{\partial\theta}\Big)^2 + r^2(\phi,\theta)\Big] \\ &- \tfrac{\partial r}{\partial\phi}\Big[r(\phi,\theta)\sin\theta\Big(\cos\theta-\cos\phi\Big) + \tfrac{\partial r}{\partial\theta}\Big(\cos\phi\cos\theta+\sin^2\theta\Big)\Big]\Big\}^{1/2} d\phi\,d\theta \\ &= A(\phi,\theta)\,d\phi\,d\theta \end{aligned} \tag{4.41}$$

where

$$\begin{aligned} A(\phi,\theta) =& \left[R+\varepsilon\cos(\beta\phi)\cos(\alpha\theta)\right] \\ &\times\sqrt{\varepsilon^2\beta^2\sin^2(\beta\phi)\cos^2(\alpha\theta) + \varepsilon^2\alpha^2\sin^2\theta\,\cos^2(\beta\phi)\sin^2(\alpha\theta) + \left[R+\varepsilon\cos(\beta\phi)\cos(\alpha\theta)\right]^2\sin^2\theta} \end{aligned} \tag{4.42}$$

Following the same methodology as before, to model the scattering of a plane wave by this surface we employ the Lippmann–Schwinger equation (LIPPMANN; SCHWINGER, 1950) in position representation,

$$\psi(\boldsymbol{r}) = \varphi(\boldsymbol{r}) + \frac{2m}{\hbar^2}\int_{\mathcal{S}} G_0^+(\boldsymbol{r}|\boldsymbol{r}')\,V(\boldsymbol{r}')\,\psi(\boldsymbol{r}')\,d\boldsymbol{r}', \tag{4.43}$$

where $G_0^+(\boldsymbol{r}|\boldsymbol{r}')$ is the free-particle Green's function and $V(\boldsymbol{r}')$ is the chosen potential. The Green's function, again, can be written via its bilinear expansion

$$G_0^+(\boldsymbol{r}|\boldsymbol{r}') = -ik\sum_{\ell=0}^{\infty}\sum_{m=-\ell}^{\ell} j_\ell(kr_<)\,h_\ell^{(1)}(kr_>)\,Y_\ell^m(\theta,\phi)\,Y_\ell^{*m}(\theta',\phi'), \tag{4.44}$$

where j_ℓ and $h_\ell^{(1)}$ are spherical Bessel and Hankel functions, respectively. As before,

$$\begin{cases} r_> = \max(r,r'), \\ r_< = \min(r,r'). \end{cases} \tag{4.45}$$

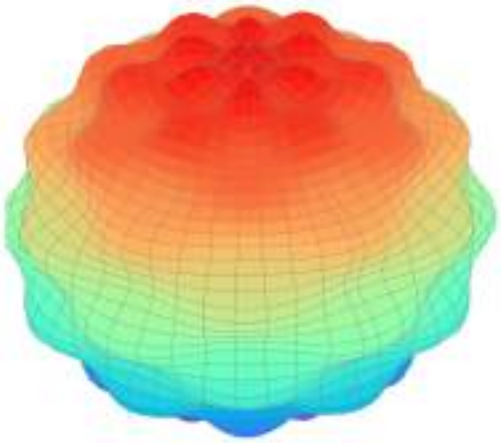

Figure 15 – Close-up view of the wavy spherical surface defined by $r = R + \varepsilon\cos(\beta\phi)\cos(\alpha\theta)$. We used $R = 2.0$, $\varepsilon = 0.15$, $\beta = 6$ and $\alpha = 12$. Here, we use the colormap just for the sake of beautifulness of the figure, so the colors used are not important.

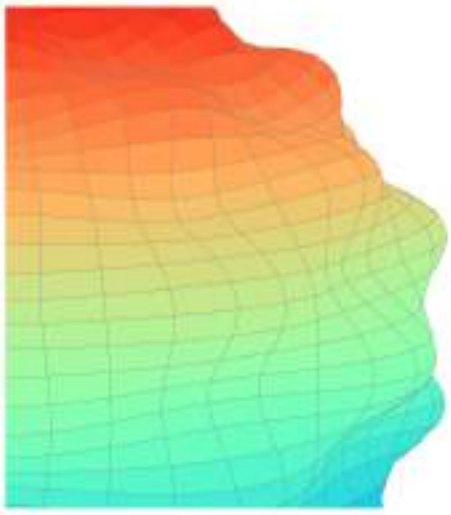

Figure 16 – Another close-up of the wavy spherical surface with $r = R + \varepsilon\cos(\beta\phi)\cos(\alpha\theta)$. Parameters: $R = 2.0$, $\varepsilon = 0.15$, $\beta = 6$, $\alpha = 12$. Again, we use the colormap just for the sake of beautifulness of the figure, so the colors used are not important.

To model the barrier potential we express it from the parametric equation of the

surface,

$$V(r,\phi,\theta) = \int_0^{2\pi}\int_0^{\pi} \gamma(\phi',\theta')\,\delta(r-r')\,\delta(\phi-\phi')\,\delta(\theta-\theta')\,\frac{A(\phi',\theta')}{r^2\sin\theta}\,d\phi'\,d\theta', \tag{4.46}$$

with $A(\phi',\theta')$ from (4.41). Inserting (4.44) and (4.46) into (4.43) gives

$$\begin{aligned}\psi(\boldsymbol{r}) = \varphi(\boldsymbol{r}) - ik\mu\sum_{\ell=0}^{\infty}\sum_{m=-\ell}^{\ell} Y_\ell^m(\theta,\phi)\int_0^{\infty}\int_0^{2\pi}\int_0^{\pi} dr'd\phi'd\theta' r'^2\sin(\theta') \\ j_\ell(kr_<)h_\ell^{(1)}(kr_>)\left[\int_0^{2\pi}\int_0^{\pi} d\phi''d\theta''\delta(r'-r'')\delta(\phi'-\phi'')\delta(\theta'-\theta'')\right. \\ \left.\gamma(\phi'',\theta'')\frac{A(\phi'',\theta'')}{r'^2\sin(\theta')}\right] Y_\ell^{*m}(\theta',\phi')\psi(r',\phi',\theta')\end{aligned} \tag{4.47}$$

where $\mu = 2m/\hbar^2$. Using the filtering property of the Dirac delta, we arrive at

$$\begin{aligned}\psi(\boldsymbol{r}) = \varphi(\boldsymbol{r}) - ik\mu\sum_{\ell=0}^{\infty}\sum_{m=-\ell}^{\ell} Y_\ell^m(\theta,\phi)\int_0^{2\pi}\int_0^{\pi} d\phi'd\theta'\gamma(\phi',\theta')A(\phi',\theta') \\ j_\ell(kr_<)h_\ell^{(1)}(kr_>)Y_\ell^{*m}(\theta',\phi')\psi(r',\phi',\theta')\end{aligned} \tag{4.48}$$

4.2.1 Case $\alpha = 0$

Since $r' = r'(\phi',\theta')$, to solve equation (4.48) we must properly define $r_<$ and $r_>$. In order to improve the understanding of this matter, we initially consider the special case where $\alpha = 0$, and in this case, $r' = R + \varepsilon\cos(\beta\phi')$ is the parametrized curve that we will use to define $r_<$ and $r_>$.

Evidently, for $r < R-\varepsilon$, we define $r_< = r$ and $r_> = R-\varepsilon$. Similarly, for $r > R+\varepsilon$, we define $r_< = R+\varepsilon$ and $r_> = r$. However, in the domain $R-\varepsilon < r < R+\varepsilon$, the values of $r_<$ and $r_>$ vary point by point, revealing that we must employ a more careful approach.

Therefore, consider $r_0 = R + \varepsilon\cos(\beta\phi)$. We know that if $R-\varepsilon \le r_0 \le R+\varepsilon$, the points of intersection will be given by

$$\phi' = \frac{1}{\beta}\arccos\left(\frac{r_0 - R}{\varepsilon}\right) \tag{4.49}$$

We then notice that the integration interval $[0,2\pi]$ with respect to the azimuthal angle will be divided as a function of β, so that we can consider

$$[0,2\pi]_\beta = \bigcup_{n=0}^{\beta-1}\left[\frac{2n\pi}{\beta} - \phi', \frac{2n\pi}{\beta} + \phi'\right] \cup \left[\frac{2n\pi}{\beta} + \phi', \frac{(2n+1)\pi}{\beta} - \phi'\right]. \tag{4.50}$$

The first term on the right-hand side of the equality in (4.50) corresponds to the intervals where $r_> = R + \varepsilon\cos(\beta\phi)$ and $r_< = r$, and the second term, consequently,

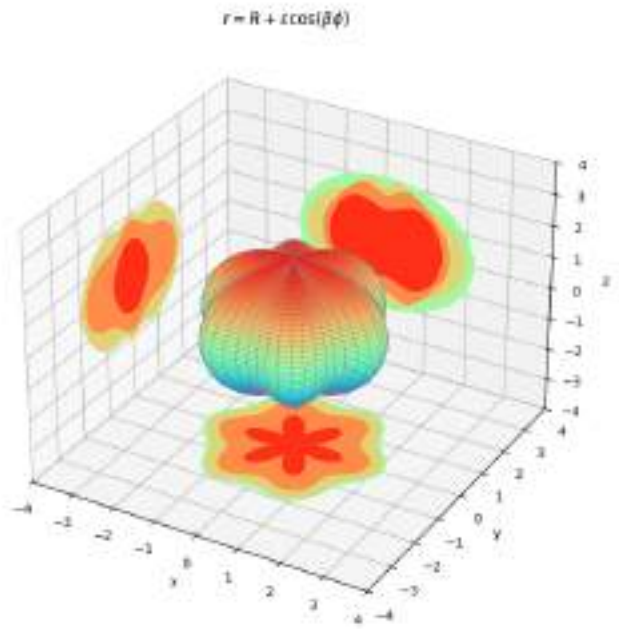

Figure 17 – Wavy spherical surface considering $\alpha = 0$ with the respective contour curves in the xy, xz, and yz plane. We use $R = 2.0$, $\varepsilon = 0.15$, and $\beta = 6$. Again, the colors used are not important.

corresponds to the intervals where $r_< = R + \varepsilon\cos(\beta\phi)$ and $r_> = r$. Using dummy variables, we can write

$$\begin{aligned}\psi(\boldsymbol{r}) =&\varphi(\boldsymbol{r}) - ik\mu\sum_{\ell=0}^{\infty}\sum_{m=-\ell}^{\ell} Y_\ell^m(\theta,\phi)\Bigg[\sum_{n=0}^{\beta-1}\int_{\frac{2n\pi}{\beta}-\phi''}^{\frac{2n\pi}{\beta}+\phi''}\int_0^{\pi} d\phi' d\theta' A(\phi',\theta')\gamma(\phi',\theta')\\ &h_\ell^{(1)}(k(R+\varepsilon\cos(\beta\phi')))Y_\ell^{*m}(\theta',\phi')\psi(R+\varepsilon\cos(\beta\phi'),\phi',\theta')\Bigg] j_\ell(kr) \quad +\\ &Y_\ell^m(\theta,\phi)\Bigg[\sum_{n=0}^{\beta-1}\int_{\frac{2n\pi}{\beta}+\phi''}^{\frac{(2n+1)\pi}{\beta}-\phi''}\int_0^{\pi} d\phi' d\theta' A(\phi',\theta')\gamma(\phi',\theta') j_\ell(k(R+\varepsilon\cos(\beta\phi')))\\ &Y_\ell^{*m}(\theta',\phi')\psi(R+\varepsilon\cos(\beta\phi'),\phi',\theta')\Bigg] h_\ell^{(1)}(kr)\end{aligned} \tag{4.51}$$

Defining

$$\begin{aligned}R_{\ell,m}(r) = \sum_{n=0}^{\beta-1}\int_{\frac{2n\pi}{\beta}-\phi''}^{\frac{2n\pi}{\beta}+\phi''}\int_0^{\pi} d\phi' d\theta' A(\phi',\theta')\gamma(\phi',\theta') h_\ell^{(1)}(k(R+\varepsilon\cos(\beta\phi')))\\ Y_\ell^{*m}(\theta',\phi')\psi(R+\varepsilon\cos(\beta\phi'),\phi',\theta')\end{aligned} \tag{4.52}$$

$$T_{\ell,m}(r) = \sum_{n=0}^{\beta-1} \int_{\frac{2n\pi}{\beta}+\phi''}^{\frac{(2n+1)\pi}{\beta}-\phi''} \int_0^{\pi} d\phi' d\theta' A(\phi',\theta')\gamma(\phi',\theta') j_\ell(k(R+\varepsilon\cos(\beta\phi'))) \\ Y_\ell^{*m}(\theta',\phi')\psi(R+\varepsilon\cos(\beta\phi'),\phi',\theta') \tag{4.53}$$

We can write equation (4.51) as

$$\psi(\boldsymbol{r}) = \varphi(\boldsymbol{r}) - ik\mu \sum_{\ell=0}^{\infty} \sum_{m=-\ell}^{\ell} Y_\ell^m(\theta,\phi)\Big[R_{\ell,m}(r) j_\ell(kr) + T_{\ell,m}(r) h_\ell^{(1)}(kr)\Big] \tag{4.54}$$

Where the functions $R_{\ell,m}(r)$ and $T_{\ell,m}(r)$ are coefficients to be determined and vary point by point. To determine such coefficients, we can aim to use orthogonality properties of the functions in equation (4.54). By multiplying equation (4.54) by $A(\phi,\theta)\gamma(\phi,\theta)Y_{\ell'}^{*m'}(\theta,\phi)h_{\ell'}^{(1)}(k(R+\varepsilon\cos(\beta\phi)))$, integrating over ϕ and θ in the intervals $[\frac{2n\pi}{\beta}-\phi', \frac{2n\pi}{\beta}+\phi']$, evaluating at $r = R+\varepsilon\cos(\beta\phi) = r'$, and summing over n, we find:

$$R_{\ell',m'}(r) = \underbrace{\sum_{n=0}^{\beta-1} \int_{\frac{2n\pi}{\beta}-\phi'}^{\frac{2n\pi}{\beta}+\phi'} \int_0^{\pi} d\phi d\theta A(\phi,\theta)\gamma(\phi,\theta) h_{\ell'}^{(1)}(kr') Y_{\ell'}^{*m'}(\theta,\phi)\varphi(r',\phi,\theta)}_{f_{\ell',m'}(r)} \\ - ik \sum_{n=0}^{\beta-1} \sum_{\ell=0}^{\infty} \sum_{m=-\ell}^{\ell} \left\{ \int_{\frac{2n\pi}{\beta}-\phi'}^{\frac{2n\pi}{\beta}+\phi'} \int_0^{\pi} d\phi d\theta A(\phi,\theta)\gamma(\phi,\theta) h_{\ell'}^{(1)}(kr') \times \right. \\ \left. Y_{\ell'}^{*m'}(\theta,\phi) Y_\ell^m(\theta,\phi)\Big[R_{\ell,m}(r') j_\ell(kr') + T_{\ell,m}(r') h_\ell^{(1)}(kr')\Big] \right\} \tag{4.55}$$

Similarly, for $T_{\ell,m}(r)$, we multiply equation (4.54) by $A(\phi,\theta)\gamma(\phi,\theta)Y_{\ell'}^{*m'}(\theta,\phi)j_{\ell'}(k(R+\varepsilon\cos(\beta\phi)))$, integrate over ϕ and θ in the intervals $[\frac{2n\pi}{\beta}+\phi', \frac{(2n+1)\pi}{\beta}+\phi']$, evaluate at $r = R+\varepsilon\cos(\beta\phi) = r'$, and sum over n to obtain:

$$T_{\ell',m'}(r) = \underbrace{\sum_{n=0}^{\beta-1} \int_{\frac{2n\pi}{\beta}+\phi'}^{\frac{(2n+1)\pi}{\beta}-\phi'} \int_0^{\pi} d\phi d\theta A(\phi,\theta)\gamma(\phi,\theta) j_{\ell'}(kr') Y_{\ell'}^{*m'}(\theta,\phi)\varphi(r',\phi,\theta)}_{g_{\ell',m'}(r)} \\ - ik \sum_{n=0}^{\beta-1} \sum_{\ell=0}^{\infty} \sum_{m=-\ell}^{\ell} \left\{ \int_{\frac{2n\pi}{\beta}+\phi'}^{\frac{(2n+1)\pi}{\beta}-\phi'} \int_0^{\pi} d\phi d\theta A(\phi,\theta)\gamma(\phi,\theta) j_{\ell'}(kr') \times \right. \\ \left. Y_{\ell'}^{*m'}(\theta,\phi) Y_\ell^m(\theta,\phi)\Big[R_{\ell,m}(r') j_\ell(kr') + T_{\ell,m}(r') h_\ell^{(1)}(kr')\Big] \right\} \tag{4.56}$$

The position-dependent functions (4.55) and (4.56) form a system of coupled linear equations, which can be solved numerically, since an exact solution has not yet been found. However, it is possible to further develop this system by taking its derivatives. Note that,

in the system of equations given by (4.55) and (4.56), the variable ϕ' in the integration limit is a function of r, as we can recognize through equation (4.49). The Leibniz integral rule[4], gives us

$$\begin{aligned}\frac{dR_{\ell',m'}(r)}{dr} =& \frac{df_{\ell',m'}}{dr} - \frac{ikh_{\ell'}^{(1)}(kr)}{\beta\sqrt{1-\left(\frac{r-R}{\varepsilon}\right)}}\times \\ & \sum_{n=0}^{\beta-1}\sum_{\ell=0}^{\infty}\sum_{m=-\ell}^{\ell}\left\{\int_0^{\pi} d\theta A(\chi_2,\theta)\gamma(\chi_2,\theta)Y_{\ell'}^{*m'}(\theta,\chi_2)Y_{\ell}^{m}(\theta,\chi_2)\right. \\ & \left. - \int_0^{\pi} d\theta A(\chi_1,\theta)\gamma(\chi_1,\theta)Y_{\ell'}^{*m'}(\theta,\chi_1)Y_{\ell}^{m}(\theta,\chi_1)\right\} \\ & \times\left[R_{\ell,m}(r)j_{\ell}(kr) + T_{\ell,m}(r)h_{\ell}^{(1)}(kr)\right]\end{aligned} \tag{4.57}$$

$$\begin{aligned}\frac{dT_{\ell',m'}(r)}{dr} =& \frac{dg_{\ell',m'}}{dr} - \frac{ikj_{\ell'}(kr)}{\beta\sqrt{1-\left(\frac{r-R}{\varepsilon}\right)}}\times \\ & \sum_{n=0}^{\beta-1}\sum_{\ell=0}^{\infty}\sum_{m=-\ell}^{\ell}\left\{\int_0^{\pi} d\theta A(\chi_4,\theta)\gamma(\chi_4,\theta)Y_{\ell'}^{*m'}(\theta,\chi_4)Y_{\ell}^{m}(\theta,\chi_4)\right. \\ & \left. - \int_0^{\pi} d\theta A(\chi_3,\theta)\gamma(\chi_3,\theta)Y_{\ell'}^{*m'}(\theta,\chi_3)Y_{\ell}^{m}(\theta,\chi_3)\right\} \\ & \times\left[R_{\ell,m}(r)j_{\ell}(kr) + T_{\ell,m}(r)h_{\ell}^{(1)}(kr)\right]\end{aligned} \tag{4.58}$$

where $\chi_1 = \frac{2n\pi}{\beta} - \phi'$, $\chi_2 = \chi_3 = \frac{2n\pi}{\beta} + \phi'$, and $\chi_4 = \frac{(2n+1)\pi}{\beta} - \phi'$. Moreover, note that when we apply the Leibniz rule, $r' \to r$. Using the results from Appendix 2 and by convention taking $A(\chi_p,\theta) = A(\phi',\theta)$, $\gamma(\chi_p,\theta) = \gamma(\phi',\theta)$, for $p = 1,\ldots,4$, we have:

$$\begin{aligned}\frac{dR_{\ell',m'}(r)}{dr} =& \frac{df_{\ell',m'}}{dr} - \frac{ikh_{\ell'}^{(1)}(kr)}{\sqrt{1-\left(\frac{r-R}{\varepsilon}\right)}} \\ & \sum_{\ell=0}^{\infty}\left\{\exp\left(+iq\phi'\right)\int_0^{\pi} d\theta A(\phi',\theta)\gamma(\phi',\theta)P_{\ell}^{m'+q\beta}(\cos\theta)P_{\ell'}^{m'}(\cos\theta)\right. \\ & \left. - \exp\left(-iq\phi'\right)\int_0^{\pi} d\theta A(\phi',\theta)\gamma(\phi',\theta)P_{\ell}^{m'+q\beta}(\cos\theta)P_{\ell'}^{m'}(\cos\theta)\right\} \\ & \times\left[R_{\ell,m}(r)j_{\ell}(kr) + T_{\ell,m}(r)h_{\ell}^{(1)}(kr)\right]\end{aligned} \tag{4.59}$$

[4] The Leibniz integral rule is given by

$$\frac{d}{dx}\int_{f_1(x)}^{f_2(x)} g(t)dt = g(f_2(x))\frac{df_2}{dx} - g(f_1(x))\frac{df_1}{dx}$$

and therefore,

$$\begin{aligned}\frac{dR_{\ell',m'}(r)}{dr} =& \frac{df_{\ell',m'}}{dr} + 2kh_{\ell'}^{(1)}(kr)U_{q-1}\left(\frac{r-R}{\varepsilon}\right)\times \\ & \sum_{\ell=0}^{\infty} S_\ell\Big[R_{\ell,m}(r)j_\ell(kr) + T_{\ell,m}(r)h_\ell^{(1)}(kr)\Big]\end{aligned} \tag{4.60}$$

Similarly, we have:

$$\begin{aligned}\frac{dT_{\ell',m'}(r)}{dr} =& \frac{dg_{\ell',m'}}{dr} - \frac{ikj_{\ell'}(kr)}{\sqrt{1-\left(\frac{r-R}{\varepsilon}\right)}} \\ & \sum_{\ell=0}^{\infty}\Bigg\{(-1)^q\exp\left(-iq\phi'\right)\int_0^\pi d\theta A(\phi',\theta)\gamma(\phi',\theta)P_\ell^{m'+q\beta}(\cos\theta)P_{\ell'}^{m'}(\cos\theta) \\ & -\exp\left(+iq\phi'\right)\int_0^\pi d\theta A(\phi',\theta)\gamma(\phi',\theta)P_\ell^{m'+q\beta}(\cos\theta)P_{\ell'}^{m'}(\cos\theta)\Bigg\} \\ & \times\Big[R_{\ell,m}(r)j_\ell(kr) + T_{\ell,m}(r)h_\ell^{(1)}(kr)\Big]\end{aligned} \tag{4.61}$$

which leads to

$$\begin{aligned}\frac{dT_{\ell',m'}(r)}{dr} =& \frac{dg_{\ell',m'}}{dr} - \frac{ikj_{\ell'}(kr)}{\sqrt{1-\left(\frac{r-R}{\varepsilon}\right)}}W_q\left(\frac{r-R}{\varepsilon}\right) \\ & \sum_{\ell=0}^{\infty} S_\ell\Big[R_{\ell,m}(r)j_\ell(kr) + T_{\ell,m}(r)h_\ell^{(1)}(kr)\Big]\end{aligned} \tag{4.62}$$

where W_ℓ is given by:

$$W_q\left(\frac{r-R}{\varepsilon}\right) = \begin{cases} 2iU_{q-1}\left(\frac{r-R}{\varepsilon}\right)\sqrt{1-\left(\frac{r-R}{\varepsilon}\right)^2}, & q \quad \text{even} \\ -2T_q\left(\frac{r-R}{\varepsilon}\right), & q \quad \text{odd} \end{cases} \tag{4.63}$$

and the term S_ℓ is given by

$$S_\ell = \int_0^\pi d\theta A(\phi',\theta)\gamma(\phi',\theta)P_\ell^{m'+q\beta}(\cos\theta)P_{\ell'}^{m'}(\cos\theta) \tag{4.64}$$

for q being a non-zero integer. The pair of equations (4.60) and (4.62) form a system of coupled first-order differential equations that must be solved numerically, due to the absence of an exact solution. By solving the system, it is possible to find the valid wave function in the domain $R-\varepsilon \leq r \leq R+\varepsilon$.

We can observe from (4.54) that the solution described in the domain $R-\varepsilon \leq r \leq R+\varepsilon$ represents a superposition of partial waves that have undergone multiple reflections and have been transmitted to infinity.

For the domain $r \leq R - \varepsilon$, note that the Hankel function $h_\ell^{(1)}(kr)$ is singular at the origin, and therefore we must take $T_{\ell,m} = 0$ for a physically plausible solution. Therefore, using equation (4.48), we can show that the wave function is expressed by

$$\psi(\boldsymbol{r}) = \varphi(\boldsymbol{r}) - ik\mu \sum_{\ell=0}^{\infty} \sum_{m=-\ell}^{\ell} Y_\ell^m(\theta, \phi) \lambda_{\ell,m} j_\ell(kr) \tag{4.65}$$

where the coefficient $\lambda_{\ell,m}$ is a constant to be determined, given by

$$\lambda_{\ell,m} = \int_0^{2\pi} \int_0^{\pi} d\phi' d\theta' \gamma(\phi', \theta') A(\phi', \theta') h_\ell^{(1)}(k(R-\varepsilon)) Y_\ell^{*m}(\theta', \phi') \psi(r', \phi', \theta') \tag{4.66}$$

Similarly, for the domain $r > R + \varepsilon$, the spherical Bessel function diverges at infinity, and therefore we take $R_{\ell,m} = 0$ for a physically plausible solution. Therefore, we have

$$\psi(\boldsymbol{r}) = \varphi(\boldsymbol{r}) - ik\mu \sum_{\ell=0}^{\infty} \sum_{m=-\ell}^{\ell} Y_\ell^m(\theta, \phi) \omega_{\ell,m} h_\ell^{(1)}(kr) \tag{4.67}$$

where the coefficient $\omega_{\ell,m}$, is also a constant to be determined, whose expression is given by

$$\omega_{\ell,m} = \int_0^{2\pi} \int_0^{\pi} d\phi' d\theta' \gamma(\phi', \theta') A(\phi', \theta') j_\ell(k(R+\varepsilon)) Y_\ell^{*m}(\theta', \phi') \psi(r', \phi', \theta') \tag{4.68}$$

Note that equation (4.92) represents a superposition of stationary waves originating from the interaction of the wave with multiple reflections within the barrier, while equation (4.94) represents a superposition of so-called propagating waves.

In both cases, $\psi(r', \phi', \theta')$ represents the wave function evaluated under the potential barrier(PEREIRA; CUNHA; SCHMIDT, 2024). To determine the connection between the position-dependent functions $R_{\ell,m}(r)$ and $T_{\ell,m}(r)$ and the coefficients $\lambda_{\ell,m}$ and $\omega_{\ell,m}$, we need appropriate boundary conditions.

Through the continuity of the wave function, we have

$$\lambda_{\ell,m} j_\ell(k(R-\varepsilon)) = R_{\ell,m}(R-\varepsilon) j_\ell(k(R-\varepsilon)) + T_{\ell,m}(R-\varepsilon) h_\ell^{(1)}(k(R-\varepsilon))$$

in addition,

$$\omega_{\ell,m} h_\ell^{(1)}(k(R+\varepsilon)) = R_{\ell,m}(R+\varepsilon) j_\ell(k(R+\varepsilon)) + T_{\ell,m}(R+\varepsilon) h_\ell^{(1)}(k(R+\varepsilon)) \,.$$

By comparing the real and imaginary parts, we conclude that

$$\lambda_{\ell,m} = R_{\ell,m}(R-\varepsilon), \tag{4.69}$$

$$\omega_{\ell,m} = T_{\ell,m}(R+\varepsilon). \tag{4.70}$$

We can therefore define two new position-dependent functions, named $\tilde{R}_{\ell,m}(r)$ and $\tilde{T}_{\ell,m}(r)$, which represent the complete solution of the Lippmann-Schwinger equation (4.43):

$$\psi(\boldsymbol{r}) = \varphi(\boldsymbol{r}) - ik\mu \sum_{\ell=0}^{\infty} \sum_{m=-\ell}^{\ell} Y_\ell^m(\theta,\phi)\Big[\tilde{R}_{\ell,m}(r) j_\ell(kr) + \tilde{T}_{\ell,m}(r) h_\ell^{(1)}(kr)\Big] \tag{4.71}$$

where we have

$$\tilde{R}_{\ell,m}(r) = \begin{cases} R_{\ell,m}(R-\varepsilon), & r < R-\varepsilon, \\ R_{\ell,m}(r), & R-\varepsilon \le r \le R+\varepsilon, \\ 0, & r > R+\varepsilon, \end{cases} \tag{4.72}$$

and

$$\tilde{T}_{\ell,m}(r) = \begin{cases} 0, & r < R-\varepsilon, \\ T_{\ell,m}(r), & R-\varepsilon \le r \le R+\varepsilon, \\ T_{\ell,m}(R+\varepsilon), & r > R+\varepsilon. \end{cases} \tag{4.73}$$

where the functions $R_{\ell,m}(r)$ and $T_{\ell,m}(r)$ are computed through the differential equation system (4.60) and (4.62).

From the expressions of the functions $\tilde{R}_{\ell,m}(r)$ and $\tilde{T}_{\ell,m}(r)$, we observe that both have physically relevant interpretations in their respective regimes of validity. For $r < R-\varepsilon$, $\tilde{T}_{\ell,m}(r) = 0$ is a necessary and sufficient condition for $|\psi(0)|^2 < 0$. On the other hand, for $r > R-\varepsilon$, there should be no stationary waves—only propagating ones—and therefore, in this domain, $\tilde{R}_{\ell,m}(r) = 0$.

4.2.2 Case $\alpha \neq 0$

We start from equation (4.48) and, once again, we must properly define $r_<$ and $r_>$. Letting $r(\phi,\theta) = R + \varepsilon\cos(\beta\phi)\cos(\alpha\theta)$, we observe that now the intersections with the maxima and minima of the surface depend on both ϕ and θ.

Consider $R-\varepsilon \le r \le R+\varepsilon$. For the intersection with $R-\varepsilon$, that is, the minimum points of the surface, we have

$$R-\varepsilon = R+\varepsilon\cos(\beta\phi)\cos(\alpha\theta) \quad \rightarrow \quad \begin{cases} \cos(\beta\phi) = 1 \text{ and } \cos(\alpha\theta) = -1 \\ \cos(\beta\phi) = -1 \text{ and } \cos(\alpha\theta) = 1 \end{cases}$$

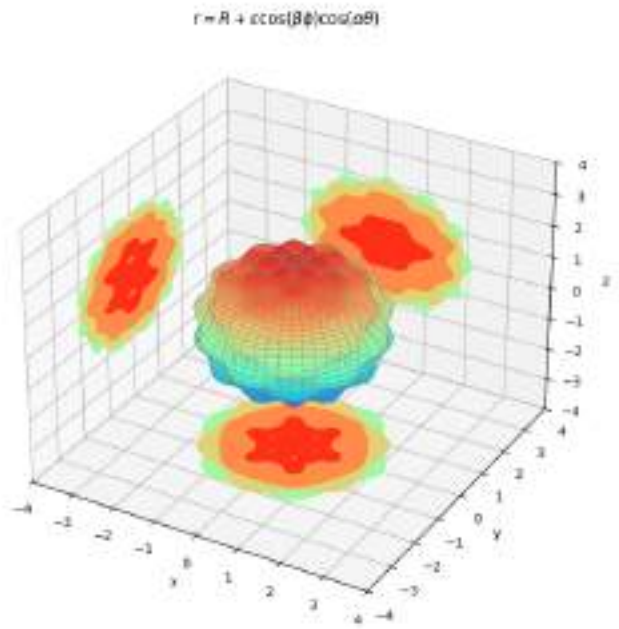

Figure 18 – Wavy spherical surface with the respective contour curves in the xy, xz, and yz planes using $R = 2$, $\varepsilon = 0.15$, $\beta = 6$, and $\alpha = 12$. The colors used are not important.

While for the intersections with $R + \varepsilon$, that is, the maximum points, we have

$$R + \varepsilon = R + \varepsilon \cos(\beta\phi)\cos(\alpha\theta) \quad \rightarrow \quad \begin{cases} \cos(\beta\phi) = 1 \text{ and } \cos(\alpha\theta) = 1 \\ \cos(\beta\phi) = -1 \text{ and } \cos(\alpha\theta) = -1 \end{cases}$$

where $\phi \in [0, 2\pi]$ and $\theta \in [0, \pi]$. Due to the impossibility of decoupling ϕ and θ, we must analyze the cosine functions geometrically in order to identify how $r(\phi, \theta)$ transitions between the surface's maxima and minima.

To do this, we analyze the functions $\cos(\beta\phi)$ and $\cos(\alpha\theta)$ separately. The first function behaves exactly as defined in the special case $\alpha = 0$, and through equation (4.50) we identify the intervals of ϕ where the transition from maximum to minimum (and vice versa) occurs. For the second function, however, the analysis must consider that the domain of θ does not cover a full period of the cosine function, since $\theta \in [0, \pi]$.

Taking into account that the function $\cos(\alpha\theta)$ has roots at $\theta' = \frac{\pi}{2\alpha} + \frac{\pi s}{\alpha}$, where $s = 1, \ldots, \alpha - 1$, it is possible to define the transition interval between the surface's maxima and minima as

$$[0,\pi]_\alpha = \left[0, \frac{\pi}{2\alpha}\right] \cup \left\{ \bigcup_{s=1}^{\alpha-1} \left[\frac{\pi}{2\alpha} + \frac{(s-1)\pi}{\alpha}, \frac{\pi}{2\alpha} + \frac{\pi s}{\alpha} \right] \right\} \cup \left[\frac{\pi}{2\alpha} + \frac{\pi(\alpha-1)}{\alpha}, \pi \right], \tag{4.74}$$

subject to

$$\begin{cases} \forall\theta \in \left(\dfrac{\pi}{2\alpha} + \dfrac{\pi(\alpha-1)}{\alpha}, \pi \right] \quad \rightarrow \quad \cos(\alpha\theta) > 0, \quad \text{when } \alpha \text{ is even} \\ \\ \forall\theta \in \left(\dfrac{\pi}{2\alpha} + \dfrac{\pi(\alpha-1)}{\alpha}, \pi \right] \quad \rightarrow \quad \cos(\alpha\theta) < 0, \quad \text{when } \alpha \text{ is odd} \end{cases} \tag{4.75}$$

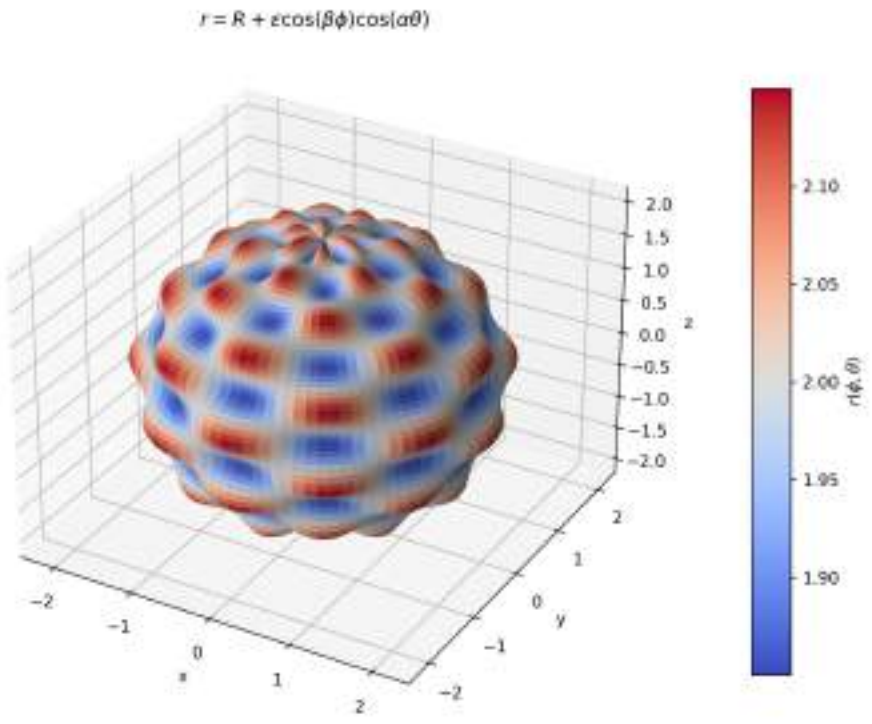

Figure 19 – Location of the surface's maxima and minima. The following values were used: $R = 2$, $\varepsilon = 0.15$, $\beta = 6$, and $\alpha = 12$.

Thus, using the same methodology applied to the case $\alpha = 0$, we can write, analogously to equation (4.54), the wave function for the general case as

$$\psi(\boldsymbol{r}) = \varphi(\boldsymbol{r}) - ik\mu \sum_{\ell=0}^{\infty} \sum_{m=-\ell}^{\ell} Y_\ell^m(\theta,\phi) \Big[R_{\ell,m}(r) j_\ell(kr) + T_{\ell,m}(r) h_\ell^{(1)}(kr) \Big] \tag{4.76}$$

where the coefficient $R_{\ell,m}$ is given, in this case, by:

$$
\begin{aligned}
R_{\ell,m} = &\left\{ \int_0^{\frac{\pi}{2\alpha}} d\theta' \left[\sum_{n=0}^{\beta-1} \int_{\frac{2n\pi}{\beta}-\phi''}^{\frac{2n\pi}{\beta}+\phi''} d\phi' \right] + \sum_{\substack{s=2,\\ s \text{ even}}}^{\alpha-1} \int_{\frac{\pi}{2\alpha}+\frac{\pi(s-1)}{\alpha}}^{\frac{\pi}{2\alpha}+\frac{\pi s}{\alpha}} d\theta' \left[\sum_{n=0}^{\beta-1} \int_{\frac{2n\pi}{\beta}-\phi''}^{\frac{2n\pi}{\beta}+\phi''} d\phi' \right] \right. \\
&+ \sum_{\substack{s=1,\\ s \text{ odd}}}^{\alpha-1} \int_{\frac{\pi}{2\alpha}+\frac{\pi(s-1)}{\alpha}}^{\frac{\pi}{2\alpha}+\frac{\pi s}{\alpha}} d\theta' \left[\sum_{n=0}^{\beta-1} \int_{\frac{2n\pi}{\beta}+\phi''}^{\frac{2(n+1)\pi}{\beta}-\phi''} d\phi' \right] \\
&\left. + \int_{\frac{\pi}{2\alpha}+\frac{2\pi(\alpha-1)}{\alpha}}^{\pi} d\theta' \left[\sum_{n=0}^{\beta-1} \int_{\frac{2n\pi}{\beta}-\phi''}^{\frac{2n\pi}{\beta}+\phi''} d\phi' \right] \right\} \times \\
&A(\phi',\theta')\gamma(\phi',\theta')h_\ell^{(1)}(kr')Y_\ell^{m*}(\theta',\phi')\psi(r',\phi',\theta'), \quad \alpha \text{ even}
\end{aligned}
\tag{4.77}
$$

$$
\begin{aligned}
R_{\ell,m} = &\left\{ \int_0^{\frac{\pi}{2\alpha}} d\theta' \left[\sum_{n=0}^{\beta-1} \int_{\frac{2n\pi}{\beta}-\phi''}^{\frac{2n\pi}{\beta}+\phi''} d\phi' \right] + \sum_{\substack{s=2,\\ s \text{ even}}}^{\alpha-1} \int_{\frac{\pi}{2\alpha}+\frac{\pi(s-1)}{\alpha}}^{\frac{\pi}{2\alpha}+\frac{\pi s}{\alpha}} d\theta' \left[\sum_{n=0}^{\beta-1} \int_{\frac{2n\pi}{\beta}-\phi''}^{\frac{2n\pi}{\beta}+\phi''} d\phi' \right] \right. \\
&+ \sum_{\substack{s=1,\\ s \text{ odd}}}^{\alpha-1} \int_{\frac{\pi}{2\alpha}+\frac{\pi(s-1)}{\alpha}}^{\frac{\pi}{2\alpha}+\frac{\pi s}{\alpha}} d\theta' \left[\sum_{n=0}^{\beta-1} \int_{\frac{2n\pi}{\beta}+\phi''}^{\frac{2(n+1)\pi}{\beta}-\phi''} d\phi' \right] \\
&\left. + \int_{\frac{\pi}{2\alpha}+\frac{2\pi(\alpha-1)}{\alpha}}^{\pi} d\theta' \left[\sum_{n=0}^{\beta-1} \int_{\frac{2n\pi}{\beta}+\phi''}^{\frac{2(n+1)\pi}{\beta}-\phi''} d\phi' \right] \right\} \times \\
&A(\phi',\theta')\gamma(\phi',\theta')h_\ell^{(1)}(kr')Y_\ell^{m*}(\theta',\phi')\psi(r',\phi',\theta'), \quad \alpha \text{ odd}
\end{aligned}
\tag{4.78}
$$

and the coefficient $T_{\ell,m}$ is given by

$$
\begin{aligned}
T_{\ell,m} = &\left\{ \int_0^{\frac{\pi}{2\alpha}} d\theta' \left[\sum_{n=0}^{\beta-1} \int_{\frac{2n\pi}{\beta}+\phi''}^{\frac{2(n+1)\pi}{\beta}-\phi''} d\phi' \right] + \sum_{\substack{s=2,\\ s \text{ even}}}^{\alpha-1} \int_{\frac{\pi}{2\alpha}+\frac{\pi(s-1)}{\alpha}}^{\frac{\pi}{2\alpha}+\frac{\pi s}{\alpha}} d\theta' \left[\sum_{n=0}^{\beta-1} \int_{\frac{2n\pi}{\beta}+\phi''}^{\frac{2(n+1)\pi}{\beta}-\phi''} d\phi' \right] \right. \\
&+ \sum_{\substack{s=1,\\ s \text{ odd}}}^{\alpha-1} \int_{\frac{\pi}{2\alpha}+\frac{\pi(s-1)}{\alpha}}^{\frac{\pi}{2\alpha}+\frac{\pi s}{\alpha}} d\theta' \left[\sum_{n=0}^{\beta-1} \int_{\frac{2n\pi}{\beta}-\phi''}^{\frac{2n\pi}{\beta}+\phi''} d\phi' \right] \\
&\left. + \int_{\frac{\pi}{2\alpha}+\frac{2\pi(\alpha-1)}{\alpha}}^{\pi} d\theta' \left[\sum_{n=0}^{\beta-1} \int_{\frac{2n\pi}{\beta}+\phi''}^{\frac{2(n+1)\pi}{\beta}-\phi''} d\phi' \right] \right\} \times \\
&A(\phi',\theta')\gamma(\phi',\theta')j_\ell(kr')Y_\ell^{m*}(\theta',\phi')\psi(r',\phi',\theta'), \quad \alpha \text{ even}
\end{aligned}
\tag{4.79}
$$

$$
\begin{aligned}
T_{\ell,m} = &\left\{ \int_0^{\frac{\pi}{2\alpha}} d\theta' \left[\sum_{n=0}^{\beta-1} \int_{\frac{2n\pi}{\beta}+\phi''}^{\frac{2(n+1)\pi}{\beta}-\phi''} d\phi' \right] + \sum_{\substack{s=2,\\ s \text{ even}}}^{\alpha-1} \int_{\frac{\pi}{2\alpha}+\frac{\pi(s-1)}{\alpha}}^{\frac{\pi}{2\alpha}+\frac{\pi s}{\alpha}} d\theta' \left[\sum_{n=0}^{\beta-1} \int_{\frac{2n\pi}{\beta}+\phi''}^{\frac{2(n+1)\pi}{\beta}-\phi''} d\phi' \right] \right. \\
&+ \sum_{\substack{s=1,\\ s \text{ odd}}}^{\alpha-1} \int_{\frac{\pi}{2\alpha}+\frac{\pi(s-1)}{\alpha}}^{\frac{\pi}{2\alpha}+\frac{\pi s}{\alpha}} d\theta' \left[\sum_{n=0}^{\beta-1} \int_{\frac{2n\pi}{\beta}+\phi''}^{\frac{2n\pi}{\beta}-\phi''} d\phi' \right] \\
&\left. + \int_{\frac{\pi}{2\alpha}+\frac{2\pi(\alpha-1)}{\alpha}}^{\pi} d\theta' \left[\sum_{n=0}^{\beta-1} \int_{\frac{2n\pi}{\beta}-\phi''}^{\frac{2n\pi}{\beta}+\phi''} d\phi' \right] \right\} \times \\
&A(\phi',\theta')\gamma(\phi',\theta')j_\ell(kr')Y_\ell^{m*}(\theta',\phi')\psi(r',\phi',\theta'), \quad \alpha \text{ odd}
\end{aligned}
\tag{4.80}
$$

where ϕ' and r' are given by

$$\phi' = \frac{1}{\beta}\arccos\left[\frac{\left(\frac{r-R}{\varepsilon}\right)}{\cos(\alpha\theta)}\right], \qquad r' = R + \varepsilon\cos(\beta\phi)\cos(\alpha\theta) \tag{4.81}$$

Analogously to the case $\alpha = 0$, we can use orthogonality properties of the basis functions to determine a system of linear equations for $R_{\ell,m}$ and $T_{\ell,m}$. In fact, defining

$$\begin{aligned}
&\left\{\int_0^{\frac{\pi}{2\alpha}} d\theta\left[\sum_{n=0}^{\beta-1}\int_{\frac{2n\pi}{\beta}-\phi'}^{\frac{2n\pi}{\beta}+\phi'} d\phi\right] + \sum_{\substack{s=2,\\ s\text{ even}}}^{\alpha-1}\int_{\frac{\pi}{2\alpha}+\frac{\pi(s-1)}{\alpha}}^{\frac{\pi}{2\alpha}+\frac{\pi s}{\alpha}} d\theta\left[\sum_{n=0}^{\beta-1}\int_{\frac{2n\pi}{\beta}-\phi'}^{\frac{2n\pi}{\beta}+\phi'} d\phi\right]\right.\\
&+ \sum_{\substack{s=1,\\ s\text{ odd}}}^{\alpha-1}\int_{\frac{\pi}{2\alpha}+\frac{\pi(s-1)}{\alpha}}^{\frac{\pi}{2\alpha}+\frac{\pi s}{\alpha}} d\theta\left[\sum_{n=0}^{\beta-1}\int_{\frac{2n\pi}{\beta}+\phi'}^{\frac{2(n+1)\pi}{\beta}-\phi'} d\phi\right]\\
&+ \int_{\frac{\pi}{2\alpha}+\frac{2\pi(\alpha-1)}{\alpha}}^{\pi} d\theta\left[\sum_{n=0}^{\beta-1}\int_{\frac{2n\pi}{\beta}+\phi'}^{\frac{2(n+1)\pi}{\beta}-\phi'} d\phi\right](\alpha \bmod 2)\\
&\left.+ \int_{\frac{\pi}{2\alpha}+\frac{2\pi(\alpha-1)}{\alpha}}^{\pi} d\theta\left[\sum_{n=0}^{\beta-1}\int_{\frac{2n\pi}{\beta}-\phi'}^{\frac{2n\pi}{\beta}+\phi'} d\phi\right](1-\alpha \bmod 2)\right\} = \left\{\int(\theta,\phi)\right\}_{R_{\ell,m}}^{\alpha,\beta}
\end{aligned} \tag{4.82}$$

and also

$$\begin{aligned}
&\left\{\int_0^{\frac{\pi}{2\alpha}} d\theta\left[\sum_{n=0}^{\beta-1}\int_{\frac{2n\pi}{\beta}+\phi'}^{\frac{2(n+1)\pi}{\beta}-\phi'} d\phi\right] + \sum_{\substack{s=2,\\ s\text{ even}}}^{\alpha-1}\int_{\frac{\pi}{2\alpha}+\frac{\pi(s-1)}{\alpha}}^{\frac{\pi}{2\alpha}+\frac{\pi s}{\alpha}} d\theta\left[\sum_{n=0}^{\beta-1}\int_{\frac{2n\pi}{\beta}+\phi'}^{\frac{2(n+1)\pi}{\beta}-\phi'} d\phi\right]\right.\\
&+ \sum_{\substack{s=1,\\ s\text{ odd}}}^{\alpha-1}\int_{\frac{\pi}{2\alpha}+\frac{\pi(s-1)}{\alpha}}^{\frac{\pi}{2\alpha}+\frac{\pi s}{\alpha}} d\theta\left[\sum_{n=0}^{\beta-1}\int_{\frac{2n\pi}{\beta}-\phi'}^{\frac{2n\pi}{\beta}+\phi'} d\phi\right]\\
&+ \int_{\frac{\pi}{2\alpha}+\frac{2\pi(\alpha-1)}{\alpha}}^{\pi} d\theta\left[\sum_{n=0}^{\beta-1}\int_{\frac{2n\pi}{\beta}-\phi'}^{\frac{2n\pi}{\beta}+\phi'} d\phi\right](\alpha \bmod 2)\\
&\left.+ \int_{\frac{\pi}{2\alpha}+\frac{2\pi(\alpha-1)}{\alpha}}^{\pi} d\theta\left[\sum_{n=0}^{\beta-1}\int_{\frac{2n\pi}{\beta}+\phi'}^{\frac{2(n+1)\pi}{\beta}-\phi'} d\phi\right](1-\alpha \bmod 2)\right\} = \left\{\int(\theta,\phi)\right\}_{T_{\ell,m}}^{\alpha,\beta}
\end{aligned} \tag{4.83}$$

Multiplying (4.76) by $A(\phi,\theta)\gamma(\phi,\theta)h_\ell^{(1)}(k(R+\varepsilon\cos(\beta\phi)\cos(\alpha\theta)))Y_{\ell'}^{*m'}(\theta,\phi)$, evaluating at $r'(\phi,\theta) = R+\varepsilon\cos(\beta\phi)\cos(\alpha\theta)$ and integrating over (4.82), for $R_{\ell,m}$ we obtain:

$$
\begin{aligned}
R_{\ell',m'}(r') =& \underbrace{\left\{\int(\theta,\phi)\right\}_{R_{\ell,m}}^{\alpha,\beta} A(\phi,\theta)\gamma(\phi,\theta)h_\ell^{(1)}(kr')Y_{\ell'}^{*m'}(\theta,\phi)\varphi(r',\phi,\theta)}_{f_{\ell',m'}^{\alpha,\beta}(r)} \\
&- ik\mu\sum_{\ell=0}^{\infty}\sum_{m=-\ell}^{\ell}\left\{\int(\theta,\phi)\right\}_{R_{\ell,m}}^{\alpha,\beta} A(\phi,\theta)\gamma(\phi,\theta)h_\ell^{(1)}(kr')Y_{\ell'}^{*m'}(\theta,\phi)Y_\ell^m(\theta,\phi) \\
&\left[R_{\ell,m}(r')j_\ell(kr') + T_{\ell,m}(r')h_\ell^{(1)}(kr')\right]
\end{aligned}
\tag{4.84}
$$

In the same way, for $T_{\ell,m}$, multiplying (4.76) by $A(\phi,\theta)\gamma(\phi,\theta)j_\ell(kr')Y_{\ell'}^{*m'}(\theta,\phi)$, evaluating at $r'(\phi,\theta) = R + \varepsilon\cos(\beta\phi)\cos(\alpha\theta)$ and integrating over (4.83), we find:

$$
\begin{aligned}
T_{\ell',m'}(r') =& \underbrace{\left\{\int(\theta,\phi)\right\}_{T_{\ell,m}}^{\alpha,\beta} A(\phi,\theta)\gamma(\phi,\theta)j_\ell(kr')Y_{\ell'}^{*m'}(\theta,\phi)\varphi(r',\phi,\theta)}_{g_{\ell',m'}^{\alpha,\beta}(r)} \\
&- ik\mu\sum_{\ell=0}^{\infty}\sum_{m=-\ell}^{\ell}\left\{\int(\theta,\phi)\right\}_{T_{\ell,m}}^{\alpha,\beta} A(\phi,\theta)\gamma(\phi,\theta)j_\ell(kr')Y_{\ell'}^{*m'}(\theta,\phi)Y_\ell^m(\theta,\phi) \\
&\left[R_{\ell,m}(r')j_\ell(kr') + T_{\ell,m}(r')h_\ell^{(1)}(kr')\right]
\end{aligned}
\tag{4.85}
$$

Following the same procedure as in the particular case $\alpha = 0$, it is desirable to obtain the equations in their differential form, so that a numerical solution can be reached. For this reason, we differentiate equations (4.84) and (4.85) with respect to r. The Leibniz rule yields:

$$
\begin{aligned}
\frac{dR_{\ell',m'}}{dr} =& \frac{df_{\ell',m'}^{\alpha,\beta}}{dr} - ik\mu\frac{h_{\ell'}^{(1)}(kr)}{\sqrt{1-[\mu(r,\theta)]^2}} \\
&\sum_{\ell=0}^{\infty}\left\{\int\right\}_{\partial_r R_{\ell,m'}}^{\alpha,\beta} A(\phi',\theta)\gamma(\phi',\theta)P_\ell^{m'+q\beta}P_{\ell'}(\cos\theta)P_{\ell'}^{m'}(\cos\theta)\times \\
&\left[R_{\ell,m'}(r)j_\ell(kr) + T_{\ell,m'}(r)h_\ell^{(1)}(kr)\right], \qquad q\in\mathbb{Z}
\end{aligned}
\tag{4.86}
$$

$$
\begin{aligned}
\frac{dT_{\ell',m'}}{dr} =& \frac{dg_{\ell',m'}^{\alpha,\beta}}{dr} - ik\mu\frac{j_{\ell'}(kr')}{\sqrt{1-[\mu(r,\theta)]^2}} \\
&\sum_{\ell=0}^{\infty}\left\{\int\right\}_{\partial_r T_{\ell,m'}}^{\alpha,\beta} A(\phi',\theta)\gamma(\phi',\theta)P_\ell^{m'+q\beta}P_{\ell'}(\cos\theta)P_{\ell'}^{m'}(\cos\theta)\times \\
&\left[R_{\ell,m'}(r)j_\ell(kr) + T_{\ell,m'}(r)h_\ell^{(1)}(kr)\right], \qquad q\in\mathbb{Z}
\end{aligned}
\tag{4.87}
$$

where we define

$$\mu(r,\theta) = \frac{\frac{(r-R)}{\varepsilon}}{\cos(\alpha\theta)}, \qquad \phi' = \frac{1}{\beta}\arccos\left[\mu(r,\theta)\right] \tag{4.88}$$

The terms related to the integrals, using the results from Appendix A, are given by:

$$\begin{aligned}\left\{\int\right\}^{\alpha,\beta}_{\partial_r R_{\ell,m'}} = \Bigg\{ & \int_0^{\frac{\pi}{2\alpha}} \left[-2iU_{q-1}(\mu(r,\theta))\sqrt{1-(\mu(r,\theta))^2}\right] d\theta + \\ & \sum_{\substack{s=2,\\ s \text{ even}}}^{\alpha-1} \int_{\frac{\pi}{2\alpha}+\frac{\pi(s-1)}{\alpha}}^{\frac{\pi}{2\alpha}+\frac{\pi s}{\alpha}} \left[-2iU_{q-1}(\mu(r,\theta))\sqrt{1-(\mu(r,\theta))^2}\right] d\theta + \\ & \sum_{\substack{s=1,\\ s \text{ odd}}}^{\alpha-1} \int_{\frac{\pi}{2\alpha}+\frac{\pi(s-1)}{\alpha}}^{\frac{\pi}{2\alpha}+\frac{\pi s}{\alpha}} W_q(\mu(r,\theta)) d\theta + \\ & \int_{\frac{\pi}{2\alpha}+\frac{2\pi(\alpha-1)}{\alpha}}^{\pi} W_q(\mu(r,\theta)) d\theta (\alpha \bmod 2) + \\ & \int_{\frac{\pi}{2\alpha}+\frac{2\pi(\alpha-1)}{\alpha}}^{\pi} \left[-2iU_{q-1}(\mu(r,\theta))\sqrt{1-(\mu(r,\theta))^2}\right] d\theta (1-\alpha \bmod 2) \Bigg\}\end{aligned} \tag{4.89}$$

$$\begin{aligned}\left\{\int\right\}^{\alpha,\beta}_{\partial_r T_{\ell,m'}} = \Bigg\{ & \int_0^{\frac{\pi}{2\alpha}} W_q(\mu(r,\theta)) d\theta + \sum_{\substack{s=2,\\ s \text{ even}}}^{\alpha-1} \int_{\frac{\pi}{2\alpha}+\frac{\pi(s-1)}{\alpha}}^{\frac{\pi}{2\alpha}+\frac{\pi s}{\alpha}} W_q(\mu(r,\theta)) d\theta + \\ & \sum_{\substack{s=1,\\ s \text{ odd}}}^{\alpha-1} \int_{\frac{\pi}{2\alpha}+\frac{\pi(s-1)}{\alpha}}^{\frac{\pi}{2\alpha}+\frac{\pi s}{\alpha}} \left[-2iU_{q-1}(\mu(r,\theta))\sqrt{1-(\mu(r,\theta))^2}\right] d\theta + \\ & \int_{\frac{\pi}{2\alpha}+\frac{2\pi(\alpha-1)}{\alpha}}^{\pi} \left[-2iU_{q-1}(\mu(r,\theta))\sqrt{1-(\mu(r,\theta))^2}\right] d\theta (\alpha \bmod 2) + \\ & \int_{\frac{\pi}{2\alpha}+\frac{2\pi(\alpha-1)}{\alpha}}^{\pi} \left[-2iU_{q-1}(\mu(r,\theta))\sqrt{1-(\mu(r,\theta))^2}\right] d\theta (1-\alpha \bmod 2) \Bigg\}\end{aligned} \tag{4.90}$$

where

$$W_q(\mu(r,\theta)) = \begin{cases} 2iU_{q-1}(\mu(r,\theta))\sqrt{1-[\mu(r,\theta)]^2}, & q \text{ even} \\ -2T_q(\mu(r,\theta)), & q \text{ odd} \end{cases} \tag{4.91}$$

and T_q and U_{q-1} are the Chebyshev polynomials of first and second kind, respectively.

Once again, the pair of equations (4.86) and (4.87) forms a system of coupled differential equations that, when solved, provides the wave function solution valid in the domain $R-\varepsilon \leq r \leq R+\varepsilon$.

As same as before, for the domain $r \leq R-\varepsilon$, note that the Hankel function $h_\ell^{(1)}(kr)$ is singular at the origin, and therefore we must take $T_{\ell,m} = 0$ for a physically plausible solution. Using equation (4.76), the wave equation in this domain is then given by:

$$\psi(\boldsymbol{r}) = \varphi(\boldsymbol{r}) - ik\mu \sum_{\ell=0}^{\infty} \sum_{m=-\ell}^{\ell} Y_\ell^m(\theta,\phi)\lambda_{\ell,m} j_\ell(kr) \tag{4.92}$$

where the coefficient $\lambda_{\ell,m}$ is a constant to be determined, given by

$$\lambda_{\ell,m} = \int_0^{2\pi} \int_0^{\pi} d\phi' d\theta' \gamma(\phi',\theta') A(\phi',\theta') h_\ell^{(1)}(k(R-\varepsilon)) Y_\ell^{*m}(\theta',\phi') \psi(r',\phi',\theta') \tag{4.93}$$

Also, for the domain $r > R + \varepsilon$, the spherical Bessel function diverges at infinity, and therefore we take $R_{\ell,m} = 0$ for a physically plausible solution in this case. Thus, we have:

$$\psi(\boldsymbol{r}) = \varphi(\boldsymbol{r}) - ik\mu \sum_{\ell=0}^{\infty} \sum_{m=-\ell}^{\ell} Y_\ell^m(\theta,\phi)\omega_{\ell,m} h_\ell^{(1)}(kr) \tag{4.94}$$

where the coefficient $\omega_{\ell,m}$ is also a constant to be determined, given by

$$\omega_{\ell,m} = \int_0^{2\pi} \int_0^{\pi} d\phi' d\theta' \gamma(\phi',\theta') A(\phi',\theta') j_\ell(k(R+\varepsilon)) Y_\ell^{*m}(\theta',\phi') \psi(r',\phi',\theta') \tag{4.95}$$

Once again, we will have a superposition of standing waves originating from the interaction of the wave with multiple reflections generated inside the barrier, in addition to a superposition of so-called propagating waves. Analogously to the case $\alpha = 0$, in both cases, $\psi(r',\phi',\theta')$ represents the wave function evaluated under the potential barrier (PEREIRA; CUNHA; SCHMIDT, 2024).

It is intuitive to note that, in both cases ($\alpha = 0$ and $\alpha \neq 0$), the expressions for the coefficients $\lambda_{\ell,m}$ and $\omega_{\ell,m}$ are the same. This is an expected result, since both cases describe scattering by the same surface, with the exception of more specific characteristics in the general case ($\alpha \neq 0$). However, it is important to note that the values of ϕ' change when we consider $\alpha \neq 0$, which can be observed by comparing equations (4.49) and (4.81). This change is, essentially, what distinguishes the coefficients in each case.

To determine the connection between the position-dependent functions $R_{\ell,m}(r)$ and $T_{\ell,m}(r)$ and the coefficients $\lambda_{\ell,m}$ and $\omega_{\ell,m}$, we use the same boundary conditions as in the case $\alpha = 0$, where we have, from the continuity of the wave function,

$$\lambda_{\ell,m} j_\ell(k(R-\varepsilon)) = R_{\ell,m}(R-\varepsilon) j_\ell(k(R-\varepsilon)) + T_{\ell,m}(R-\varepsilon) h_\ell^{(1)}(k(R-\varepsilon)),$$

$$\omega_{\ell,m} h_\ell^{(1)}(k(R+\varepsilon)) = R_{\ell,m}(R+\varepsilon) j_\ell(k(R+\varepsilon)) + T_{\ell,m}(R+\varepsilon) h_\ell^{(1)}(k(R+\varepsilon)).$$

By comparing the real and imaginary parts, we conclude that

$$\lambda_{\ell,m} = R_{\ell,m}(R-\varepsilon), \tag{4.96}$$

$$\omega_{\ell,m} = T_{\ell,m}(R+\varepsilon). \tag{4.97}$$

Thus, we define two new position-dependent functions, named $\tilde{R}_{\ell,m}(r)$ and $\tilde{T}_{\ell,m}(r)$, which represent the full solution of the Lippmann-Schwinger equation (4.43):

$$\psi(\boldsymbol{r}) = \varphi(\boldsymbol{r}) - ik\sum_{\ell=0}^{\infty}\sum_{m=-\ell}^{\ell} Y_\ell^m(\theta,\phi)\left[\tilde{R}_{\ell,m}(r)j_\ell(kr) + \tilde{T}_{\ell,m}(r)h_\ell^{(1)}(kr)\right] \tag{4.98}$$

where,

$$\tilde{R}_{\ell,m}(r) = \begin{cases} R_{\ell,m}(R-\varepsilon), & r < R-\varepsilon, \\ R_{\ell,m}(r), & R-\varepsilon \le r \le R+\varepsilon, \\ 0, & r > R+\varepsilon, \end{cases} \tag{4.99}$$

and

$$\tilde{T}_{\ell,m}(r) = \begin{cases} 0, & r < R-\varepsilon, \\ T_{\ell,m}(r), & R-\varepsilon \le r \le R+\varepsilon, \\ T_{\ell,m}(R+\varepsilon), & r > R+\varepsilon. \end{cases} \tag{4.100}$$

are functions computed through the differential equation system (4.86) and (4.87).

4.2.3 Scattering Amplitude and Physical Quantities

The scattering amplitude, in both cases, is given by:

$$f(\phi,\theta) = \mu\sum_{\ell=0}^{\infty}\sum_{m=-\ell}^{\ell}(-i)^\ell Y_\ell^m(\theta,\phi)T_{\ell,m}(R+\varepsilon) \tag{4.101}$$

with the caveat of the definition of ϕ', which introduces intrinsic changes in the computation of $T_{\ell,m}$ for each case ($\alpha = 0$ and $\alpha \neq 0$). Therefore, the differential and total cross-sections, are given by:

$$\begin{aligned}\frac{d\sigma}{d\Omega} = |f(\phi,\theta)|^2 = \mu^2\sum_{\ell,m}\sum_{\ell',m'}(-i)^\ell(+i)^{\ell'}(-1)^{m'} \\ Y_\ell^m(\theta,\phi)Y_{\ell'}^{-m'}(\theta,\phi)\left|T_{\ell,m}(R+\varepsilon)\right|^2\end{aligned} \tag{4.102}$$

$$\sigma_{total} = \int\frac{d\sigma}{d\Omega}d\Omega = \mu^2\sum_{\ell=0}^{\infty}\sum_{m=-\ell}^{\ell}\left|T_{\ell,m}(R+\varepsilon)\right|^2 \tag{4.103}$$

remembering that the definition of $T_{\ell,m}$ changes in each case ($\alpha = 0$ and $\alpha \neq 0$).

Observe that for $r > R + \varepsilon$ the surface's maxima and minima no longer intersect. Consequently, all the special treatments we introduced to define $r_<$ and $r_>$, and to integrate correctly in spherical coordinates, can be replaced by the standard solid-angle integration. Therefore, the equation (4.79) reduces to

$$T_{\ell,m}(R+\epsilon) = \int_0^{2\pi}\int_0^{\pi} A(\phi,\theta)\gamma(\phi,\theta)j_\ell(k(R+\varepsilon)))Y_\ell^{m*}(\theta,\phi)\psi(R+\varepsilon,\phi,\theta)d\theta d\phi \quad (4.104)$$

To evaluate the coefficient $T_{\ell,m}(R+\epsilon)$ we can also use the simplified version of the equation (4.85),

$$\begin{aligned} T_{\ell',m'}(R+\varepsilon) = & \underbrace{\int_0^{2\pi}\int_0^{\pi} A(\phi,\theta)\gamma(\phi,\theta)j_{\ell'}(k(R+\varepsilon))Y_{\ell'}^{*m'}(\theta,\phi)\varphi((R+\varepsilon),\phi,\theta)d\theta d\phi}_{g^{\alpha,\beta}_{\ell',m'}} \\ & - ik\mu\sum_{\ell=0}^{\infty}\sum_{m=-\ell}^{\ell} T_{\ell,m}(R+\epsilon)h_\ell^{(1)}(k(R+\varepsilon)))j_\ell(k(R+\varepsilon)) \\ & \int_0^{2\pi}\int_0^{\pi} A(\phi,\theta)\gamma(\phi,\theta)Y_{\ell'}^{*m'}(\theta,\phi)Y_\ell^m(\theta,\phi)d\theta d\phi \end{aligned} \quad (4.105)$$

which yields a system of equations that can be solved using numerical methods.

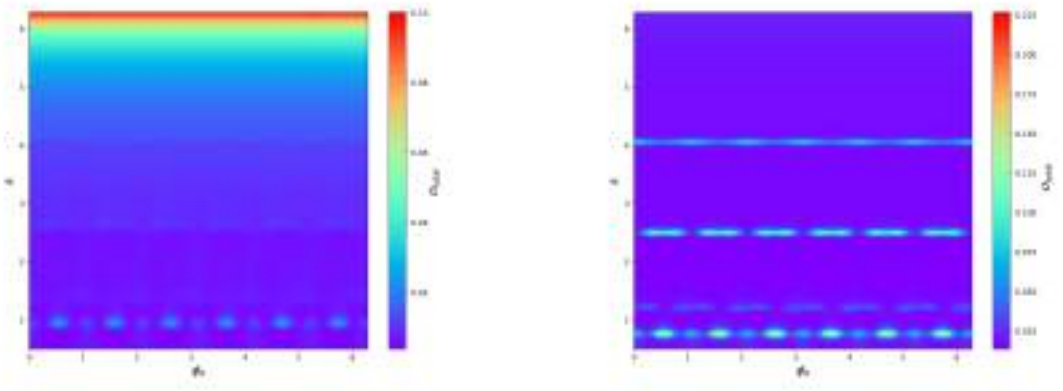

Figure 20 – Total cross-section for the scattering of a plane wave with wavenumber k and incident angle ϕ_0. Here, we also use $\theta_0 = \pi/2$ and the parameters $\alpha = 0$, $\beta = 6$, $\varepsilon = 0.1$, $R = 1.0$ and a constant coupling strength $\gamma = 50$ (left) and $\gamma = -50$ (right).

In figure 20 we present a density plot for the total cross-section of a plane wave scattered by a wavy sphere with $\alpha = 0$ and $\beta = 6$, using $\varepsilon = 0.1$ and a constant coupling strength. We notice that the symmetry of wavy surface is manifested in the figure, providing certain directions which maximize the cross-section. For some values of k we have local maxima points, in both figures, that represents incident waves that hits the barrier and then are scattered. For an attractive potential $\gamma < 0$, we can notice that other values of k represents waves that can penetrate the barrier and then suffers multiple scattering within

the barrier and cannot escape. For an repulsive potential $\gamma > 0$, this still happen, but when k increase, e.g, $k \approx 2\pi$, the wavelength becomes small and then the incident wave passes through the barrier without necessarily interacting with it.

This behavior is expected, since it also happens in the similar two-dimensional problem (PEREIRA; CUNHA; SCHMIDT, 2024). So we can conclude that for barriers with this kind of surface symmetry will provide certain directions which maximize the cross-section, enhanced the scattering process.

5 Conclusions

In this work, we study the definition and construction of Green's Functions and how these mathematical objects connect to differential operators. In this context, we developed a bilinear expansion of the Green's Function in three spatial dimensions, applied to spherical coordinates. This expansion was then used in an application involving quantum scattering phenomena. The quantum scattering problem was formulated from the perspective of the Lippmann-Schwinger equation, through which we analyzed key quantities related to the problem, such as the scattering cross-section and the quantum refractive index. This formulation was applied to two problems of similar nature, where plane waves were scattered by boundary wall type spherical potential barriers(LUZ; LUPU-SAX; HELLER, 1997).

The first and simpler problem involved a smooth spherical barrier. We detailed the methodology used and analyzed two cases: one where the coupling strength of the barrier is constant, and another where we modeled an oscillatory behavior on the barrier through a position-dependent coupling strength, which we called Wavy Coupling, that can be used to model roughness or porosity. The second and more challenging problem focused on modeling a surface with imperfections (or roughness) through the definition of a rippled sphere, which we referred to as the Wavy Sphere.

In the first problem, we developed analytical solutions for the Lippmann-Schwinger equation in both cases. We also studied the physical quantities of the scattering process, such as the cross-section and the quantum refractive index, for various problem parameters.

In the second problem, due to the nature of the kernel in the integral equation, it was not possible to find an analytical solution. However, we developed a methodology capable of transforming the coupled integral equation system into a coupled differential equation system, which provides numerical solutions with better convergence. In this case, we also analyzed the related physical quantities for different initial configurations of the problem.

The methodology developed in this work proved to be effective in characterizing and analyzing this type of scattering phenomenon. In both problems addressed, the results allowed us to draw parallels with the important physical properties, demonstrating the effectiveness of this approach for modeling scattering phenomena of this type of target object. Furthermore, the methodology presented can be extended to other problems of the same nature, in higher spatial dimensions(SCHMIDT; PEREIRA, 2023), and is not limited to Euclidean spaces(JESUS; MAIOLI; SCHMIDT, 2021).

Therefore, there are possibilities for continuing this work. For example, instead

of using a methodology based on plane wave incidence, one could study the behavior of these problems under the incidence of wave packets. Other directions include the addition of multiple barriers centered at different points in space, leading to multiple scattering phenomena and even more complex configurations. Last but not least, there are possibilities to study this same problem in a opposite perspective, i.e, the inverse scattering phenomena, using an approach based on neural networks to capture the patterns of different configures of the potential operator(MAIOLI, 2020).

References

ABLOWITZ, M. J.; FOKAS, A. S. *Complex variables: introduction and applications*. [S.l.]: Cambridge University Press, 2003. Cited on page 42.

ABRAMOWITZ, M.; STEGUN, I. A. *Handbook of mathematical functions with formulas, graphs, and mathematical tables*. [S.l.]: US Government printing office, 1948. v. 55. Cited on page 52.

AL, E. A. et. Glory and resonance effects in the index of refraction for atomic waves. *Europhysics Letters*, v. 37, n. 4, p. 311, 1997. Cited on page 45.

ARFKEN, G. B.; WEBER, H. J. *Mathematical methods for physicists*. [S.l.]: American Association of Physics Teachers, 1999. Cited 5 times on pages 33, 44, 48, 53, and 55.

AUDOUARD, E.; DUPLAA, P.; VIGUÉ, J. Glory and resonance effects in the index of refraction for atomic waves. *EPL (Europhysics Letters)*, IOP Publishing, v. 32, n. 5, p. 397, 1995. Cited on page 45.

AZADO, P. C.; MAIOLI, A. C.; SCHMIDT, A. G. M. Quantum scattering by a spherical barrier with an arbitrary coupling strength. *Physica Scripta*, IOP Publishing, v. 96, n. 8, p. 085205, 2021. Cited 3 times on pages 32, 50, and 55.

BARATA, J. C. A. *Notas para um curso de Física-Matemática*. [S.l.]: Departamento de Física Matemática, USP, 2020. Cited on page 23.

BELKIC, D. *Principles of Quantum Scattering Theory*. [S.l.]: Institute of Physics Publishing, 2004. Cited on page 14.

BOHR, N. *Phil. Mag* ***25*** *10*, 1913. Cited on page 14.

BUTKOV, E. *Mathematical Physics*. 1ed. ed. [S.l.]: Addison-Wesley Educational Publisher, 1968. Cited 4 times on pages 19, 23, 27, and 30.

CHAMPENOIS, C. et al. Index of refraction of gases for matter waves: Effect of the motion of the gas particles on the calculation of the index. *Physical Review A*, APS, v. 77, n. 1, p. 013621, 2008. Cited 2 times on pages 16 and 45.

CHEN, Y.-J.; LEE, C.-C.; CHEN, S.-H.; FLORY, F. Extra high reflection coating with negative extinction coefficient. *Optics letters*, Optical Society of America, v. 38, n. 17, p. 3377–3379, 2013. Cited on page 56.

CHIANG, W.-S.; GEORGI, D.; YILDIRIM, T.; CHEN, J.-H.; LIU, Y. A non-invasive method to directly quantify surface heterogeneity of porous materials. *Nature communications*, Nature Publishing Group UK London, v. 9, n. 1, p. 784, 2018. Cited on page 14.

COHEN-TANNOUDJI, C.; DIU, B.; LALOE, F. Quantum mechanics, volume 1. *Quantum Mechanics*, v. 1, p. 898, 1986. Cited on page 37.

DUFFY, D. G. *Green's Functions with Applications*. 2ed. ed. [S.l.]: Chapman and Hall, 2015. Cited 3 times on pages 27, 28, and 29.

E., R. *Phil. Mag* ***21*** *669*, 1911. Cited 2 times on pages 14 and 36.

FOLDY, L. L. The multiple scattering of waves. i. general theory of isotropic scattering by randomly distributed scatterers. *Physical review*, APS, v. 67, n. 3-4, p. 107, 1945. Cited on page 44.

FOLLAND, G. B. *Fourier Analysis and its Applications*. [S.l.]: University of Washington, 1992. Cited on page 18.

FORREY, R. C.; YOU, L.; KHARCHENKO, V.; DALGARNO, A. Index of refraction of noble gases for sodium matter waves. *Physical Review A*, APS, v. 54, n. 3, p. 2180, 1996. Cited on page 45.

FRANCK, F.; HERTZ, G. *Verhandl. Deut. Phys. Ges.* ***16*** *459*, 1914. Cited on page 14.

GOLDBERGER, M. L.; WATSON, K. M. *Collision Theory*. 3ed. ed. [S.l.]: Wiley, 1967. Cited on page 42.

GONIS, A.; BUTLER, W. H. *Multiple Scattering in Solids*. [S.l.]: Springer, 2000. Cited 3 times on pages 17, 40, and 41.

GOTTFRIED, K. *Quantum mechanics: fundamentals*. [S.l.]: CRC Press, 2018. Cited on page 49.

GRADSHTEYN, I. S.; RYZHIK, I. M. *Table of integrals, series, and products*. [S.l.]: Academic press, 2014. Cited on page 52.

GRIER, D. A. Irene stegun, the handbook of mathematical functions, and the lingering influence of the new deal. *The American Mathematical Monthly*, Taylor & Francis, v. 113, n. 7, p. 585–597, 2006. Cited on page 52.

GRIFFITHS, D. J.; SCHROETER, D. F. *Introduction to Quantum Mechanics*. 3ed. ed. [S.l.]: Cambridge University Press, 2018. Cited 2 times on pages 30 and 43.

GU, S.; LAN, C. Q. Biosorption of heavy metal ions by green alga neochloris oleoabundans: Effects of metal ion properties and cell wall structure. *Journal of Hazardous Materials*, v. 418, p. 126336, 2021. ISSN 0304-3894. Disponível em: <https://www.sciencedirect.com/science/article/pii/S0304389421013005>. Cited 2 times on pages 9 and 15.

HAUKSBEE, F. Vi. a description of the apparatus for making experiments on the refractions of fluids: with a table of the specifick gravities, angles of observations, and ratio of refractions of several fluids. *Philosophical Transactions of the Royal Society of London*, The Royal Society London, v. 27, n. 328, p. 204–207, 1710. Cited on page 44.

HERMANSSON, P.; FORSSELL, G.; FAGERSTROM, J. A review of models for scattering from rough surfaces. *Linköping: FOI-Swedish Defence Research Agency*, 2003. Cited on page 14.

HÖRMANDER, L. *The Analysis of Linear Partial Differential Operators I: Distribution Theory and Fourier Analysis*. Springer Berlin Heidelberg, 2015. (Classics in Mathematics). ISBN 9783642614972. Disponível em: <https://books.google.fr/books?id=aaLrCAAAQBAJ>. Cited on page 21.

JESUS, A. L. de; MAIOLI, A. C.; SCHMIDT, A. G. M. Scattering in the poincaré disk and in the poincaré upper half-plane. *Physica Scripta*, IOP Publishing, v. 96, n. 12, p. 125264, 2021. Cited on page 80.

JOACHAIN, C. J. *Quantum Collision Theory*. [S.l.]: Elsevier Science Ltd, 1979. Cited on page 43.

JOSE, J. V.; SALETAN, E. J. *Classical Dynamics*. [S.l.]: Cambridge University Press, 1998. Cited on page 36.

KAHNERT, M.; NOUSIAINEN, T.; LINDQVIST, H. Model particles in atmospheric optics. *Journal of Quantitative Spectroscopy and Radiative Transfer*, Elsevier, v. 146, p. 41–58, 2014. Cited 2 times on pages 9 and 15.

KAHNERT, M.; NOUSIAINEN, T.; LINDQVIST, H. Model particles in atmospheric optics. *Journal of Quantitative Spectroscopy and Radiative Transfer*, Elsevier, v. 146, p. 41–58, 2014. Cited on page 15.

LANDIM, E. O. A.; RODRIGUES, A. F. Espalhamento elétron-pósitron. *Revista Brasileira de Ensino de Fisica*, SciELO Brasil, v. 44, p. e20210338, 2022. Cited 2 times on pages 40 and 41.

LAX, M. Multiple scattering of waves. *Reviews of Modern Physics*, APS, v. 23, n. 4, p. 287, 1951. Cited on page 44.

LAZAREVICH, A. K.; THOMAS, M. E.; DUNCAN, D. D.; MITCHELL, C. A. Determination of bacterial aerosol spectral cross sections. In: SPIE. *Chemical and Biological Sensing V*. [S.l.], 2004. v. 5416, p. 194–201. Cited on page 15.

LEÓN-PÉREZ, F. de; BRUCOLI, G.; GARCÍA-VIDAL, F.; MARTÍN-MORENO, L. Theory on the scattering of light and surface plasmon polaritons by arrays of holes and dimples in a metal film. *New Journal of Physics*, IOP Publishing, v. 10, n. 10, p. 105017, 2008. Cited on page 14.

LIPPMANN, B.; SCHWINGER, J. *Phys. Rev.* ***79*** *469*, 1950. Cited 2 times on pages 14 and 61.

LUZ, M. D.; LUPU-SAX, A.; HELLER, E. Quantum scattering from arbitrary boundaries. *Physical Review E*, APS, v. 56, n. 3, p. 2496, 1997. Cited 2 times on pages 47 and 80.

MAIOLI, A. C. Deep learning regression for inverse quantum scattering. *arXiv preprint arXiv:2009.09944*, 2020. Cited on page 81.

MAIOLI, A. C.; SCHMIDT, A. G. M. *J. Math. Phys.* ***59*** *122102*, 2018. Cited 2 times on pages 14 and 50.

MISHCHENKO, M. I.; LACIS, A. A. Morphology-dependent resonances of nearly spherical particles in random orientation. *Appl. Opt.*, Optica Publishing Group, v. 42, n. 27, p. 5551–5556, Sep 2003. Disponível em: <https://opg.optica.org/ao/abstract.cfm?URI=ao-42-27-5551>. Cited on page 15.

MISHCHENKO, M. I.; TRAVIS, L. D. Capabilities and limitations of a current fortran implementation of the t-matrix method for randomly oriented, rotationally symmetric scatterers. *Journal of Quantitative Spectroscopy and Radiative Transfer*, Elsevier, v. 60, n. 3, p. 309–324, 1998. Cited on page 15.

MOON, P.; SPENCER, D. E. Separability conditions for the laplace and helmholtz equations. *Journal of the Franklin Institute*, Citeseer, v. 253, n. 6, p. 585–600, 1952. Cited on page 31.

MORSE, P. M.; FESHBACH, H. *Methods of theoretical physics*. [S.l.]: Technology Press, 1946. Cited on page 31.

MULLER, M. E. A note on a method for generating points uniformly on n-dimensional spheres. *Communications of the ACM*, ACM New York, NY, USA, v. 2, n. 4, p. 19–20, 1959. Cited on page 51.

NEWTON, I. *Opticks, or, a treatise of the reflections, refractions, inflections & colours of light*. [S.l.: s.n.], 1730. Cited on page 44.

OLIVEIRA, J. V. J. e E. C. de. *Métodos Matemáticos, vol 3*. [S.l.]: Editora Unicamp, 2016. Cited 2 times on pages 18 and 19.

PEREIRA, M. E.; CUNHA, P. H.; SCHMIDT, A. G. Quantum scattering in a wavy circle. *Physica E: Low-dimensional Systems and Nanostructures*, Elsevier, v. 161, p. 115965, 2024. Cited 3 times on pages 68, 76, and 79.

PINSKER, F. Multiple scattering induced negative refraction of matter waves. *Scientific Reports*, Nature Publishing Group, v. 6, n. 1, p. 1–9, 2016. Cited on page 56.

PRUVOST, J.; VOOREN, G. V.; GOUIC, B. L.; COUZINET-MOSSION, A.; LEGRAND, J. Systematic investigation of biomass and lipid productivity by microalgae in photobioreactors for biodiesel application. *Bioresource technology*, Elsevier, v. 102, n. 1, p. 150–158, 2011. Cited on page 15.

PéREZ, D. E. Distribution Theory and Fundamental Solutions of Differential Operators. Final Degree Dissertation. Universidad del País Vasco, 2015. Cited 3 times on pages 17, 21, and 41.

SAKURAI, J. J.; NAPOLITANO, J. *Modern Quantum Mechanics*. 2ed. ed. [S.l.]: Cambridge University Press, 2017. Cited 4 times on pages 37, 42, 43, and 45.

SCHMIDT, A. G.; PEREIRA, M. E. Quantum refractive index for two-and three-dimensional systems. *Annals of Physics*, Elsevier, v. 452, p. 169273, 2023. Cited 2 times on pages 56 and 80.

SMITH, E. T.; RUBENSTEIN, R. A.; KOKOROWSKI, D. A.; PRITCHARD, D. E. Matter-wave index of refraction, inertial sensing, and quantum decoherence in an atom interferometer. *Brazilian Journal of Physics*, v. 27, n. 2, p. 193, 1997. Cited on page 45.

TAYLOR, J. R. *Classical Mechanics*. [S.l.]: University Science Books, 2004. Cited on page 35.

TRIFONOV, D. Nist handbook of mathematical functions by frank wj olver, daniel w. lozier, ronald f. boisvert and charles w. clark. 2011. Cited on page 53.

VACCHINI, B.; HORNBERGER, K. Quantum linear boltzmann equation. *Physics Reports*, Elsevier, v. 478, n. 4-6, p. 71–120, 2009. Cited on page 45.

VAZ, J. M.; OLIVEIRA, E. C. de. *Métodos matemáticos*. [S.l.], 2016. Cited on page 18.

VIGUÉ, J. Index of refraction of dilute matter in atomic interferometry. *Physical Review A*, APS, v. 52, n. 5, p. 3973, 1995. Cited on page 45.

WOLF, A.; TERHEIDEN, B.; BRENDEL, R. Light scattering and diffuse light propagation in sintered porous silicon. *Journal of applied physics*, AIP Publishing, v. 104, n. 3, 2008. Cited on page 14.

YOUNG, T. *A course of lectures on natural philosophy and the mechanical arts*. [S.l.]: Taylor and Walton, 1845. v. 1. Cited on page 44.

ZANETTI, F.; VICENTINI, E.; LUZ, M. da. Eigenstates and scattering solutions for billiard problems: A boundary wall approach. *Annals of Physics*, Elsevier, v. 323, n. 7, p. 1644–1676, 2008. Cited on page 14.

ZHU, Y. et al. Persisting volcanic ash particles impact stratospheric so2 lifetime and aerosol optical properties. *Nature communications*, Nature Publishing Group UK London, v. 11, n. 1, p. 4526, 2020. Cited on page 15.

APPENDIX A – Expansion of the Coupling γ in Spherical Harmonics

The coupling function $\gamma(\phi, \theta)$ we wish to expand is a wavy coupling expressed as:

$$\gamma(\phi, \theta) = \gamma_0 + \eta \cos(\beta\phi) \cos(\alpha\theta) \tag{A.1}$$

The azimuthal dependence in the spherical harmonics is given by $e^{im\phi}$. Using Euler's formula, we can write:

$$\cos(\beta\phi) = \frac{e^{i\beta\phi} + e^{-i\beta\phi}}{2}.$$

This implies that only the terms with $m = \pm\beta$ in Y_ℓ^m will be non-zero.

The polar angle dependence in spherical harmonics is given by the associated Legendre polynomials $P_\ell^m(\cos\theta)$. To decompose $\cos(\alpha\theta)$, we use the fact that it can be expanded as:

$$\cos(\alpha\theta) = \sum_{\ell=|\beta|}^{\infty} c_\ell P_\ell^\beta(\cos\theta),$$

where $P_\ell^0(x)$ are the Legendre polynomials of degree ℓ, and the coefficients c_ℓ are determined by orthogonality:

$$c_\ell = \frac{2\ell+1}{2} \frac{(l-\beta)!}{(l+\beta)!} \int_0^\pi \cos(\alpha\theta) P_\ell^\beta(\cos(\theta)) \sin\theta d\theta$$

which is the standard procedure for Fourier-Legendre series. The spherical harmonics $Y_\ell^m(\theta, \phi)$ are defined as:

$$Y_\ell^m(\theta, \phi) = N_\ell^m P_\ell^m(\cos\theta) e^{im\phi},$$

where N_ℓ^m is a normalization constant.

Combining the expressions for $\cos(\beta\phi)$ and $\cos(\alpha\theta)$, we obtain:

$$\cos(\beta\phi)\cos(\alpha\theta) = \frac{1}{2}\left(e^{i\beta\phi} + e^{-i\beta\phi}\right) \sum_{\ell=0}^{\infty} c_\ell P_\ell^\beta(\cos\theta).$$

we can rewrite this as:

$$\cos(\beta\phi)\cos(\alpha\theta) = \frac{1}{2}\sum_{\ell=|\beta|}^{\infty} c_\ell P_\ell^\beta(\cos\theta) e^{i\beta\phi} + \frac{1}{2}\sum_{\ell=|\beta|}^{\infty} c_\ell P_\ell^{-\beta}(\cos\theta) e^{-i\beta\phi}.$$

The terms $e^{i\beta\phi}$ and $e^{-i\beta\phi}$ correspond, respectively, to the spherical harmonics with $m = \beta$ and $m = -\beta$. Therefore, the expression can be written as:

$$\cos(\beta\phi)\cos(\alpha\theta) = \frac{1}{2}\sum_{\ell=|\beta|}^{\infty} c_\ell N_\ell^\beta P_\ell^\beta(\cos\theta) e^{i\beta\phi} + \frac{1}{2}\sum_{\ell=|\beta|}^{\infty} c_\ell N_\ell^{-\beta} P_\ell^{-\beta}(\cos\theta) e^{-i\beta\phi}.$$

$$\begin{aligned}\cos(\beta\phi)\cos(\alpha\theta) &= \frac{1}{2}\sum_{\ell=|\beta|}^{\infty} c_\ell Y_\ell^{\beta}(\theta,\phi) + \frac{1}{2}\sum_{\ell=|\beta|}^{\infty} c_\ell Y_\ell^{-\beta}(\theta,\phi) \\ &= \frac{1}{2}\left[\sum_{\ell=|\beta|} c_\ell \left(Y_\ell^{\beta}(\theta,\phi) + Y_\ell^{-\beta}(\theta,\phi)\right)\right]\end{aligned} \tag{A.2}$$

Since we have the constraint $|\beta| \leq \ell$, we finally obtain the expression:

$$\cos(\beta\phi)\cos(\alpha\theta) = \sum_{\ell=|\beta|}^{\infty} \frac{c_\ell}{2}\left(Y_\ell^{\beta}(\theta,\phi) + Y_\ell^{-\beta}(\theta,\phi)\right) \tag{A.3}$$

APPENDIX B – Spherical Harmonics on the Wavy Surface

Consider the following expression:

$$\sum_{n=0}^{\beta-1}\sum_{\ell=0}^{\infty}\sum_{m=-\ell}^{\ell} Y_{\ell}^{m}(\theta,\frac{2n\pi}{\beta}\pm\phi')Y_{\ell'}^{*m'}(\theta,\frac{2n\pi}{\beta}\pm\phi') \tag{B.1}$$

we know that

$$Y_{\ell'}^{*m'}(\theta,\phi)=(-1)^{-m'}Y_{\ell}^{m'}(\theta,\phi)=(-1)^{-m'}e^{-im'\phi}P_{\ell}^{-m'}(\cos\theta)$$

therefore, expression (B.1) can be rewritten as:

$$\begin{aligned}\sum_{n=0}^{\beta-1}\sum_{\ell=0}^{\infty}\sum_{m=-\ell}^{\ell} Y_{\ell}^{m}(\theta,\frac{2n\pi}{\beta}\pm\phi')Y_{\ell'}^{*m'}(\theta,\frac{2n\pi}{\beta}\pm\phi') = \\ \sum_{n=0}^{\beta-1}\sum_{\ell=0}^{\infty}\sum_{m=-\ell}^{\ell}(-1)^{-m'}\exp\left[\frac{2n\pi i(m-m')}{\beta}\right]e^{[\pm i(m-m')\phi']}\times \\ P_{\ell}^{m}(\cos\theta)P_{\ell'}^{-m'}(\cos\theta)\end{aligned} \tag{B.2}$$

Using the sum of roots of unity to our advantage, we notice that

$$\sum_{n=0}^{\beta-1}\exp\left[\frac{2n\pi i(m-m')}{\beta}\right]=\begin{cases}\beta, & \text{if} \quad m=m'+q\beta, \quad q\in\mathbb{Z}\\ 0, & \text{otherwise}\end{cases}$$

thus, expression (B.2) can be simplified and expressed as:

$$\begin{aligned}\sum_{n=0}^{\beta-1}\sum_{\ell=0}^{\infty}\sum_{m=-\ell}^{\ell} Y_{\ell}^{m}(\theta,\frac{2n\pi}{\beta}\pm\phi')Y_{\ell'}^{*m'}(\theta,\frac{2n\pi}{\beta}\pm\phi') = \sum_{\ell=0}^{\infty}\sum_{m=-\ell}^{\ell}\delta_{m,m'+q\beta}e^{\pm i(m-m')\phi'} \\ (-1)^{m'}P_{\ell}^{m}(\cos\theta)P_{\ell'}^{-m'}(\cos\theta)\end{aligned} \tag{B.3}$$

simplifying,

$$\begin{aligned}\sum_{n=0}^{\beta-1}\sum_{\ell=0}^{\infty}\sum_{m=-\ell}^{\ell} Y_{\ell}^{m}(\theta,\frac{2n\pi}{\beta}\pm\phi')Y_{\ell'}^{*m'}(\theta,\frac{2n\pi}{\beta}\pm\phi') = \sum_{\ell=0}^{\infty}(-1)^{-m'}\beta e^{\pm iq\beta\phi'} \\ P_{\ell}^{m'+q\beta}(\cos\theta)P_{\ell'}^{-m'}(\cos\theta)\end{aligned} \tag{B.4}$$

for $q \in \mathbb{Z}$. Recalling that $\phi' = \frac{1}{\beta}\arccos\left(\frac{r-R}{\epsilon}\right)$ and also that $P_{\ell'}^{-m'} = (-1)^{m'} P_{\ell'}^{m'}$, we can write

$$\sum_{n=0}^{\beta-1}\sum_{\ell=0}^{\infty}\sum_{m=-\ell}^{\ell} Y_\ell^m(\theta, \frac{2n\pi}{\beta} \pm \phi') Y_{\ell'}^{*m'}(\theta, \frac{2n\pi}{\beta} \pm \phi') = \beta \exp\left[\pm iq\left(\arccos\left(\frac{r-R}{\epsilon}\right)\right)\right] \sum_{\ell=0}^{\infty} P_\ell^{m'+q\beta}(\cos\theta) P_{\ell'}^{m'}(\cos\theta) \tag{B.5}$$

Moreover, the complex exponential refers to the Chebyshev polynomials:

$$\exp\left[\pm iq\left(\arccos\left(\frac{r-R}{\epsilon}\right)\right)\right] = T_q\left(\frac{r-R}{\epsilon}\right) \pm iU_{q-1}\left(\frac{r-R}{\epsilon}\right)\sqrt{1-\left(\frac{r-R}{\epsilon}\right)^2} \tag{B.6}$$

where T_q is the Chebyshev polynomial of the first kind of order q, and U_{q-1} is the Chebyshev polynomial of the second kind of order $q-1$.